Rhodopsin 7 and Cryptochrome – circadian photoreception in *Drosophila*

A thesis submitted to

Julius-Maximilians-Universität Würzburg

Department of Neurobiology and Genetics

in partial fulfillment of the requirements for the degree of

Doctor rerum naturalium (Dr. rer. nat.)

by

Christa Rita Kistenpfennig

from Regensburg

Würzburg, June 2012

Date of submission: 2012/06/18

Members of the Thesis Committee:

Chairperson: ……..

Supervisor: Prof. Dr. Charlotte Förster
Julius-Maximilians-Universität Würzburg, Lehrstuhl für Neurobiologie und Genetik

Reviewer: PD Dr. Alois Hofbauer
Universität Regensburg, Institut für Zoologie

Date of public defense: ……

Date of receipt of certificates: ……

“What we know is a drop, what we don´t know is an ocean.”

Isaac Newton

Dedicated to my family.

Affidavit

I hereby declare that this thesis entitled “Rhodopsin 7 and Cryptochrome – circadian photoreception in *Drosophila”* is the result of my own research and has been written independently with no other sources and aids than those specified in the text.
Furthermore, I confirm that this thesis has not been submitted or accepted as part of another examination process neither in identical nor in similar form.

Würzburg, June 2012 _____

Christa Kistenpfennig

Parts of this thesis have already been published:
Kistenpfennig C, Hirsh J, Yoshii T and Helfrich-Förster C (2012) Phase-Shifting the Fruit Fly Clock without Cryptochrome. *Journal of Biological Rhythms* 27:117-25.

Contents

Figures

Tables

Abbreviations

#	number sign
ø	diameter
°C	degree Celsius
A	ampere
aa	amino acid(s)
ad	to (fill up to)
ADP	adenosine diphosphate
Amp	ampicillin
aMe	accessory medulla
ATP	adenosine triphosphate
α-tub	*α-tubulin*
bit	binary digit
BL	Bloomington Stock Center
bp	base pares
c	centi
C-	carboxy-
Cam	chloramphenicol
CCW	counterclockwise
cDNA	complementary DNA
CIAP	calf intestinal alkaline phosphatase
CRY	cryptochrome
Ct	cycle threshold
CT	circadian time
CW	clockwise
Δ	difference
DAM	*Drosophila* Activity Monitoring
dd	double distilled
DD	constant darkness
DNA	deoxyribonucleic acid
DRA	dorsal rim area
DroID	*Drosophila* Interactions Database
DRY	aspartic acid-arginine-tyrosine
EA	evening activity
e.g.	exempli gratia (for example)
et al.	et alii (and others)
EM	electron micrograph
EO	evening oscillator
EtOH	ethanol
FAD	flavin-adenine dinucleotide
Fig.	figure
g	gram
h	hour
H	height
HEK	histidine-glutamic acid-lysine
i.a.	inter alia (among other things)
JO	Johnston's organ
K	lysine
kb	kilobase
l	liter
La	lamina
LED	light-emitting diode
LD	light/dark
LL	constant light
LM	light/moonlight
Lo	lobula
Lp	lobula plate
LP	light pulse
µ	micro
m	milli
M	medulla
M1	guinea pig animal number 1
M2	guinea pig animal number 2
MA	morning activity
MeOH	methanol
min	minute
MO	morning oscillator
Mrh	metarhodopsin
MTHF	methenyltetrahydrofolate
n	number (of tested animals)
N-	amino-
nm	nano meter
NaN_3	sodium acide
NGS	normal goat serum
No.	number
p	pale
PB	phosphate buffer
PBS	phosphate buffered saline
PBT	PB with Triton-X
PC	pigment cell
PCR	polymerase chain reaction
PDA	prolonged depolarization afterpotential
PER	period protein
PFA	paraformaldehyde
PHR	photolyase homology region
PR	photoreceptor
PRC	phase response curve
qPCR	quantitative PCR
R	retina
R1	rabit animal number 1
R2	rabit animal number 2

Rh	rhodopsin
RNA	ribonucleic acid
RNAi	RNA interference
rp49	*ribsomal protein 49*
rpm	rounds per minute
RT	room temperature
SDS	sodium dodecyl sulfate
SDS-PAGE	SDS-polyacrylamide gel electrophoresis
sec	second
SEM	standard error of the mean
τ	free-running rhythm
T	period of *Zeitgeber* cycle
TBS	tris buffered saline
TBST	TBS with Tween-20
TIM	timeless protein
TM	transmembrane
UAS	upstream activating sequence
UV	ultraviolet
V	volt
v.s.	vide supra (see above)
W	watt
y	yellow
ZT	*Zeitgeber* time

1 Introduction

1.1 Circadian clocks

As the earth rotates on its axis once every 24 h, virtually all living organisms evolved endogenous time-keeping systems, so called circadian clocks, to adapt physiological, biochemical and behavioral processes to daily environmental variations and seasonal changes, e.g., in light intensity, temperature or food availability. On the one hand, endogenous clocks provide internal temporal organization and ensure coordination of biological processes. On the other hand, they allow individuals to anticipate and thus, to prepare for predictable periodic changes. In general, circadian rhythms are defined by the following three fundamental properties:

First of all, they are generated by a self-sustained oscillator which persists with an endogenous free running rhythm close to, but not exactly, 24 h in the absence of all environmental cues, and are thus referred to as “circadian” rhythms deriving from the Latin phrase “circa diem”, which means “approximately a day” (Halberg et al., 1959). Second, they can be synchronized to the environmental 24-h day by external time cues, so called *Zeitgebers* (from the German “time givers”; Aschoff, 1960). The most predominant *Zeitgeber* accomplishing this process of circadian “entrainment” is the daily change of light and darkness, a clearly defined and rather noise-free marker of local time (Pittendrigh, 1960). Third, circadian rhythms are temperature compensated, meaning that their periodicity is relatively stable over a wide range of physiological temperatures (Pittendrigh, 1954).

Following a simplified linear model, circadian systems can principally be divided into three components (Johnson and Hastings, 1986) according to their function: Different input pathways (1) detect and transmit *Zeitgeber* information to an endogenous central circadian oscillator (2) which keeps time and generates output signals (3) governing biological rhythms, e.g., in behavior or physiology (Fig. 1).

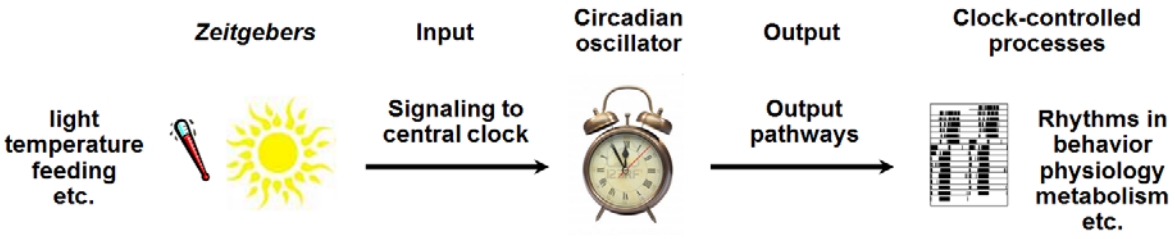

Figure 1: Simplified linear model of a circadian oscillator.

The basic model of a circadian clock comprises three parts: Input pathways, a central oscillator and output pathways. For details, see text.

1.2 The circadian clock of *Drosophila melanogaster*

In *Drosophila*, the history of chronobiology began in 1971, when Konopka and Benzer discovered the first clock gene, *period (per)*, in a forward genetic screen. It took more than 20 years until the second major clock gene, *timeless (tim)*, was identified (Sehgal et al., 1994). However, many other core components and clock-related genes followed during the last decades. Since then, the circadian oscillator of *Drosophila* has been extensively studied at the molecular, cellular and neural levels.

At the molecular levels, cell-autonomous rhythm-generating mechanisms are thought to rely on a central, self-sustained, negative feedback loop in which *per* and *tim* gene products, PER and TIM, ultimately repress their own transcription (Fig. 2). Briefly, the heterodimeric helix-loop-helix transcription factors CLOCK (CLK) and CYCLE (CYC) bind to E-Box sequences in *per* and *tim* promoters, thereby directly activating gene expression around midday (Allada et al., 1998; Darlington et al., 1998; Rutila et al., 1998). In the early night, PER and TIM accumulate and dimerize in the cell cytoplasm before translocation into the nucleus takes place around midnight (Curtin et al., 1995). Inside the nucleus, PER binds to CLK and thereby terminates transcriptional activation in the late night (Lee et al., 1999). Subsequent degradation of PER restarts the cycle and activates clock gene transcription (Hardin et al., 1990). A current, elaborate model of the molecular circadian oscillator, including further references, is summarized in a recent review by Peschel and Helfrich-Förster (2011).

Under LD 12:12 cycles in which 12 h of light alternate with 12 h of darkness, *Per* and *tim* transcript levels peak in the earlier and protein levels during the late night (So and Rosbash, 1997). This temporal delay between transcription and translation including posttranslational modifications (phosphorylation, dephosphorylation or ubiquitination) and changes in subcellular localization of PER and TIM generate the ~24-h cycle. Furthermore, additional interlocked feedback loops, which will not be introduced here, regulate gene expression of further clock components, e.g., rhythmic expression of CLK (for review: Allada and Chung, 2011).

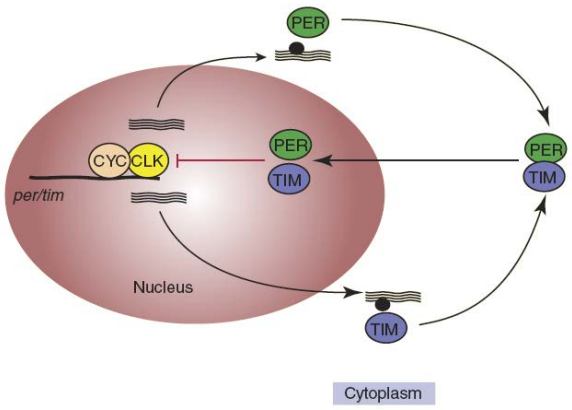

Figure 2: Simplified model of the molecular circadian core clock mechanism in *Drosophila.*

The schematic diagram illustrates the transcriptional negative feedback loop underlying circadian oscillation within single clock neurons in which PER und TIM repress their own CLK-CYC mediated transcription (from Nitabach and Taghert, 2008).

For details, see text.

Anatomically, the master clock of the fruit fly comprises ~150 clock neurons per brain hemisphere. Depending on their location, these are roughly divided into dorsal (DNs) and lateral (LNs) pacemaker neurons comprising the following seven clusters: Three groups of dorsal cells (DN_1, DN_2 and DN_3), the dorsal lateral neurons (LN_d), the lateral posterior neurons (LPN) and the lateral ventral cells (LN_v) which are, according to their size, subdivided into small (s-LN_v) and large (l-LN_v) neurons, respectively. These clock neurons send their axonal projections to distinct areas of the brain, thereby generating a neuronal clock network (for review: Helfrich-Förster et al., 2007). Alternatively, the pacemaker neurons could be classified according to their function in the control of circadian behavior (for review: Helfrich-Förster, 2009) or to the neuropeptides which they use for signaling (for review: Nitabach and Taghert, 2008).

Besides this central master clock in the fly brain, additional "slave" clocks have been discovered in many peripheral tissues, e.g., in the Malpighian tubules, the eyes or the antennae (Plautz et al., 1997; Giebultowicz, 2001).

Since daylight is also the strongest *Zeitgeber* in the fruit fly, its visual system will be elucidated in the following sections before proceeding to circadian light entrainment in *Drosophila*.

1.3 The visual system of Drosophila melanogaster

Like many other insects, the adult fruit fly possesses a highly developed visual system comprising three photoreceptive organs, namely, the compound eyes, the ocelli and the Hofbauer-Buchner (H-B) eyelet (Fig. 3). The most prominent visual structure is the pair of compound eyes which mainly mediates shape, color and motion vision (Menne and Spatz, 1977; Yamaguchi et al., 2010). Low levels of light and subtle changes in light intensity are detected by the ocelli, three small simple eyes located in a triangle at the vertex of the fly head (Goodman, 1970; Hu et al., 1978). The H-B eyelet is a cluster of four neurons residing between the retina and the lamina of each compound eye (Hofbauer and Buchner, 1989). This extraretinal photoreceptor derives from the larval visual system, termed Bolwig's organ (Bolwig, 1946), projects to the region of the accessory medulla (aMe) and is involved in circadian entrainment (Yasuyama and Meinertzhagen, 1999; Helfrich-Förster et al., 2002; Rieger et al., 2003).

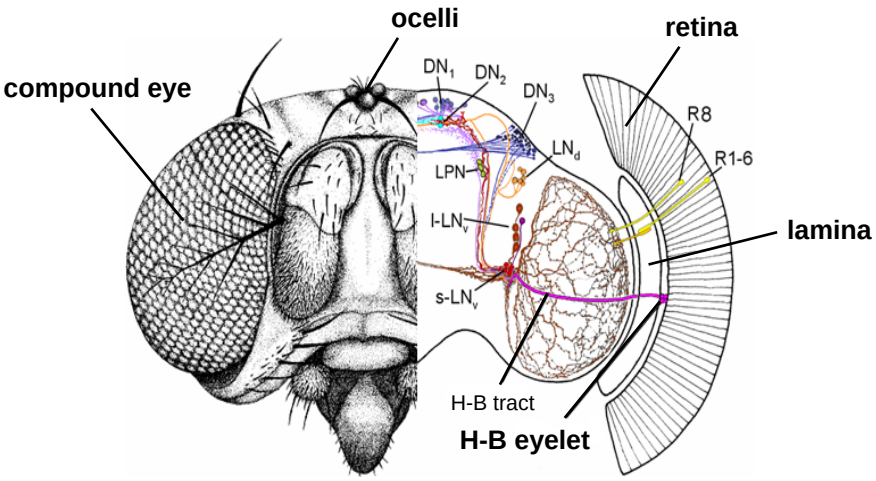

Figure 3: Visual system of *Drosophila melanogaster*.
Left: Frontal perspective view of the head of a CS wild-type fly. Right: View onto the optic lobe and the brain after removal of the cranium. Photoreceptive organs and structures are highlighted; the neural network of the circadian clock is indicated. For details, see text (modified from Helfrich and Engelmann, 1983; Helfrich-Förster et al., 2007).

1.4 The compound eyes of Drosophila melanogaster

The compound eye is the main visual system of insects. As the name suggests, each compound eye is composed of single optical units, the ommatidia, which are arranged in a regular hexagonal pattern. In *Drosophila*, each of the 750-800 ommatidia contains 20 cells including 8 photoreceptor (PR) neurons (R1-R8) and 12 accessory cells, such as cone, bristle and pigment cells. The latter optically isolate adjacent ommatidia from each other, thereby causing the red color of wild-type ommatidia (Ready et al., 1976). Each cluster of PR cells comprises six larger peripheral PRs (R1-R6) extending the entire depth of the retina to the basal lamina and two slender central ones (R7+R8) arranged in tandem with R7 located on top of R8 along the distal-proximal axis of the retina (Fig. 4A, B; for review: Wolff and Ready, 1993). The dioptric apparatus formed by the transparent biconvex corneal lens (at the outer surface) and the pseudocone (extracellular fluid-filled cavity below) borders the ommatidium and focuses light onto the photosensitive organelle of the PR, the rhabdomere. As shown in the EM cross section through an adult ommatidium (Fig. 4C), rhabdomeres are oriented towards the center (interrhabdomeral space) and arranged in an asymmetrical trapezoidal pattern. Structurally, rhabdomeres are organized in stacks of up to 60,000 densely packed microvilli, each up to 2 µm long and 60 nm in diameter (Fig. 4D; Leonard et al., 1992). The rhabdomere houses the visual pigments of the ommatidia, the rhodopsins (~1000 molecules per microvillus) and other components of the phototransduction machinery (for review: Hardie, 2001; Katz and Minke, 2009; Montell, 2012).

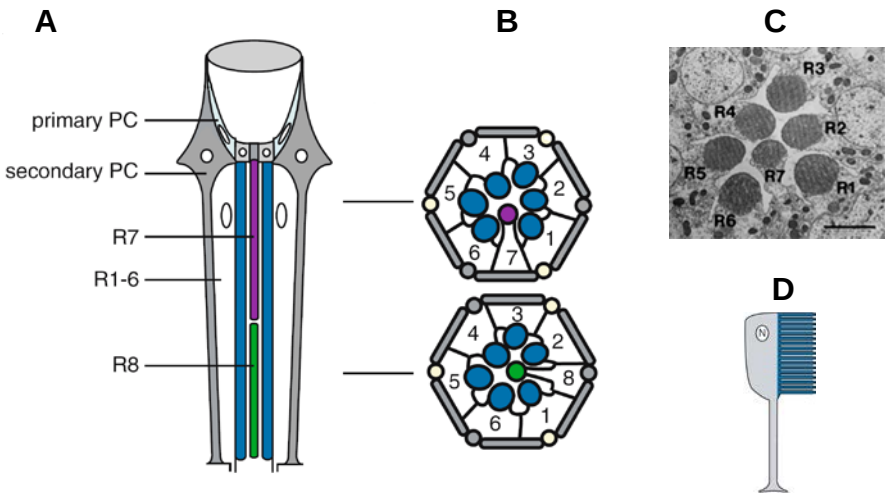

Figure 4: Structure of the *Drosophila* ommatidium.

Schematic diagram of an adult ommatidium representing a longitudinal (A) and a cross section (B). One single ommatidium contains a cluster of 8 PRs encircled by auxiliary cells, i.a. pigment cells (PCs). Six large peripheral PRs (R1-R6) surround two slender central ones (R7+R8), arranged in tandem with R7 distal and R8 proximal. Their highlighted photosensitive rhabdomeres orient to the centre of the ommatidium and build an open rhabdom (from Wang and Montell, 2007).

C: EM image of a cross section through the distal region of a wild-type ommatidium. Cell bodies of PRs are numbered. Rhabdomeres of R1-R6 are organized in a chiral trapezoid with the smaller R7 rhabdomere in its center. Scale bar: 2 µm (from Pearn et al., 1996).

D: Cartoon showing a longitudinal view of a PR cell including cell body (with nucleus, N), axon and the stack of rhabdomeral microvilli (highlighted in blue). Theses contain F-actin filaments (Arikawa, 1990), but no cell organelles (adapted from Wang and Montell, 2007).

The axons of R1-R6 terminate in the first optic neuropil, the lamina, providing synaptic input to first-order interneurons which are grouped in cartridges (Trujillo-Cenoz, 1965; Braitenberg, 1967). In contrast, R7 and R8 axons directly project into distinct layers of the medulla (M6 and M3, respectively), the second neuropil of the optic lobe (Fig. 5A; Fischbach and Dittrich, 1989). According to the principle of neural superposition, one lamina cartridge receives synaptic input from outer PR cells (one each) with identical optical axes of six neighboring ommatidia, thereby increasing the absolute sensitivity (Fig. 5B; Kirschfeld, 1973).

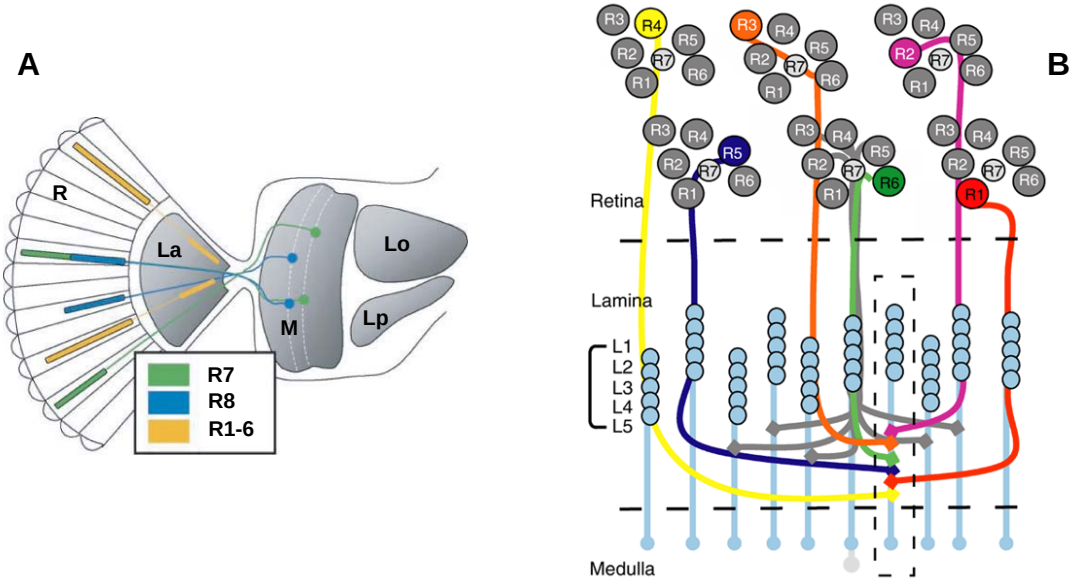

Figure 5: Structure of the optic lobe and projection patterns of retinal photoreceptors.

A: The optic lobe comprises four successive neuropils, the retina (R), the lamina (La), the medulla (M), the lobula (Lo) and the lobula plate (Lp). R1-R6 axons terminate in the lamina, whereas axons of R7 and R8 directly project into the medulla (modified from Petrovic and Hummel, 2008).

B: The axons of six peripheral PRs from six neighboring ommatidia (one each) project to the same lamina cartridge (dashed box), a complex arrangement called neural superposition (from Morante and Desplan, 2005).

1.5 Rhodopsin signaling in *Drosophila*

Rhodopsins (Rhs) are the major visual pigments in *Drosophila* and present in all PRs, where they locate to rhabdomeral microvilli. In general, rhodopsin molecules belong to the G protein-coupled receptor superfamily which is structurally characterized by seven transmembrane (7TM) domains (Fig. 6; Zuker et al., 1985). They consist of an apoprotein, referred to as the opsin, and a light-sensitive part, the covalently bound chromophore, 11-*cis* 3-hydoxyretinal in *Drosophila* (Vogt and Kirschfeld, 1984).

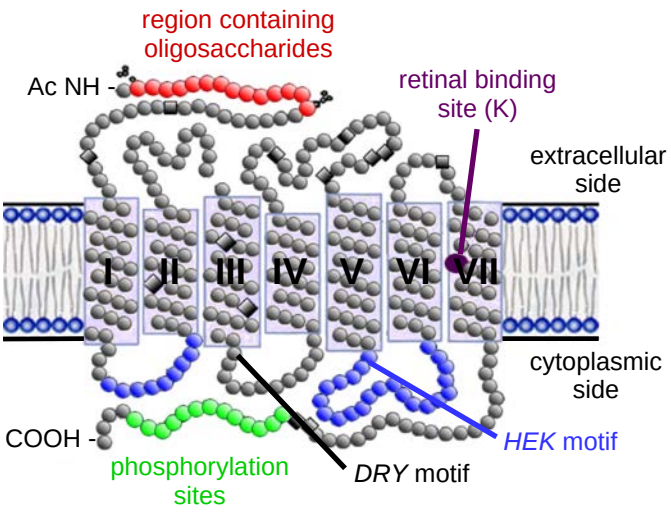

Figure 6: Secondary structural model of rhodopsin.

Rhs are GPCRs with a 7TM architecture (α-helical domains) linked to intra- and extracellular loops. TM VII contains the retinal binding site (lysine residue; K) and is followed by an 8th helix running in parallel to the cytoplasmic membrane surface. Regions important for synthesis, post-translational modification and function of Rhs as well as conserved amino acid motifs are highlighted (Gärtner, 2000; Hargrave, 2001; adapted from Hargrave et al., 1984).

Exposure to light causes an isomerization to the all-*trans* retinal, thereby inducing a conformational change of the opsin subunit. This biologically active “metarhodopsin” (Mrh) induces the G_q protein-coupled signaling cascade (Scott et al., 1995), which ultimately results in PR depolarization. Thereby generated electrical signals convey visual information to the fly’s brain. Recent reviews from Hardie (2012) and Montel (2012) describe a current model of the *Drosophila* phototransduction cascade (Fig. 7). Briefly, photoactivated Mrh activates a heterotrimeric G_q protein, promoting GDP-GTP exchange. The dissociated $G_q\alpha$ subunit, in turn, stimulates phospolipase Cβ (PLCβ), thereby initiating phosphoinositol signaling. Although the underlying mechanism is still under discussion, this leads to opening of TRP and TRPL ion channels resulting in a cation, mainly Ca^{2+}, influx into the PR neuron. Finally, CalX, a co-localized Na^+/ Ca^{2+} exchanger, mediates Ca^{2+} extrusion (see Wang and Montell, 2007 and references cited therein).

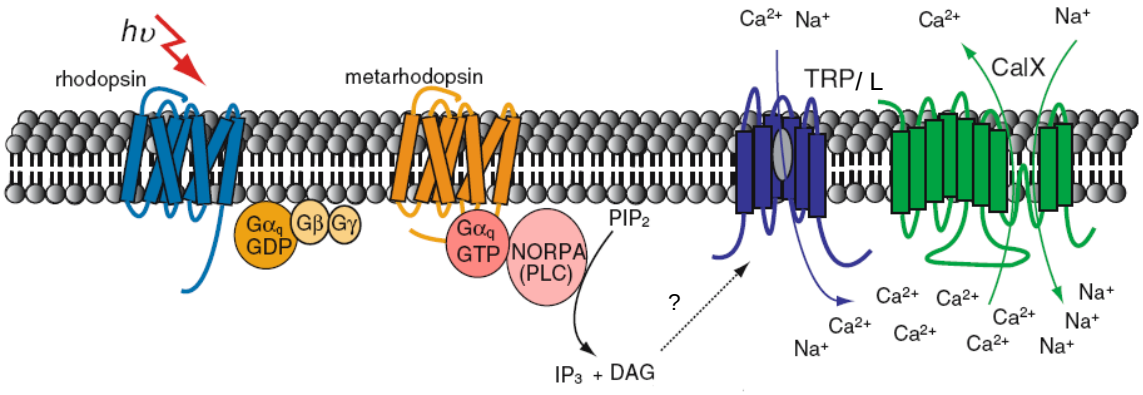

Figure 7: Schematic model of the rhodopsin photoransduction cascade in *Drosophila*.
Light-activated Mrh initiates G_q protein based phosphoinositol signaling which results in ion channel opening and subsequent PR depolarization (modified from Wang and Montell, 2007). For details, see text.

The termination of visual signaling is achieved by selective binding of arrestin1 and, mainly, arrestin2 to phosphorylated Mrh, thereby uncoupling Mrh from the $G_q\alpha$ subunit (Dolph et al., 1993). Subsequent to photoisomerization, the 11-*cis* form of the retinal is either regenerated by absorption of a second photon of light or recycled within an enzymatic visual cycle (Wang et al., 2010; Wang et al., 2012).

Histamine is the primary neurotransmitter released from PR cells upon light-induced depolarization (Hardie, 1987). PRs contain histidine decarboxylase (Hdc), an enzyme that is crucial for histamine biosynthesis from histidine (Burg et al., 1993).

1.6 Rhodopsin expression in *Drosophila*

Six different rhodopsins, named Rh1 to Rh6, each with a distinct spectral sensitivity and expression pattern, have been identified in *Drosophila* so far. Rh1, discovered by its ERG phenotype in 1985 and encoded by the *ninaE* gene *(neither inactivation nor afterpotential E)*, was the first visual pigment to be characterized (Nichols and Pak, 1985; O`Tousa et al., 1985; Zuker et al., 1985). Rh1 is expressed in R1-R6 PRs of all ommatidia (Fig. 8A) and thus the major pigment in the fly's visual system. Regarding its spectral properties, Rh1 is a blue-green-sensitive PR with a broad spectral range and a sensitivity peak at ~486 nm (Fig. 8B; Zuker et al., 1985; Salcedo et al., 1999). Functionally, R1-R6 PRs are responsible for the high light sensitivity of the compound eyes and mainly mediate shape and motion vision (Heisenberg and Buchner, 1977; Yamaguchi et al., 2008). In contrast, R7 and R8 work at higher light intensities and are involved in color vision, phototaxis and the detection of the e-vector of polarized light (Menne and Spatz, 1977; Wernet et al., 2003; Yamaguchi et al., 2010).

To fulfill all these functions, the retina is endowed with different ommatidial subtypes characterized by the Rh expression in their central PR cells (see Fig. 8A). In the ~70% of "yellow" (y) ommatidia, expression of Rh6 in R8 comes along with Rh4 in R7, whereas in the remaining ~30% of "pale" (p) ommatidia expression of Rh3 in R7 is combined with Rh5 in R8. The two types of ommatidia are randomly distributed over the retina. Visual pigments of R7 cells, Rh3 and Rh4 are UV-sensitive with maximum absorption at 331 nm and 355 nm, respectively. Rh5 is most sensitive to blue light (λ_{max} 442 nm), whereas Rh6 is a green-light sensitive (λ_{max} 515 nm) PR (see Fig. 8B; Chou et al., 1996; Papatsenko et al., 1997; Salcedo et al., 1999). Except for Rh3 and Rh4, the presence of a sensitizing pigment causes additional sensitivity in the UV range (Kirschfeld and Franceschini, 1977).

In addition, specialized y-type ommatidia along the dorsal margin of the compound eye (dorsal rim area, DRA) which detect polarized light, express Rh3 in their enlarged R7 and R8 rhabdomeres (Fortini and Rubin, 1990; Wernet et al., 2003). Moreover, another minor type of y-ommatidia (~10% of the total ~70%) is present in the dorsal third of the retina and characterized by co-expression of Rh3 and Rh4 in R7 (Mazzoni et al., 2008).

Rh6 was additionally detected in the neurons of the H-B eyelet (Helfrich-Förster et al., 2002; Sprecher and Desplan, 2008). Finally, the violet-absorbing Rh2 (λ_{max} ~418 nm) is exclusively expressed in the ocelli (Pollock and Benzer, 1988).

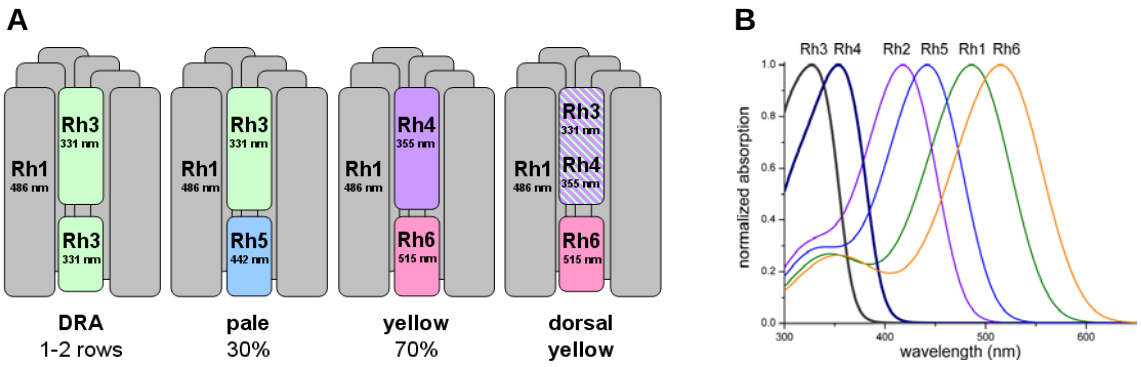

Figure 8: Rhodopsin expression in retinal photoreceptors.

A: The four types of retinal ommatidia differ in their Rh expression in central PRs, whereas Rh1 is expressed in R1-R6 of all subtypes.

B: Absorption spectrum of *Drosophila* Rhodopsins (Stavenga and Arikawa, 2008).

For details, see text.

The photoconversion of the Rh state into the active Mrh form leads to a strong shift in absorbance to longer wavelength ranges (Stavenga, 1992). Rh6 is the only exception to this rule, since its Mrh absorbs at shorter wavelengths than its Rh state. Thus, the spectral composition of the light source and the absorption spectra determine the ratio between both forms in the photosteady state (Salcedo et al., 1999).

Table 1 summarizes the characteristics of *Drosophila* Rhs described in this section.

Table 1: Basic features of *Drosophila* rhodopsins.

Rh: Rhodpsin state; Mrh: Metarhodpsin state. Data from absorption spectra: Salcedo et al., 1999. For details, see text.

Rhosopsin	Expression pattern	Absorption maximum Rh (nm)	Absorption maximum Mrh (nm)
Rh1	Ommatidia, R1-R6	~486	~566
Rh2	Ocellar PR cells	~418	~506
Rh3	Ommatidia (~30%), R7	~331	~468
Rh4	Ommatidia (~70%), R8	~355	~470
Rh5	Ommatidia (~30%), R7	~442	~494
Rh6	Ommatidia (~70%), R8 PR cells of the HB eyelet	~515	~468

Remarkably, Rh1 has an additional, vision-independent function in the development and maintenance of PR cells in adult flies. In 1995, Kumar and Ready discovered a massive degeneration in R1-R6 rhabdomeres of Rh1 null mutants and concluded a structural requirement of Rh1 during PR morphogenesis. Even though small amounts of Rhs were shown to be sufficient for normal PR development (Leonard et al., 1992;

Kumar and Ready, 1995), their proper maturation and trafficking to rhabdomeral membranes play an essential role in PR development. Besides, a function of Rh1 in the thermosensation cascade of *Drosophila* larvae was demonstrated in a more recent publication (Shen et al., 2011). Another additional and important role, especially of ommatidal Rhs, in the entrainment of the fly's circadian clock to light will be addressed in a separate section later on.

1.7 *Drosophila* cryptochrome

Cryptochrome (CRY), an intracellular photopigment in *Drosophila* does not contribute to the classic visual signaling pathway, but is mainly required for light-mediated entrainment of the clock (Stanewsky et al., 1998; Emery et al., 1998). Besides, CRY is involved in magnetoreception (Gegear et al., 2008; Yoshii et al., 2009), mediates the response of the circadian clock to temperature (Kaushik et al., 2007) and plays a light-independent role in the function of peripheral oscillators (Krishnan et al., 2001).

First identified in *Arabidopsis thaliana* by Ahmad and Cashmore in 1993, CRYs are sensitive to light in the UV-A/blue range and present in many organisms ranging from cyanobacteria (Hitomi et al., 2000) to mammals (Todo et al., 1996). However, the two known mammalian CRY homologues do not overtake PR function, but are part of the central oscillator (Griffin et al., 1999). CRYs are flavoproteins and phylogenetically closely related to DNA photolyases, but lack DNA repair function (Cashmore, 1999).

Drosophila CRY (dCRY in the following) is a member of the photolyase/cryptochrome family (Emery, 1998). It is characterized by an N-terminal photolyase homology (PHR) domain including a catalytic cofacor, FAD (flavin-adenine dinucleotide) and a second, light-harvesting chromophore, MTHF (methenyltetrahydrofolate), a pterine (Cashmore 2003). Its C-terminal domain is not required for photoreception, but regulates i.a. protein stability (Busza et al., 2004).

As shown in the absorption spectrum (Fig. 9A) from Öztürk et al. (2011), dCRY both its dark and its light activated form, show sensitivity peaks in the UV-A (~360 nm) and a plateau in the near blue range (~430-460 nm). Upon light exposure, the C-terminal extensions of dCRY undergo a conformational change (Öztürk et al., 2011), thus explaining the importance of the C-terminus for proper signaling function (Rosato et al., 2001; Busza et al., 2004).

In the adult fly head, CRY is detected in the cytoplasm of PR cells and it is expressed in certain pacemaker neurons (Fig. 9B), in all LN_vs, in the 5^{th} s-LN_v, in three LN_ds and some DN_1s. Besides, a couple of non-clock neurons show CRY immunoreactivity (Yoshii et al., 2008).

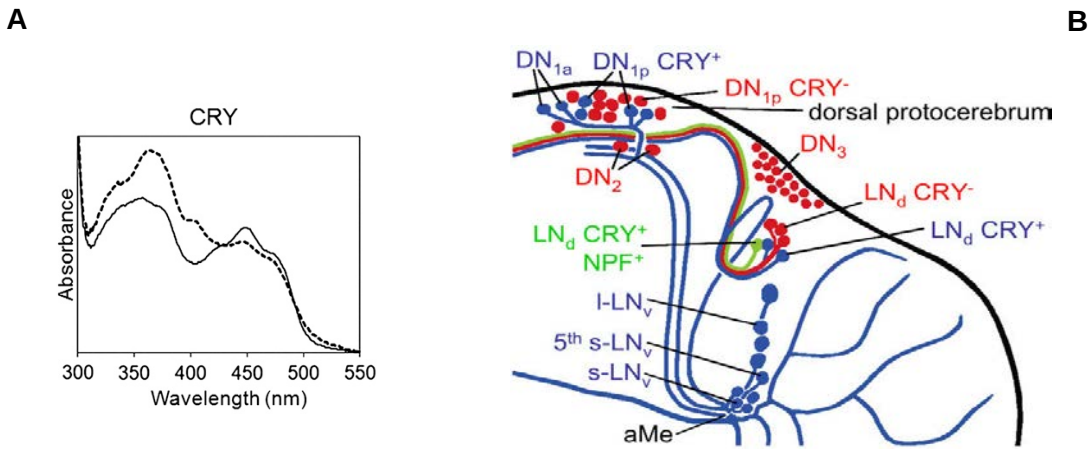

Figure 9: CRY is an internal blue-light photoreceptor in *Drosophila*.

A: Absorption spectrum of CRY. CRY shows sensitivity in the UV-A (~330-370 nm) and in the blue (430-460 nm) wavelength range. Solid line: Spectrum of FAD oxidized form; dashed line: Spectrum of $FAD^{\cdot}$ anion radical form (from Öztürk et al., 2011).

B: Expression of CRY in the central pacemaker neurons in the brain. CRY-positive neurons and their projections are highlighted in blue; the additionally NPF-positive LN_d is labeled in green (from Yoshii et al., 2008). For details, see text.

In whole head extracts, levels of *cry* transcript cycle with a peak around dawn and a trough around midnight under LD 12:12 conditions and are thus in anti-phase with *per* and *tim* mRNA cycling. In contrast, protein levels are light-regulated with low levels of CRY in the presence of light and CRY accumulation in darkness (Emery et al., 1998). Concerning its subcellular localization, CRY is present in both the nucleus and the cell cytoplasm (Ceriani et al., 1999).

CRY signaling, its role in photic entrainment and the effect of light on the circadian clock in general, will be discussed in the following sections.

1.8 The effects of light on the circadian clock of *Drosophila*

Locomotor activity rhythms are one reliable and robust output of the circadian clock in *Drosophila* and widely used to investigate clock function, since they are relatively accessible and locomotor activity recording is automated. Fruit flies are diurnal to crepuscular, meaning that they are predominantly active around dawn and dusk. Based on the dual oscillator model originally proposed for rodents by Pittendrigh and Daan (1976), this bimodal activity pattern comprising morning and evening activity bouts is regulated by two separate but interacting oscillators (morning and evening oscillator, respectively) which show different responses to light (Rieger et al., 2006).

In general, light has different effects on the circadian clock, which will be described on the levels of activity rhythms. One effect was briefly mentioned before – entrainment

(Fig. 10A). *Zeitgebers*, primarily light, synchronize activity rhythms to the external 24-h day. Therefore, the endogenous free-running rhythm (τ), which slightly deviates from 24 h, needs to adjust to the exactly 24-h period of the *Zeitgeber* cycle (T) daily and to keep a stable phase relationship. Moreover, after release into constant conditions, here constant darkness (DD), rhythms resume with their endogenous period but with a phase determined by the *Zeitgeber*. Meaning, if the onset of free-running activity does not coincide with the phase of entrainment, animals did not entrain and one speaks of "masking". These are direct effects of light on the circadian clock which can conceal or even distort the clock-controlled activity (Minors and Waterhouse, 1989). Masking effects can easily be observed in the activity patterns of clock mutants, e.g., in per^0 flies (Wheeler et al., 1993). However, masking is not restricted to mutants but also present in wild-type animals (Fig. 10B). Fruit flies, for example, often respond with a sudden increase in locomotor activity ("startle response") to the light being switched on at the beginning of the LD 12:12 cycle (Hamblen-Coyle et al., 1992), and with an abrupt decrease in activity to lights-off, respectively (for review: Mrosovsky, 1999).

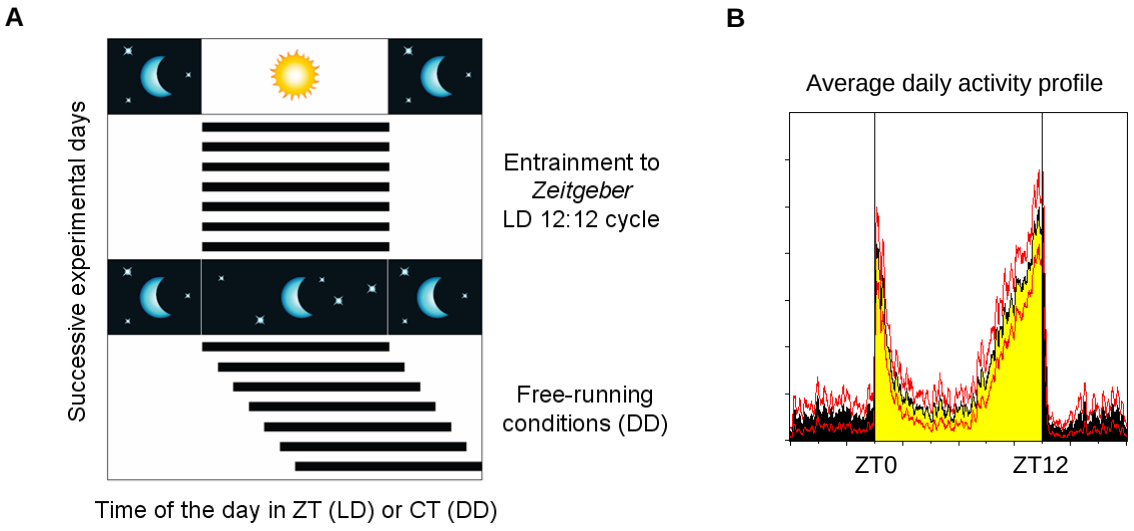

Figure 10: Entrainment of circadian rhythms to light.

A: Schematic actogram of a day-active animal under LD 12:12 cycles. Activity rhythms adjust their endogenous period to the period of the *Zeitgeber*. Upon release into DD, circadian rhythms resume with their endogenous period (here > 24 h), but the initial onset of activity in DD coincides with the onset under LD cycles, thereby confirming proper entrainment. ZT: *Zeitgeber* time; ZT0 is defined as lights-on; CT: Circadian time, defined by the endogenous period and the activity pattern under free-running conditions (adapted from Golombek and Rosenstein, 2010).

B: Average daily activity profile of a wild-type *Drosophila*. Both lights-on (ZT0) and lights-off (ZT12) directly provoke an abrupt increase and decrease in activity, respectively. This masking effect is typical for day-active animals, whereas activity in nocturnal animals would be suppressed by light (Mrosovsky, 1999).

There are two other effects of light that were used to propose models for entrainment, so called parametric (sometimes also tonic or continuous) and non-parametric (phasic or discrete) effects of light (Daan, 1977; Roenneberg and Merrow, 2003).

In general, parametric light effects affect the period length (τ) of a circadian oscillator. Usually, longer photoperiods or constant light (LL) continuously shorten τ of diurnal animals and lengthen τ of nocturnal animals, a correlation referred to as Aschoff's rule (Pittendrigh, 1960). According to Aschoff (1960), τ is a function of the intensity of illumination under LL and shortens with increasing light intensity, while activity levels increase at the same time. However, this rule does not apply to all diurnal animals; some lengthen their period with increasing light intensity. In *Drosophila* constant light of low irradiance, such as moonlight of 0.01 lux intensity, lengthens τ (> 1 h in experiments of this thesis using wild-type flies) and increases the overall locomotor activity in comparison to DD (Bachleitner et al., 2007). On the other hand, fruit flies become immediately arrythmic under LL conditions (Konopka et al., 1989).

Non-parametric light effects basically affect the phase of the free-running rhythm and have been studied more extensively. The model of non-parametric light entrainment in which light is supposed to change the phase of an endogenous oscillator daily in order to compensate for the difference between T and τ (see entrainment) was postulated by Aschoff's opponent, Pittendrigh (1966). According to this model, light at different circadian times affects the phase of an oscillator differently to allow entrainment. This can be studied by constructing a phase response curve (PRC) in which phase shifts of a circadian rhythm are plotted depending on the circadian phase (CT) a *Zeitgeber* is applied (Pittendrigh, 1960; for review: Johnson, 1999). The idealized PRC based on the enclosed actograms illustrates the effect of a light pulse (LP) on the locomotor activity rhythm of a night-active free-running animal (Fig. 11).

Light during the subjective day (CT0-CT12) generally provokes little or no behavioral responses (see data points 1, 2, 5) regarding the onset of activity, thus, this part of the PRC is called dead zone. On the contrary, light pulses presented during the subjective night (CT12-CT0) phase-shift the free-running activity rhythm. They induce phase delays (3) during the early subjective night (mimicking delayed dusk) and phase advances (4) during the late subjective night (mimicking advanced dawn), respectively.

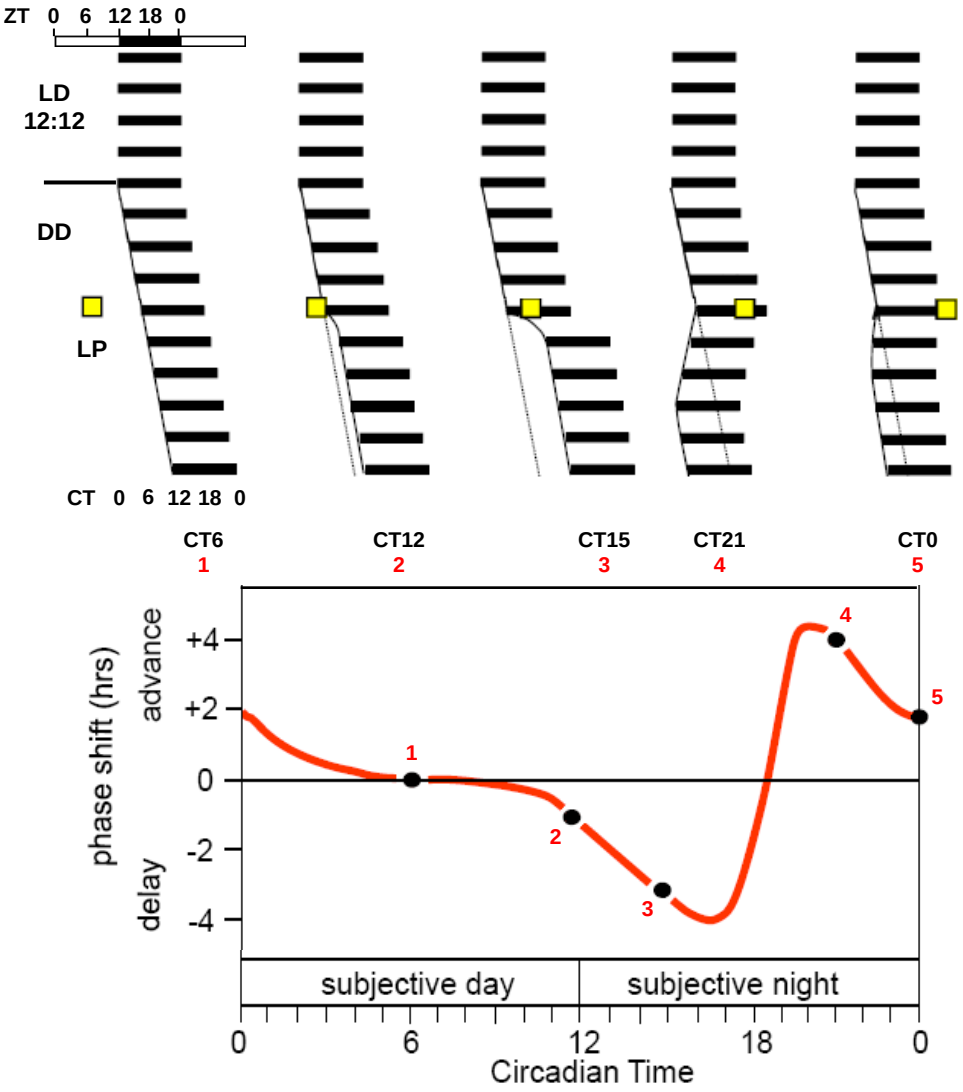

Figure 11: Idealized type 1 PRC to a photic stimulus.

The top panel shows actograms representing the response of locomotor activity rhythms (nocturnal animal) to a light pulse (LP) presented at different circadian phases during the subjective day (CT0-CT12) and night (CT12-CT0). The responses are plotted below in an idealized PRC. A LP during the earlier subjective night (CT15) phase delays the activity rhythm (negative value), whereas a LP during the late subjective night (CT21) phase advances the rhythm (positive value). For details, see text (adapted from Moore-Ede et al., 1982).

The shape and the amplitude of a PRC is species-specific and depends on different parameters, e.g., the strength (duration or intensity) of the stimulus (Pittendrigh, 1981). Besides, not all organisms generate a slow-resetting type 0 PRC like shown above, but respond with stronger phase shifts (up to 12 h) resulting in a discontinuous, abrupt transition between delays and advances characterizing a type 0 PRC (Winfree, 1970). Remarkably, type 1 and type 0 resetting are observed in the same animal depending on the strength of the stimulus (e.g. Saunders, 1978).

However, under laboratory LD conditions, an organism experiences parametric and non-parametric light effects represented by the continuous presence of light during the

artificial day and the lights-on and lights-off transition, respectively. Thus, both effects are assumed to contribute to circadian entrainment (for review and further references: Johnson et al., 2003; Roenneberg and Merrow, 2003; Golombek and Rosenstein, 2010).

1.9 Photic entrainment in *Drosophila*

As previously mentioned, CRY is the major circadian photoreceptor in *Drosophila* – but how does it transfer light information to the endogenous oscillator and do the Rhs in the photoreceptive organs contribute to photic entrainment? In comparison to the classical phototransduction cascade, the signaling of CRY to the circadian clock is far less understood. At the molecular levels, activated CRY directly interferes with the core clock mechanism by interaction with TIM, thereby resetting the clock. A current model of CRY signaling is discussed in a recent reviewed by Peschel and Helfrich-Förster (2011). Briefly, light-activated CRY binds to TIM inducing its ubiquitination and the following proteasomal degradation (Naidoo et al., 1999). The F-Box protein Jetlag (JET), a component of an E3 ubiquitin ligase complex, mediates TIM degradation and is required for subsequent degradation of CRY (Koh et al., 2006; Peschel et al., 2006). In the absence of TIM, PER is not stabilized and thus undergoes degradation via the ubiquitin-proteasomal pathway. Biochemical principles of CRY activation and signaling are highlighted in Öztürk et al. (2011).

Light-dependent degradation of TIM explains the response of the clock to light pulses in the PRC. A photic stimulus presented during the early night leads to a delay in TIM accumulation, thereby causing phase delays, whereas a short light pulse during the late night advances disappearance of TIM resulting in phase advances of the rhythm.

Initial experiments showed that ocular TIM is not degraded upon exposure to light and that rhythmic core clock luciferase-reporter gene expression is abolished in cry^{b} flies which carry a point mutation in the conserved FAD-binding domain (Stanewsky et al., 1998). However, oscillation of PER and TIM persists in the absence of CRY in most of the clock neurons, although partly with a reduced amplitude (e.g., Helfrich-Förster et al., 2001; Yoshii et al., 2004).

Unexpectedly, mutants lacking functional CRY (cry^{b} and cry^{01}) entrain their locomotor activity rhythms to LD 12:12 cycles and show normal free-running rhythms under DD. Despite their ability to entrain, mutant flies are less sensitive to light and require longer time to re-entrain to a shifted (phase advanced or delayed) LD cycle (Stanewsky et al., 1998; Emery et al., 2000b; Kistenpfennig et al., 2012). Unlike wild-type flies (Konopka et al., 1989), *cry* mutants do not become arrythmic under LL (Emery et al., 2000a), but

exhibit free-running rhythms that dissociate in two components, especially at higher irradiances (Yoshii et al, 2004; Dolezelova et al., 2007).

In various experiments, impairment of *cry* function was combined with other mutations affecting the visual system to confirm that light entrainment does not exclusively rely on CRY and to investigate these contributions. The results basically suggested that especially the compound eyes, but also the extraretinal photoreceptors (H-B eyelets and ocelli) including an unknown photopigment in the DN_3s, provide additional input into the circadian clock, thereby mediating light entrainment (e.g., Rieger et al., 2003; Veleri et al., 2007). The compound eyes and the HB-eyelets project to the region of the circadian pacemaker center in the brain; their axons terminate in proximity to dendritic arborizations of the LN_vs (Helfrich-Förster et al., 2002; Malpel et al., 2002). However, their complex interactions as well as potential signaling pathways remained rather unclear (for review: Helfrich-Förster, 2005).

Within these studies, circadianly blind flies lacking all known photoreceptors showed still direct responses to light, raising the possibility of the presence of a yet unidentified photoreceptor and making Rh7 a possible candidate (Helfrich-Förster et al., 2001).

1.10 Rhodopsin 7 – a candidate for a new photoreceptor in *Drosophila*

Twelve years ago, when the *Drosophila* genome was published (Adams et al., 2000) a yet uncharacterized gene, annotated CG5638, was denominated *rh7* due to sequence homologies to the known *Drosophila* Rhs, although its function was unknown.

The *rh7* gene is located on the left arm of the third chromosome, spans 11.3 kb in total and contains three coding exons (E2-4). These encode a protein of 483 amino acids (aa) with a predicted molecular weight of 53.7 kDa (FlyBase). The *rh7* promoter region contains two common sequence elements required for transcription of all *rh* promoters, the TATA box and the ~15-30 bp upstream located rhodopsin conserved sequence I (RCSI; Papatsenko et al., 2001).

Rh7 is highly conserved across the *Drosophila* genus (Senthilan, personal communication). In comparison to Rh1-Rh6, its predicted sequence is remarkably longer (~100 aa) due to C- and N-terminal extensions, but otherwise shows a shortened third intracellular loop (Izutsu et al., 2012). However, Rh7 shares some characteristics of the *Drosophila* Rh family (see Fig. 6), a predicted 7TM architecture (FlyBase), a lysine residue (K) within TM VII (chromophore binding site; Gärtner, 2000) and a DRY motif at the boundary between TM III and the second intracellular loop (for interaction with G proteins and arrestins, for regulation of conformational states; Marion et al., 2006) – but also lacks a conserved HEK feature at the beginning of the

third cytoplasmic loop (for G protein coupling; Gärtner, 2000). Within the *Drosophila melanogaster* species, Rh7 shows the highest sequence similarity (>30%) to Rh5 (for sequence comparisons: Veleri, 2005).
Available mRNA expression data (from FlyBase, modENCODE Temporal Expression Data; Gravely et al., 2011 and from FlyAtlas, Anatomical Expression Data; Chintapalli et al., 2007) suggests generally low levels of *rh7* expression with highest values for young adult males in terms of developmental stages and for the adult eye and brain in terms of tissue-specific expression.

1.11 Aims of this thesis

The first part of this thesis addresses the synchronization and entrainment properties of cry^{01} mutant flies. Despite CRYs role as main circadian photoreceptor in *Drosophila*, it has been shown that CRY-independent signaling via the photoreceptive organs is sufficient for entrainment to LD cycles (Stanewsky et al., 1998). However, responses to light are slower in the absence of CRY, and mutants take considerably longer than wild-type flies to re-entrain their locomotor activity rhythms to 8-h shifts of the LD cycle (Emery et al., 2000b). Furthermore, the phase-shifting behavior was impaired in cry^{b}, a *cry* loss-of-function mutant (Stanewsky et al., 1998). In mammals, light entrainment is exclusively mediated by the eyes (Nelson and Zucker, 1981) and thus similar phase-shifting abilities could be expected. If this comparison holds true, flies lacking CRY should shift their activity rhythms upon light-pulses and display a slow-resetting, mammalian-like type 1 PRC of low amplitude.
The second and major part of this thesis investigates the expression pattern of Rh7 and its function, especially in circadian entrainment, in *Drosophila*. In adult fruit flies, all so far characterized rhodopsins are expressed in rhabdomeral membranes of photoreceptor cells in diverse visual organs (see 1.6). Flies lacking the internal blue-light photopigment CRY as well as a functional visual system still respond to light, thereby implying the presence of an unknown photoreceptor (Helfrich-Förster, 2001). According to its predicted 7TM structure and certain features characteristic of Rhs (as described above), *rh7* might indeed encode a functional photoreceptor.
This issue will mainly be addressed by analyzing the spatial expression of Rh7 and its role in circadian entrainment of locomotor activity rhythms by studying an $rh7^{0}$ mutant. To investigate a possible relationship between Rh7 and CRY photoreceptors in the circadian system, I additionally generated $rh7^{0}$ cry^{01} double mutants and analyzed their entrainment to LD cycles and their activity rhythms under free-running conditions.

2 Material and methods

2.1 Material

2.1.1 Fly strains

Table 2: Fly strains used in this thesis. BL: Bloomington Stock Center.

GAL4 driver and UAS responder lines			
Genotype	Source	Reference	Details
y[*] w[*];; P{w[+mC]=actin-GAL4}/TM6B	Stock collection of the laboratory	Ito et al., 1997	Ubiquitous expression of GAL4; homozygous lethal
w[*];; P{w[+mC]=elav-GAL4}/TM3 (Sb)	Stock collection of the laboratory	Robinow and White, 1988	Ubiquitous neuronal expression of GAL4
y[*] w[*]; P{w[+mC]=pdf-GAL4}	Stock collection of the laboratory	Renn et al., 1999	PDF neuron specific expression of GAL4
w[*]; P{w[+mC]=tim-UAS-GAL4}	Stock collection of the laboratory	Blau and Young, 1999	Clock neuron specific expression of GAL4
w[*]; P{w[+mC]=cry- GAL4-39}	Stock collection of the laboratory	Klarsfeld, 2004	CRY-positive neuron specific expression of GAL4
+; P{ry[+t7.2]=rh1-GAL4}; ry[506]	Stock collection of the laboratory	Rister and Heisenberg, 2006	Photoreceptor cell R1-R6 specific expression of GAL4
w[*]; P{GMR-GAL4.w[-]}	Stock collection of the laboratory	Moses and Rubin, 1991; Freeman, 1996	Photoreceptor specific expression of GAL4
w[*]; P{w[+mC]=lGMR-GAL4}; TM2/TM6B	Provided by J. Rister	Wernet et al., 2003	Photoreceptor specific expression of GAL4
w[*]; P{w[+mC]=rh7 (1,7)-GAL4}	Diploma thesis Bleyl, 2008		*Rh7* promoter construct; 1.7 kb promoter fragment
w[*]; P{w[+mC]=rh7 (3,1)-GAL4}	Diploma thesis Bleyl, 2008		*Rh7* promoter construct; 3.1 kb promoter fragment
w[*];; P{w[+mC]=UAS-GFP.S65T}eg[T10]	BL #1522	Dickson, 1996	Reporter; cytoplasmic GFP expression
w[1118]; P{w[+mC]=UAS-myr-mRFP}1	BL #7118	Chang, 2003	Reporter; membrane-targeted monomeric RFP expression
y[*] w[*] P{w[+mC]=UAS-2xEYFP}AX	BL #6661	Halfon et al., 2002	Reporter; expression of YPF

y[*] w[*]; +; P{w[+mC]=UAS-2xEYFP}AH3	BL #6660	Halfon et al., 2002	Reporter; YFP expression
w[*]; P{w[+mC]=UAS-rh7}	Present thesis		
Other transgenic lines			
Genotype	Source	Reference	Details
w[*]; P{w[+mC]=GMR-hid}	Stock collection of the laboratory	Bergmann et al., 1998	Expression of the *hid* apoptosis gene under the control of a *GMR* element
y[*] w[*]; Ki[*] P{Δ2-3}	Stock collection of the laboratory	Lindsley and Zimm, 1992	*y w* strain with *P* element transposase activity
y[1] w[67c35]; P{EPgy2}	BL #21406	Bellen et al., 2004	*P* element strain
w[1118]; P{GT1}Rh7[BG02264]	BL #12787	Bellen et al., 2004	GAL4 gene trap
y[*] w[*]; P{Cary[+] pRh1-Rh7}	PhD thesis Bachleitner, 2008		*Rh1* minimal promoter construct with *Rh7* CDS and *rh1* 3' UTR
y[*] w[*]; P{Cary[+] pRh1-Rh7}; sr[1] ninaE[17]	PhD thesis Bachleitner, 2008		*Rh1-Rh7* construct in sr^1 $ninaE^{17}$ background
y[*]; P{Cary[+] pRh1-Rh7}	Present thesis		*Rh1* minimal promoter construct with *Rh7* CDS and *rh1* 3' UTR in w^+ background
y[*]; P{Cary[+] pRh1-Rh7}; sr[1] ninaE[17]	Present thesis		*Rh1-Rh7* construct in sr^1 $ninaE^{17}$ and w^+ background
Wild-type, balancer and mutant flies			
Genotype	Source	Reference	Details
CS (Canton S)	Stock collection of the laboratory	Lindsley and Grell, 1968	Wild-type strain
ALA1 (Alto Adige)	Stock collection of the laboratory	PhD thesis Bhutani, 2009	Wild-type strain
w[1118]	Stock collection of the laboratory	Lindsley and Grell, 1968	Germline transformation
cry^+	Stock collection of the laboratory	Dolezelova et al., 2007	Control flies for cry^{01} (derived from w^{1118} BL #6326)
Dark-fly	Provided by N. Fuse		Nonsense mutation in *rh7* (→ truncation)

Df RC3	Provided by N. Fuse		Mutation in *rh7* (i.a.)
PBac{WH}CG9760[f00991]	Provided by N. Fuse		Control flies for Df RC3
+;so[1]	Stock collection of the laboratory	Milani, 1941	Orientation marker for paraffin sections
w[*]; *Sp/CyO*; *D3/TM6B (Tb)*	Stock collection of the laboratory	Lindsley and Zimm, 1992	Double balancer II and III chromosome
w[*]; *Sp/CyO*; *MKRS/TM6B (Tb)*	BL #3703	Lindsley and Zimm, 1992	Double balancer II and III chromosome
y[1]; T(2;3)ss[aD]/CyO; TM6B (Tb); sv	BL #2976	Hannah-Allava, 1991	Used as *y* background balancer
y[*] w[*]	PhD thesis Bachleitner, 2008		Backcross; control flies for *Rh1-Rh7*
y[*] w[*]	PhD thesis Bachleitner, 2008		Revertant; control flies for *rh7^0*
y[*]	Present thesis		Backcross; control flies for *Rh1-Rh7* in *w$^+$* background
y[*]	Present thesis		Revertant; control flies for *rh7^0* in *w$^+$* background
y[*] w[*];; rh7^0	PhD thesis Bachleitner, 2008		*Rh7* knockout mutant
y[*];; rh7^0	Present thesis		*Rh7* knockout mutant in *w$^+$* background
y[*] w[*];; sr[1] ninaE[17]	Provided by J. Bentrop	O´Tousa et al., 1985	*Rh1* null mutants; *sr^1* homozygous flies with gray stripe on thorax
w[1118];; w[+mC] cry^{01}	Stock collection of the laboratory	Dolezelova et al., 2007	*Cry* knockout mutant; *cry* coding sequence replaced by mini-*white$^+$*
w[*]; P{w[+mC]=GMR-hid}; MKRS/TM6B	Present thesis; obtained from double balancer crosses to *w[*]; P{w[+mC]=GMR-hid}; w[+mC] cry^{01}* (T. Yoshii)		Expression of the *hid* apoptosis gene under the control of a *GMR* element; balanced for chromosome III

w[*]; P{w[+mC]=hdc[JK910]}; MKRS/TM6B	Provided by T. Yoshii	Burg et al., 1993	Histidine decarboxylase deficiency; balanced for chromosome III
w[*]; P{w[+mC]=hdc[JK910]}; w[+mC] cry[01]	Provided by T. Yoshii		Double mutant for *hdc* and *cry*
w[*]; P{w[+mC]=hdc[JK910]}; rh7[0]w[+mC] cry[01]	Present thesis		Triple mutant for *hdc, rh7* and *cry*; genetically blind
w[*]; P{w[+mC]=GMR-hid}; rh7[0]w[+mC] cry[01]	Present thesis		Genetically blind flies

Flies were reared in glass vials on standard *Drosophila* medium (0.8% agar, 2.2% sugar beet molasses, 8.0% malt extract, 1.8% yeast, 1.0% soy flour, 8.0% corn flour and 0.3% hydroxybenzoic acid) under LD 12:12 cycles at either 18°C, 20°C or 25°C and a relative humidity of 60-65%. Small plastic vials were used for single crosses and crosses were mainly carried out at 25°C.

All further material, such as antibodies, solutions and technical devices, are tabulated in the appendix.

2.2 Germline transformation, genetic procedures and antibody generation

2.2.1 Microinjection

To generate UAS-*rh7* lines by myself, a pUAS-*rh7* construct (see also section 3.3) was injected into early embyros. Therefore, *w[1118]* females were first mated to *y w*; *Ki Δ2-3* males, providing transposase activity, and then transferred to collection cages with freshly yeasted egg laying plates. Embryos were collected in 30 min intervals at 25°C, the first plate was discarded. All following steps took place at 18°C. Embryos were dechorionated manually by rolling on double stick tape, then transferred and lined up in the same orientation on slides with double stick tape. After desiccation for 5-10 min on silica gel, embryos were covered with Voltalef oil. *UAS-rh7* plasmid DNA from a midi-preparation (final concentration 300 ng/µl) was mixed with 10x injection buffer and food dye (2.5%), centrifuged, and the supernatant microinjected into the posterior end of 201 embryos. Slides were kept on egg laying plates and developed larvae were collected and transferred to standard medium.

2.2.2 Establishment of stable transgenic fly lines

To establish independent transformant lines, “injected” adult flies were backcrossed to w^{1118} and the male progeny was selected for w^+ transformants lacking transposase activity (absence of the dominant marker *Ki*). Insertions were mapped and balanced by crossing twice to *w; Sp*/*CyO*; *D3/TM6B* double balancer females. The resulting fly strains are specified in section 3.3.

2.2.3 Crosses for behavior experiments

Some strains had to be crossed into the wild-type red eye background to exclude side effects on behavior due to different pigmentation. Thus, $rh7^0$ and *Rh1-Rh7* transgenic males as well as their corresponding controls were crossed to *y* w^+ balancer females, followed by sib crosses between the balanced heterozygous offspring to transfer them into the w^+ background for locomotor activity recording.

2.2.4 Generation of $rh7^0$ cry^{01} double mutants and genetically blind flies

Cry and *rh7* map to the right and left arm of the third chromosome, respectively. To obtain recombinant flies, mass crosses between *w; +;* w^+ cry^{01} females and *y w; +;* $rh7^0$ males were performed. The female offspring (including potential recombinants) were mated to *w; Sp*/*CyO*; *MKRS/TM6B* males and 330 single crosses were carried out recrossing w^+*/TM6B* progeny to double balancer flies.

To generate genetically blind flies, $rh7^0$ cry^{01} double mutants were balanced for the second chromosome. These males were either mated to hdc^{JK910}*; MKRS/TM6B* or to *GMR-hid/CyO; MKRS/TM6B* females. Homozygous triple mutant flies were obtained by crossing the F1 offspring carrying the respective balanced mutation to each other.

2.2.5 The GAL4 system

The GAL4/UAS binary system, devised by Brand and Perrimon in 1993, is a powerful tool in *Drosophila*, which allows directing gene expression in a temporally and spatially controlled manner in vivo. The system is composed of two components, which are originally present in two different fly lines and then simply brought together by crossing (Fig. 12). One of them contains GAL4, a transcriptional regulator from yeast that activates gene transcription upon binding to an upstream activation sequence (UAS). This so called driver line expresses GAL4 in a tissue-specific fashion. The second so called responder line carries the UAS transgene. In the progeny, specific binding of GAL4 to UAS activates the transcription of the gene of interest (for review and further references, see Duffy 2002). In practice, we used this approach to ectopically express Rh7 in different cells clusters or tissues.

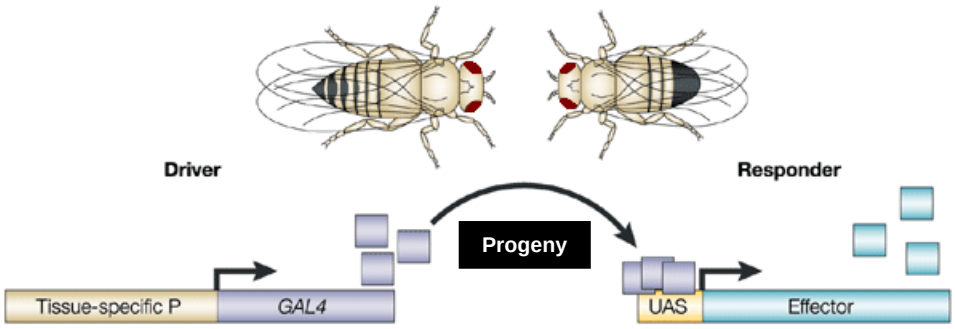

Figure 12: Schematic model of the *Drosophila* GAL4/UAS binary system.
In the progeny, GAL4 drives expression of the UAS-target gene (Effector) under a tissue-specific promoter (P). For details, see text (adapted from Wimmer, 2003).

2.2.6 Generation of antibodies against Rh7

To localize Rh7, generation of antibodies was required. For this reason, an epitope analysis of the Rh7 protein was carried out and a peptide antibody was raised in two guinea pigs and rabbits (conducted by Pineda Antikörper-Service, Berlin). They used a synthetic peptide representing amino acids 54-71 (TESSAVNVGKDHDKHVND) to generate N-terminal domain antibodies (18-mer). Before immunization, blood samples were taken to obtain preimmunoserum which served as negative control for unspecific immunoreactivity. Then, animals were immunized following a standard protocol (see company homepage for details) and the sera were immediately tested on whole mount brains (partly with attached retina and ocelli) of wild-type, *rh7*^{0} and *Rh1-Rh7; ninaE* flies. Serum samples were collected and tested after 61, 120, 150 and 210 days after the initial boost. Finally, antibodies were affinity purified using the original peptide bound to Sepharose 6B columns.

2.3 Molecular methods

2.3.1 Nucleic acids-based methods

2.3.1.1 Isolation of genomic DNA

Genomic DNA was isolated from 50 flies following a modified protocol of S. Celniker (Pflugfelder et al., 1990). After DNA precipitation, the pellet was dried for 5-10 min at room temperature (RT) and dissolved in 50 µl of double distilled H_2O (H_2O_{dd} in the following). To remove RNA from DNA preparation, the sample was incubated with 5 µl RNase A at 37°C and the reaction stopped after 1 h by addition of 20 µl of 3 M sodium acetate. DNA was purified by phenol-chloroform-isopentanol (25:24:1 v/v) extraction. After 5 min of centrifugation at 13,000 rpm, the supernatant was transferred into a new reaction tube and the DNA precipitated with 500 µl of 100% EtOH at -20°C for 2 h. The

sample was centrifuged under previous conditions, the supernatant discarded and the DNA pellet washed by adding 500 µl of 70% EtOH. The centrifugation step was repeated, the pellet air-dried and resolved in 20 µl $H_2O_{dd.}$ Genomic DNA was stored at 4°C for short term or at -20°C for long term storage, respectively.

Alternatively, if high purity was not required, genomic DNA was isolated from a single fly being squashed in 100 µl of 50 mM NaOH with a medium sized pipette tip. The sample was incubated at 95°C for 10 min, briefly spinned down, neutralized with 10 µl of 1 M Tris-HCl and centrifuged again. Later, 3 µl of the supernatant were used as template in PCR screenings for mutant flies.

2.3.1.2 Polymerase Chain Reaction

PCR allows for amplification of target DNA using a specific pair of primers. Standard reactions, which were mainly used for deletion mapping, were set up and carried out as described below.

Table 3: Standard PCR reaction.

Component	Volume
Template DNA	1-2 µl (ca. 100 ng)
10x LSB (low salt buffer)	2.5 µl
40 mM dNTPs (10 mM/base)	1 µl
10 mM 5’ primer	1 µl
10 mM 3’ primer	1 µl
Taq polymerase	1 µl
H_2O_{dd}	ad 25 µl

Table 4: Standard PCR program; x: Primer dependent; y: Product length dependent.

Step	Temperature (°C)	Duration (min:sec)	
Initialization	95°C	05:00	
Denaturation	95°C	01:00	35 cycles
Annealing	x	01:00	
Elongation	72°C	y	
Final elongation	72°C	10:00	
Final hold	8°C	hold	

Alternatively, to identify $rh7^{0}$ cry^{01} recombinant flies, PCR reactions were set up using 2x *Taq* DNA Polymerase Master Mix and carried out following the recommended PCR program:

Table 5: Alternative PCR reaction.

Component	Volume
2x Master Mix	10 µl
Template DNA	1-2 µl (ca. 100 ng)
10 mM 5' primer	1 µl
10 mM 3' primer	1 µl
H_2O_{dd}	ad 20 µl

Table 6: Alternative PCR program; x: Primer dependent; y: Product length dependent.

Step	Temperature (°C)	Duration (min:sec)	
Initialization	95°C	01:00	
Denaturation	95°C	00:30	35 cycles
Annealing	x	00:30	
Elongation	72°C	y	
Final elongation	72°C	05:00	
Final hold	8°C	hold	

The duration of the elongation step was adapted to the amplicon length calculating 1 min/kb. Using the Robocycler Gradient 40, PCR reactions had to be covered with 25 µl of mineral oil to prevent evaporation. If the optimal annealing temperature for a set of primers was unknown or not matching, an annealing temperature gradient in the range of 48°C to 62°C was used for the first trial run.

2.3.1.3 Sequencing and ethanol precipitation

Sequencing was used to determine the breakpoints of the *rh7* deletion, to confirm this deletion in *rh7*^{0} *cry*^{01} recombinants, and to test the UAS-*rh7* construct prior to injection. For sequencing reactions carried out in Regensburg, the Big Dye Terminator v1.1 Cycle Sequencing Kit was used according to the following reaction and program:

Table 7: Standard sequencing reaction.

Component	Volume
Plasmid DNA	10 ng/100 bp
5x Seq buffer	4 µl
Big Dye	1 µl
10 mM 5' or 3' primer	1 µl
H_2O_{dd}	ad 20 µl

Table 8: Sequencing program; x: Primer dependent.

Step	Temperature (°C)	Duration (min:sec)	
Denaturation	96°C	00:10	30 cycles
Annealing	x	00:05	
Elongation	60°C	00:20	
Final hold	4-8°C	hold	

Three biological replicates per genotype were prepared for the tissue of interest.
After the sequencing reaction, tubes were filled up with H_2O_{dd} to 100 µl and ethanol precipitation was carried out by addition of 10 µl of 3 M sodium acetate (pH 4.8) and 250 µl of 100% EtOH. After 15 min of centrifugation at 13,000 rpm, the supernatant was discarded, the sample washed twice with 70% EtOH and solved in 20 µl H_2O_{dd}. Sequencing was conducted by GeneArt (Regensburg) and the data was analyzed using Chromas Lite and DNASTAR software. For sequencing carried out in Würzburg, 100 ng of plasmid DNA from a midipreparation were sent to LGC Genomics, primers were selected and all further steps were carried out by the company. GENtle software was used to analyze the resulting data.

2.3.1.4 Dephosphorylation of vectors

In single restriction enzyme cloning, linearized pUAST vector was dephosphorylated at the 5' end to prevent self-ligation (relegation). Phosphate groups were removed by treatment with CIAP in the following reaction:

Table 9: Dephosphorylation reaction.

Component	Volume
Linearized vector DNA	40 µl
10x CIAP buffer	5 µl
CIAP	1 µl
H_2O_{dd}	ad 50 µl

Reactions were incubated at 37°C for 30 min and then stopped by heating at 85°C for 15 min.

2.3.1.5 Ligation

For cloning, the DNA insert was first ligated into a plasmid vector.
Ligation reactions were set up as follows:

Table 10: Standard ligation reaction.

Component	Volume
Vector	50 ng
Insert	150 ng
T4 DNA Ligase	1 µl
10x ligation buffer	2 µl
H_2O_{dd}	ad 20 µl

Reactions were incubated at 4°C overnight or for 1 h at RT prior to transformation.

2.3.1.6 Transformation

E. coli XL1-Blue competent cells are generated in the institute and aliquots of 100 µl are stored at -80°C for general use. An aliquot of competent cells was thawed on ice for 10 min. Depending on the DNA concentration 1-7 µl of the ligation reaction were added to the cells. They were incubated on ice for 20 min, then heat-shocked for 45 sec at 42°C and immediately placed back on ice for 1-2 min. For recovery, 800 µl of LB_0 medium was added before incubation at 37°C for 30-50 min. 80-100 µl of the culture was plated on pre-warmed LB_{Amp} plates. To identify recombinant colonies by blue/white screening, AXI agar plates were used for transformations with pGEM-T Easy vector. Positive recombinants were used for mini- or midipreparation of plasmid DNA.

2.3.1.7 Minipreparation of plasmid DNA

This method was used to isolate small amounts of plasmid DNA from *E. coli* cultures. A single, well-isolated colony (positive recombinant resulting from transformation) was inoculated into 2 ml of selective medium (LB_{Amp} or LB_{Cam}) for each small scale plasmid isolation and incubated at 37°C for 12-16 h. Plasmid DNA was isolated following the protocol of Sambrook et al. (1989) with minor modifications: 1 µl RNase A was added to the GTE buffer (1 µg/µl) and the pellet was resolved in 50 µl H_2O_{dd}. To obtain a DNA extract of higher purity, the QIAprep Spin Miniprep Kit was used and the plasmid DNA eluted in 30 µl H_2O_{dd}.

2.3.1.8 Midipreparation of plasmid DNA

To obtain higher amounts, plasmid DNA was isolated from a 100 ml overnight LB_{Amp} culture using either the QIAfilter Plasmid Midi Kit, following the instructions of the manual, or the GenElute Plasmid Midi Prep Kit according to the following steps: The overnight culture was split up equally between two 50 ml Falcon tubes and centrifuged

for 5 min at 5,000 rpm in a refrigerated microcentrifuge (Fresco 21, Heraeus) using a fixed angle rotor. The supernatant was roughly discarded and the pellet resolved in the residual medium before 1.2 ml Resuspension solution was added. For cell lysis, an equal amount of Lysis solution was added to the completely resolved solution and the contents were mixed by gentle inversions. After 4 min incubation time, cell debris was precipitated by adding 1.6 ml Neutralization / Binding solution, which was stored at 4°C prior to first use. The lysate was centrifuged at 10,000 g for 20-30 min using a swing bucket rotor from this step on. The column was prepared according to the protocol. The supernatant from the previous step was transferred to the column and centrifuged at 3000 rpm for 5 min. The flow-through was discarded and the collection tube reused. To wash the column, 3 ml of the prediluted Wash solution were added and the centrifugation step was repeated. The column was centrifuged once more to remove residual Wash solution. Finally, the column was transferred to a new collection tube and DNA was eluted under the same centrifugation conditions using 1 ml of H_2O_{dd}.

2.3.1.9 Restriction digestion

This method is used for analysis or to prepare DNA for cloning. Analytical restriction enzyme digestions were set up as follows:

Table 11: Standard restriction digestion.

Component	Volume
DNA	1-2 µl
10x buffer	2 µl
Enzyme(s)	1 µl (each)
H_2O_{dd}	ad 20 µl

Reactions were incubated for 1 h at 37°C.

Enzymes, corresponding buffers and BSA (if required) were added according to the manufacturers´ instructions (NEB). For preparative digestions, up to 10 µl DNA were used. To use vector inserts as a transcriptional template, vectors were linearized by adding only one restriction enzyme to the digestion reaction.

2.3.1.10 DNA Gel electrophoresis and sample purification

Agarose gel electrophoresis was used to separate DNA fragments according to their length, e.g., subsequent to a PCR to check the amplified product. Ethidium bromide or GelRed (0.05 µl/ml) was added to 1% TAE agarose gels, to visualize nucleic acids with UV light. Then, samples were mixed with 6x loading dye containing the progress

markers xylene cyanol and bromophenole blue (or only one of them) or Orange G, alternatively. To determine the size and or the amount of DNA, DNA ladders were mixed with 6x loading dye and additionally loaded to the agarose gel. Electrophoretic separation was carried out at 70-120 V in TAE buffer. Results were imaged using the MultiImage Light Cabinet or E-Box gel documentation system. Images were either printed out directly or saved and further analyzed using the E-capt software. For preparative electrophoresis, DNA fragments of interest were cut out under UV light with a clean scalpel or razor blade. DNA was subsequently purified with the QIAquick Gel Extraction Kit according to the manufacturers´ instructions prior to further usage, e.g., in sequencing or cloning.

2.3.1.11 Isolation of RNA

RNA was isolated to determine mRNA expression levels mainly of *rh7* and *ninaE* in certain tissues. Total RNA was extracted from 100 fly heads using peqGOLD TriFast reagent and following the manufacturers´ protocol. After washing, the RNA pellet was briefly air- dried and dissolved in 50 µl DEPC water.

RNA extraction from small amounts of tissue (a single fly brain or three retinas) was carried out using the *Quick-RNA* MicroPrep Kit. The tissue was rapidly dissected in PBS and roughly squashed in the homogenization buffer using a pipette tip. The initial homogenization volume was reduced to 300 µl, but the following steps of the protocol were not modified.

Concentration of RNA was determined using either the Ultrospec 3000, or NanoDrop 2000c spectrophotometer. Samples were stored at -20°C or at -80°C for long-term storage until cDNA synthesis was performed.

2.3.1.12 First strand cDNA synthesis

The QuantiTect Reverse Transcription Kit with integrated removal of genomic DNA was used for cDNA synthesis. All steps involved in conversion from RNA to cDNA were carried out according to the provided protocol and resulting cDNA was stored at 4°C. Template cDNA resulting from RNA extraction with the *Quick-RNA* MicroPrep Kit was diluted 1:5 in nuclease free water prior to use in qPCR.

2.3.1.13 Quantitative real-time PCR (qPCR)

This method is a powerful tool to quantify tissue specific expression levels of a gene of interest. The qPCR reaction contains a fluorescent dye, SYBR Green, which emits a fluorescent signal upon binding double stranded DNA molecules. This signal is

detected after every single cycle and increases in direct proportion to the amount of amplified DNA.

Two different standard reactions and programs were used for qPCR experiments: On the one hand, the QuantiTect SYBR Green Kit combined with the LightCycler II (in Regensburg) and, on the other, the Maxima SYBR Green/ROX qPCR Master Mix (2x) in combination with Rotor-Gene Q (in Würzburg). Under both conditions, a master mix containing template cDNA, water and 2x qPCR master was prepared. 5' and 3' primer pairs (10 mM) were mixed in advance to reduce potential pipetting errors. PCR reactions and conditions were set up as described below.

Table 12: 7x qPCR master.

7x master (prepared for each template cDNA)	
Component	Volume
cDNA	7 µl
2x QuantiTect SYBR Green PCR Master Mix	70 µl
H_2O_{dd}	49 µl

18 µl of the master was pipetted into each glass capillary. 2 µl of control (*rp49*) and target (*rh7*) primer mixes were added to three capillary tubes each, in order to obtain three replicates for both primer sets. Samples were mixed, briefly centrifuged, closed with capillary plugs and placed into the LightCycler sample carousel.

Table 13: Standard LightCycler II qPCR program.

Step	Temperature (°C)	Duration (min:sec)	
Initialization	95°C	15:00	
Denaturation	95°C	00:15	40 cycles
Annealing	55°C	00:30	
Elongation	72°C	00:20	
Final hold	10°C	hold	

Three biological replicates per genotype were prepared for the tissue of interest and each of them was tested in the Rotor-Gene Q PCR machine together with an internal control (*α-tub*) at least for 6 times. Master mix included template cDNA, 2x Maxima SYBR Green/ROX qPCR Master Mix and H_2O_{dd}, control and target gene primer mix were separately added. The standard qPCR program was set up as follows:

Table 14: Standard Rotor-Gene Q qPCR program.

Step	Temperature (°C)	Duration (min:sec)	
Initialization	95°C	10:00	
Denaturation	95°C	00:15	40 cycles
Annealing	60°C	00:30	
Elongation	72°C	00:30	
Melt	60-95°C (1°C steps)	01:30 (1^{st}); 00:05	

The resulting real-time data was presented relative to another gene referred to as an internal control (*rp49* / *α-tub*). Therefore, one speaks of relative expression levels that do not require any data transformation via a standard curve. For data analysis, a threshold was set up closely at the base of the exponential phase of amplification. The PCR cycle number at which the fluorescent dye signal crosses this threshold is defined as Ct (cycle threshold) and used for further calculations. The Ct is inversely related to the amount of amplicon - this means, the higher the Ct value, the lower the amount. Relative gene expression from LightCycler qPCR data was analyzed using the $2^{-\Delta\Delta Ct}$ method as described, for example, in Livak and Schmittgen (2001).

The data from Rotor-Gene Q qPCRs was analyzed with the corresponding software and processed differently: First, the difference between the Ct values of the internal control and the target gene was calculated. Next, the resulting ΔCt was subtracted from 12 (almost arbitrarily), in order to correlate high values with a high amount of amplicon in the histogram. There was one prerequisite to the value: it was chosen higher than the maximum ΔCt including all replicates of the experiment. The qPCR data of all biological and technical replicates was summarized for each genotype, the average relative expression level plotted. Finally, standard deviation and standard error of the mean (± SEM) were calculated.

SYSTAT was used for all statistical analysis and data was first tested for normal distribution by a one-sample Kolmogorov-Smirnov test (Lilliefors). If the data was normally distributed, a one-way ANOVA was run followed by pairwise comparisons. If not normally distributed, data was compared by a Kruskal-Wallis analysis followed by Wilcoxon post-hoc test with Bonferroni correction. Resulting values were regarded as highly significantly different at $p < 0.01$ and as significantly different at $p < 0.05$.

2.3.2 Protein-based methods

The following methods were used (in the specified order) to determine the expression of Rh7 protein.

2.3.2.1 Protein extraction

For each genotype, 15-30 flies were collected in a 15-ml centrifugation tube, snap frozen in liquid nitrogen and decapitated by vortexing. Tubes were emptied over a piece of meshed fabric placed on dry ice and heads were counted and transferred to pre-chilled Eppendorf tubes with a brush. Heads were then homogenized in 50 µl of ice cold protein cracking buffer using a hand-held homogenisator with plastic pestles. Lysates were centrifuged for 6 min at 13,000 rpm once or twice to remove insoluble cell debris. The clear supernatant was transferred to a new tube and stored at -20°C or immediately used for SDS-PAGE. In order to test insoluble cell debris, the pellet was resuspended in 20 µl of protein cracking buffer.

2.3.2.2 SDS-polyacrylamide gel electrophoresis

If not stated otherwise, extraction was followed by protein denaturation and samples were heated to 95°C for 4 min. The electrophoresis unit was prepared and 30 µl of each sample loaded on a 5% stacking gel and separated on a 12% resolving gel at 120 V and 20 mA for ca. 1.5 h. 10 µl of pre-stained protein marker were loaded in addition to the samples to identify target proteins according to their molecular weight.

2.3.2.3 Western Blot

After separation by SDS-PAGE, proteins were transferred from the resolving gel to a nitrocellulose membrane via a semi-dry electro blotting system. Transfer buffer was used to incubate the resolving gel and to wet six Whatman papers of same size. The membrane was soaked in water before setting up the blot sandwich. Proteins were blotted by semi-dry transfer at constant 400 mA and at 30 V for ca. 50 min.

2.3.2.4 Immunostaining and signal detection

Membranes were placed into small closable boxes with blocking buffer and incubated for 2 h at RT using a horizontal shaker from this step on. Blocking was followed by incubation in the primary antibody solution (in TBST 0.1% with 0.02% NaN_3) at 4°C overnight. After warming up to RT, membranes were washed 3 x 15 min with TBST 0.1% and incubated in fluorescence labeled secondary antibody solution (in TBST 0.1% with 0.02% NaN_3) for 2 h at RT. Both antibody solutions were re-used several times. Washing steps were repeated and the membranes briefly incubated with 1x

TBS, before scanning them with the Odyssey Infrared Imaging System at 700 nm. Resulting images were displayed with the corresponding software, exported as JPEG files and edited using Fiji or PowerPoint.

2.3.2.5 Dot blot analysis

This method was used to test the selective binding of Rh7 antibody to the purified peptide. Therefore, the peptide was first diluted with H_2O_{dd} to obtain a 10 µg/µl stock solution. 1 µl drops of decreasing peptide concentration (5, 2 and 1 µg) were pipetted on a nitrocellulose membrane with a pre-drawn grid. Spots were allowed to dry and the membrane was processed like described in immunostaining and signal detection.

2.3.3 Histological methods

2.3.3.1 Whole mount antibody staining

Adult male flies were collected in 4% PFA and fixed for about 2.5 h at RT with gentle shaking. The fixing solution did not contain Triton X-100 if fluorescent reporter lines were used (e.g., UAS-GFP) to preserve the signal. Samples were washed 3 x 15 min in PB and dissected in PBT 0.5%. Alternatively, cold-immobilized flies were dissected and subsequently fixed using a tissue specific fixation time - 2 h for brains and 0.5 h for retinas at maximum. After the washing steps (3 x 15 min in PB), pre- and post-fixed samples were treated the same: Tissue was blocked (5% NGS in PBT 0.5%) either for 2-3 h at RT or at 4°C overnight. Depending on the antibodies, tissue was incubated in the primary antibody solution (in PBT 0.5% with 5% NGS and 0.02% NaN_3) 1-3 times overnight at 4°C. The antibody solution was re-used several times. After warming up to RT, samples were washed 3-6 x 15 min in PBT 0.5%. Light-protected incubation with fluorescence labeled secondary antibodies (5% NGS in PBT 0.5%) was carried out at 4°C overnight. Washing steps were repeated and followed by a final wash in PBT 0.1%. Retinas of red-eyed flies were further incubated for 3 days at 4°C to reduce autofluorescence caused by eye pigmentation. Tissue was then mounted in Vectashield on a microscope slide, the cover slip sealed with Fixogum and slides stored protected from light at 4°C until visualization using confocal microscopy.

2.3.3.2 Paraffin sections

To prepare paraffin sections of heads, up to 14 flies were placed in a mass histology collar as described by Heisenberg and Böhl (1979). Easily identifiable *sine oculis* flies were asymmetrically threaded to allow for later identification of different genotypes. Samples were subsequently fixed in Carnoy´s solution for 3.5 - 4 h at RT, dehydrated in ethanol (2 x 30 min 99% EtOH, 1 x 60 min 100% EtOH) and incubated in methyl

benzoate overnight. The latter was removed from the tissue by incubation in paraffin-methyl benzoate solution (1:1) for 1 h, followed by 6 x 30 min incubation steps in paraffin at < 60°C. Samples were embedded in paraffin and stored at RT until serial frontal sections of 7 µm thickness were prepared. Sections were cut, carefully transferred to glycerol albumin coated glass slides, stretched with water at 45°C, and, after removing the water, dried at RT over 1-2 nights in a dust-free environment. For both, immunohistochemistry and tissue staining with toluidine blue, sections were deparaffinized in xylene (2 x 30 min, < 60°C) and rehydrated using a series of graded ethanol solutions (from 99% to 70% in 5-6 steps for 3-5 min at RT) and finally H_2O_{dd}.

2.3.3.2.1 Toluidine blue staining on paraffin sections

Paraffin embedded head sections were stained with 0.01% toluidine blue for 10 min, washed 2 x 3 min with H_2O_{dd} and mounted in glycerin gel. The staining was analyzed and representative images were taken using the microscope camera system.

2.3.3.2.2 ABC Immunohistochemistry on paraffin sections

Paraffin embedded head sections were incubated with PBT 0.1% for 5 min at RT, blocked (2% NGS in PBT 0.1%) for 1 h at RT and incubated with primary antibody solution (in PBT 0.1%) at 4°C overnight. Microscope slides were allowed to warm up to RT before being washed 2 x 5 min with PBT 0.1% and incubated with biotinylated secondary antibody (in PBT 0.1%) for 1 h at RT. Washing steps were repeated, sections were incubated in Vectastain AB (1:1) solution (2% in PBT 0.1%; A = avidin; B = biotin, HRP-conjugated) for 1.5 h at RT and washed once with PBT 0.1%. Sections were finally incubated with DAB-H_2O_2-urea staining solution, composed of 1 DAB tablet and 1 H_2O_2-urea tablet dissolved in 5 ml of 0.1% Triton X-100 (in H_2O_{dd}). After desired staining intensity was reached, the staining reaction was stopped with H_2O_{dd} and wet sections were mounted in glycerin gel. The staining was analyzed and representative images were taken using the microscope camera system.

2.3.3.3 Cryosections

Adult male flies were collected and fixed in 4% PFA for 3 h at RT with gentle shaking, then washed 4 x 5 min with PB and incubated in 25% sucrose in PB at 4°C overnight. 12-20 flies were decapitated using forceps and the heads were embedded with O.C.T. Compound medium in a disposable vinyl specimen mold (Cryomold). Heads were pushed to the bottom, orientated for vertical sections and carefully frozen in liquid nitrogen. The cube was pushed out of the mold, fixed to the chuck by freezing with O.C.T. and placed into the cryostat chamber for 20-30 min to equilibrate to chamber

temperature. 12 µm sections were cut, transferred to slides and dried for at least 1 h at RT. Sections were washed 3 x 10 min with PB and incubated with blocking solution (5% NGS in PBT 0.1%) for 45 min at RT.

Alternatively, cryosections of unfixed fly heads were prepared, sections were dried for 1 h, then fixed for 30 min, washed 4 x 5 min with PB and finally blocked as described above.

Sections were incubated with primary antibody solution (in PBT 0.1% with 5% NGS and 0.02% NaN_3) at 4°C overnight. After washing 3 x 10 min with PBT 0.03%, sections were incubated with fluorescence labeled secondary antibody (in PBT 0.1% with 2% NGS) for 2 h at RT. Sections were washed 5 x 10 min with PBT 0.03%, then 2 x 10 min with PB and finally mounted in Vectashield on microscope slides. Cover slips were sealed with nail polish and slides stored protected from light at 4°C until visualization using confocal microscopy.

2.3.3.4 Semithin sections

For semithin plastic sections, adult male fly heads were fixed in a mixture of 4% PFA and 0.5% glutaraldehyde (in PB; pH 4.7) at 4°C overnight, washed 3 x 10 min with PBT 0.1% and post-fixed in 1% osmium tetroxide (in PB) at 4°C for 2 h with gentle shaking. Washing steps were repeated and preparations were dehydrated in increasing ethanol series (30%, 50%, 70%, 80%, 95%, 99.5% and 2x100% for 30 min each). Samples were transferred into propylene oxide, incubated for 2 x 10 min before incubating in epon/propylene oxide (1:1) at RT overnight. Heads were treated with epon for 1 h at RT, transferred to epon-filled embedding moulds, orientated and allowed to polymerize at 37°C overnight and at 60°C for two days. Preparations were detached from moulds and stored at RT before horizontal 2 µm microtome sections were cut.

2.3.3.4.1 Toluidine blue staining on semithin sections

Epon embedded head sections were dried on a hot plate at 60°C and incubated with 1x toluidine blue staining solution for 1-2 min, then washed 2 x 3 min with H_2O_{dd} and mounted in DPX mounting medium. The staining was analyzed and representative images were taken using the microscope camera system.

2.3.3.5 Temporary head whole mounts

Temporary head whole mounts were mainly prepared to study *rh7* expression using different fluorescent reporter lines. Flies were immobilized on ice, decapitated and 6-8

heads were temporarily mounted on single cavity microscope slides using glycerol. Tilted head orientation allowed for confocal analysis of the second antennal segment.

2.3.3.6 Confocal laser scanning microscopy

Immunofluorescent labeled tissues and sections were analyzed using confocal laser scanning microscopy. High-magnification images were obtained using a 63x oil immersion objective and digital zoom function. Laser excitation wavelengths were 488, 532 and 635 nm. Individual channels were scanned separately, one after another, to prevent bleed-through. Fluorescent proteins were detected using special settings, a specific combination of beam splitters and emission filters, provided by the software. Unless stated otherwise, images were captured at 2 µm section intervals using a frame average of 3-4 and a resolution of 1024x1024 pixels. Z-stack images were displayed and modified using the corresponding Leica software and finally exported as 12-bit TIFF files for further editing with Fiji.

2.3.4 Behavioral assays

2.3.4.1 Locomotor activity recording

Locomotor behavior of 2-6-day-old, individual male flies was monitored at 20°C under controlled conditions (provided by an incubator or a climate chamber) using either the TriKinetics *Drosophila* Activity Monitoring (DAM) System (Hermann et al., 2012) or a home-made recording device (workshop of the university), as previously described in Helfrich-Förster (1998) and Rieger et al. (2007). In both systems, infrared light beam crosses of individual flies were consecutively collected in 1-min bins. Light of a given intensity (usually ranging from 0.01 lux to 1000 lux) was provided by white-light LEDs located either at the top (DAM System) or in front of (home-made system) the setup and controlled by the Lichtorgel software (see Figure 13).

In general, flies were recorded up to one month under successively applied conditions. The DAM System was primarily used to record locomotor activity under LD 12 h:12 h cycles (12 h of light alternating with 12 h of darkness) at 1000 lux irradiance and under constant conditions – constant darkness (DD) or constant light of 1000 lux intensity (LL). In the home made system, activity was monitored at different irradiances under LD and LM 12:12 cycles (M: moonlight; low light of 0.01 lux intensity to mimic natural moonlight conditions), under blue light LD 12:12 conditions, and under different day lengths (LD 04:20; 08:16; 16:08; 20:4).

The main difference between the two recording systems is the size of each recording unit and the resulting free moving space. In the DAM System (Fig. 13C and D), single

flies are recorded in glass tubes of 6.5 cm length and 5 mm diameter, whereas the home made system (Fig. 13A and B) is basically composed of plastic photometer cuvettes of comparably large size (4.5 x 1 x 1 cm). In these units (8 cuvettes are glued together), flies are able to move around in the frontal half of each cuvette without interrupting the infrared light beam. In contrast, DAM System recorded flies are hardly able to move without being registered, resulting in generally higher locomotor activity levels.

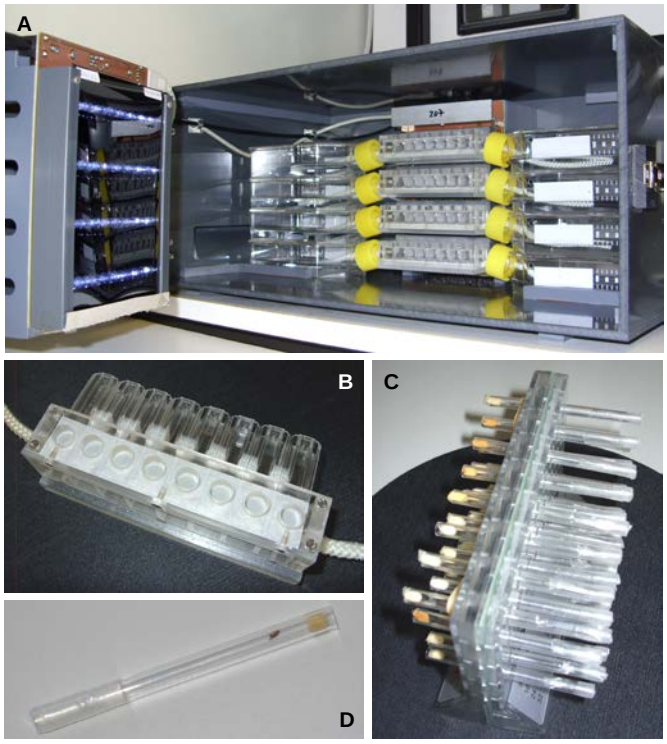

Figure 13: *Drosophila* locomotor activity monitoring systems.

A+B: Home-made recording device. This system was built in the workshops of the University of Regensburg. It comprises 32 cuvettes (4.5 x 1 x 1 cm) per experimental box, 8 of which are glued together to one unit. The infrared light beam crosses the cuvette approximately before its last third. The units are illuminated from the front by white-light or color LEDs located at the inner surface of the cubicle door. Units are ventilated and the flies have access to water (provided by a fiber optics string) and a piece of coarse sugar located in the frontal area of the cuvettes.

C+D: TriKinetics DAM System. For activity recording, 32 male flies are separately transferred into glass tubes of 6.5 cm length and 0.5 cm diameter and inserted into the monitor. The infrared light beam crosses the tube approximately after the first third of the tube. Up to six monitors fit into one experimental box which is illuminated by white-light LEDs from top. TriKinetics medium (2% agar, 4% sucrose) is placed on one end of each glass tube which is then sealed with Parafilm to prevent rapid dehydration; the other end is closed with an air-permeable foam plug.

2.3.4.2 Activity data analysis

2.3.4.2.1 Average daily activity profiles

Raw data of individual light beam interruptions was processed as follows:
Data of the first experimental day was generally excluded and individual activity was visualized in double-plotted actograms (representing 48 h) using ElTemps software. For each illumination condition (cycles of a certain light intensity and day length), the data of a minimum of 5 consecutive days was averaged for individual entrained flies. To generate average daily activity profiles (daily averages in the following) for single genotypes, the average of at least 20 flies (as far as possible) was calculated and then smoothed by applying a moving average of 11.
Due to variations in the activity level across the data collection, smoothed data was normalized by setting the average activity maximum to one in order to determine the relative average daily activity. This normalized data was used to compare the activity pattern between different genotypes and to analyze the composition of daily average activity (e.g., percentage of average activity recorded during the experimental night).
Activity calculated from successive light regimes (e.g., LD 12:12 followed by LD 16:08 or DD) did usually not include data of the first two days after the change of settings. DD data was collected to determine the period length (τ) of rhythmic flies using chi square periodogram analysis (Sokolove and Bushell, 1978). Resulting values were averaged for single genotypes and standard deviation and standard error of the mean (± SEM) were calculated.
Statistical analysis was carried out as described for qPCR data (section 2.3.1.13).

2.3.4.2.2 Analysis of activity levels

To calculate the levels of average morning activity (MA) or evening activity (EA) during a certain interval (e.g., a 4-h interval following lights-on), raw data was normalized for each single fly by setting the daily maximum of activity to one. Then, the sum of activity within the interval of interest was calculated (number of infrared beam crosses during this period) and averaged prior to subsequent statistical analysis.

2.3.4.2.3 Determination of morning activity offset and evening activity onset

For each single fly, the morning activity (MA) offset and the evening activity (EA) onset was determined from single-fly raw data (averaged for one experimental condition – e.g., 6 days of LD 12:12) under consultation of the activity profile. The MA offset or EA onset, respectively, was then averaged for the single genotypes, the resulting minute

values were statistically analyzed and finally transferred to ZT values, setting lights-on to ZT0 (independent from day length).

2.3.4.2.4 Determination of the evening activity peak

Daily averages of individual flies were smoothed over 30 data points and the relative maxima were automatically calculated and visualized within the smoothed single-fly activity profiles (excel template provided by M. Schlichting). The EA peak was visually determined from these profiles for each fly, averaged for the single genotypes and ZT values calculated in reference to lights-on (ZT0).

2.3.4.3 Blue light shift experiments

Sift experiments were carried out in the home made recording device. Blue LED light sources of a certain wavelength range and comparatively low irradiance were applied as follows: 395-400 nm at ~0.0006 µW/cm^2 and 465-470 nm at ~0.0004 µW/cm^2. Low light intensities were achieved by adding neutral density filters. Under both conditions, flies were monitored under blue LD 12:12 cycles for 7 days before a phase shift of the light regime, either a 6 h advance or delay, was applied. The Phase shifting behavior was then observed for the following 10 days until release into DD.

Single-fly actograms were used to determine the number of days that were required for resynchronization to the phase shifted LD cycle. Seven experienced members of the laboratory analyzed the shifting behavior in a blind evaluation. Average values, standard deviation, and standard error (± SEM) were calculated for each condition (light source; direction of the phase shift). Statistical analysis was carried out as described for qPCR data (2.2.1.13).

2.3.4.4 Optomotor response (OR)

Individual male flies were tested for movement-induced optomotor walking behavior. The experimental setup (Fig. 14) comprises: (1) an upright cylinder (ø 8 cm; H 4.5 cm) with vertical black and white stripes on its inner wall providing visual stimulation and (2) a centrally located transparent plexiglass arena (ø 3 cm; H 1.5 cm) with a small attached tube to insert the test fly. The cylinder could be illuminated (LED light source) and rotated either clockwise (CW) or counterclockwise (CCW) with a turning speed of 10 turns/min. OR behavior was visually observed at the same time every day and flies were starved ~3.5 h prior to testing to increase general activity. Single flies were dark adapted for 10 min within the arena, observed for 5 min under CW pattern rotation, then, separated by a 30-sec interval of dark adaptation, tested for another 5 min under CCW rotation. The number of times the fly walked a full circle in the moving direction

of the striped pattern was counted for both rotation directions to determine the behavioral response, R, which is defined as the sum of the values counted for CW and CCW rotation divided by 2 x 50. As a consequence, a fly moving with the turning speed of the cylinder would achieve an R-value of one.

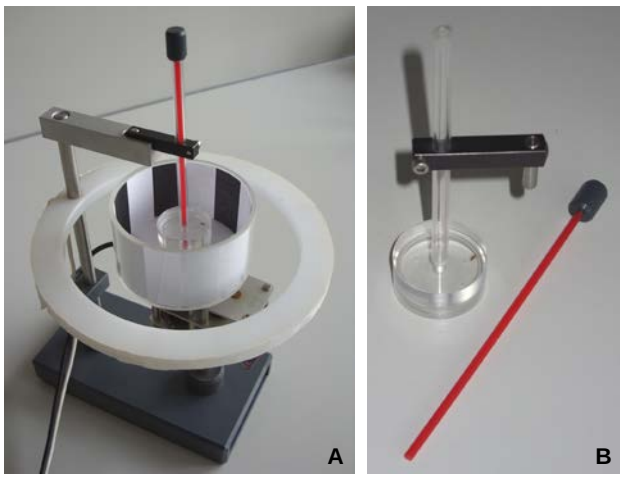

Figure 14: Experimental setup for OR tests.

The experimental device comprises a vertically black and white striped cylinder which is illuminated by a surrounding circle of white-light LEDs (A). The fly containing plexiglass arena (B) is arranged in the center of the cylinder.

For details, see text.

3 Results

3.1 Phase-shifting behavior in *cry^{01}* mutant flies

Phase response curves (PRCs) are widely used to investigate the general properties of circadian oscillators and their sensitivity towards light (see section 1.8). To study the role of CRY in phase-shifting of circadian locomotor activity rhythms, we recorded a PRC for *cry^{01}* mutants and control flies to 1-h light pulses of 1000 lux intensity and conducted re-entrainment experiments.

We showed that CRY-deficient flies are indeed able to phase shift their activity rhythm to a photic stimulus. Like wild-type flies, *cry^{01}* mutants responded with phase delays to light pulses during the early subjective night, and with phase advances to light pulses during the late subjective night, although to a much lesser extent. This phase shifting can explain the slow, but otherwise normal re-entrainment behavior in *cry^{01}* mutants observed to 8-h phase delays of the LD 12:12 cycle.

In summary, our results suggested that, in spite of the dominant role of CRY in photic entrainment, the visual system contributes to the light sensitivity of the circadian clock, mainly around dawn and dusk. General information, further experiments and results concerning this side project are presented and discussed in the following publication entitled “Phase-Shifting the Fruit Fly Clock without Cryptochrome”.

Phase-Shifting the Fruit Fly Clock without Cryptochrome

Christa Kistenpfennig,[*,†] Jay Hirsh,[‡] Taishi Yoshii,[*,†,§,1] and Charlotte Helfrich-Förster[*,†,1]

[*]*Institute of Zoology, University of Regensburg, Regensburg, Germany,*
[†]*Neurobiology and Genetics, Theodor-Boveri Institute, Biocenter, University of Würzburg, Am Hubland, Würzburg, Germany,*
[‡]*Department of Biology, University of Virginia, Charlottesville, VA, USA, and*
[§]*Graduate School of Natural Science and Technology, Okayama University, Okayama, Japan*

Abstract The blue light photopigment cryptochrome (CRY) is thought to be the main circadian photoreceptor of *Drosophila melanogaster*. Nevertheless, entrainment to light-dark cycles is possible without functional CRY. Here, we monitored phase response curves of cry^{01} mutants and control flies to 1-hour 1000-lux light pulses. We found that cry^{01} mutants phase-shift their activity rhythm in the subjective early morning and late evening, although with reduced magnitude. This phase-shifting capability is sufficient for the slowed entrainment of the mutants, indicating that the eyes contribute to the clock's light sensitivity around dawn and dusk. With longer light pulses (3 hours and 6 hours), wild-type flies show greatly enhanced magnitude of phase shift, but CRY-less flies seem impaired in the ability to integrate duration of the light pulse in a wild-type manner: Only 6-hour light pulses at circadian time 21 significantly increased the magnitude of phase advances in cry^{01} mutants. At circadian time 15, the mutants exhibited phase advances instead of the expected delays. These complex results are discussed.

Key words cryptochrome, light pulses, locomotor activity, *Drosophila melanogaster*

The clock of the fruit fly *Drosophila melanogaster* is extremely light sensitive to entrainment, using 12: 12-hour light-dark (LD) cycles of very dim light (Stanewsky et al., 1998; Ohata et al., 1998; Helfrich-Förster et al., 2001; Bachleitner et al., 2007; Hirsh et al., 2010). Adult flies re-entrain to 8-hour shifts of bright LD cycles within 1 or 2 days (Emery et al., 2000b). In contrast, mammals need a minimum of 1 week to re-entrain to such phase shifts (Aschoff et al., 1975). The fly possesses many photoreceptors, but the blue light photopigment cryptochrome (CRY) is regarded as the main photoreceptor responsible for the high light sensitivity of the fly's clock (Emery et al., 1998, 2000a, 2000b). CRY is expressed in the majority of clock neurons, where it interacts with the clock protein Timeless (TIM), provoking its light-dependent degradation (Benito et al., 2008; Yoshii et al., 2008). Without functional CRY, TIM is not degraded upon exposure to constant light (LL). As a consequence, cry^{b} mutants that carry a point mutation in the flavin binding region of cryptochrome as well as *cry*-null (cry^{0} and cry^{out}) mutants remain rhythmic under LL even at intensities above 1000 lux (Emery et al., 2000a; Yoshii et al., 2004; Rieger et al.,

1. To whom all correspondence should be addressed: Charlotte Helfrich-Förster and Taishi Yoshii, Lehrstuhl für Genetik und Neurobiologie, Universität Würzburg, Biozentrum, Am Hubland, 97074 Würzburg, Germany; e-mail: charlotte.foerster@biozentrum.uni-wuerzburg.de and taishi.yoshii@biozentrum.uni-wuerzburg.de.

JOURNAL OF BIOLOGICAL RHYTHMS, Vol. 27 No. 2, April 2012 117-125
DOI: 10.1177/0748730411434390

2006; Dolezelova et al., 2007), whereas wild-type flies and mutants without functional eyes become arrhythmic at intensities beyond 10 lux (Konopka et al., 1989; Helfrich-Förster et al., 2001). Furthermore, cry^b mutants are not able to shift their activity rhythms in response to short (10-minute) light pulses (Stanewsky et al., 1998).

Despite the importance of CRY for circadian photoreception, *cry* mutants can entrain well to LD cycles (Stanewsky et al., 1998), although they require longer time to re-entrain to 8-hour shifted LD cycles (Emery et al., 2000b). Similar slow responses to 8-hour phase shifts are rather common for mammalian species that have no photoreceptive pigment in their clock neurons. In mammals, light is exclusively perceived by the eyes and is mediated to the clock in the suprachiasmatic nuclei (SCN) via glutamate and PACAP through regular synapses onto retinorecipient clock neurons in the ventrolateral SCN core (Morin and Allen, 2006). The clock neurons of *D. melanogaster* also receive light input from photoreceptor cells of the compound eyes, the Hofbauer-Buchner eyelets (H-B eyelets), and perhaps other unidentified interneurons (Helfrich-Förster et al., 2001; Rieger et al., 2003; Veleri et al., 2003; Veleri et al., 2007), although direct synaptic connections have only been shown between photoreceptor cells and clock neurons of larvae so far (Wegener et al., 2004). This eye-mediated light input is probably sufficient for a normal entrainment of the activity rhythm that largely resembles that of mammals. If true, CRY-deficient fruit flies should show a low-amplitude phase response curve (PRC).

To determine if this is true, we characterized the phase-shifting capabilities of CRY-less flies (cry^{01} mutants) by monitoring a PRC to light pulses of 1-hour duration. We found that cry^{01} mutants are able to phase-shift their clock, although the magnitude of phase shifts was reduced to approximately 25% of control flies. Thus, our results can explain the re-entrainment characteristics of CRY-deficient flies.

MATERIALS AND METHODS

Fly Strains

To exclude any residual function of CRY, we used mutants that lack CRY completely (cry^{01}) (Dolezelova et al., 2007) instead of cry^b mutants that show just one amino acid change in the CRY flavin binding domain that is crucial for light reception (Stanewsky et al., 1998). cry^{01} flies are knockout mutants generated from w^{1118} flies by homologous recombination, in which the entire coding sequence of the cry^+ allele was replaced by *mini-white*$^+$ (Dolezelova et al., 2007). In addition, cry^{01} was outcrossed to the w^{1118} Bloomington strain no. 6326 (Dolezelova et al., 2007). This w^{1118} strain was used as a control strain in the present experiments, so that mutant ($w^{1118};;cry^{01}$) and control flies (w^{1118}) had exactly the same genetic background except for the *cry* and the *mini-white*$^+$ gene. Both strains carried the *timeless* allele *s-tim* and the wild-type *jetlag* gene (jet^+) (Dolezelova et al., 2007) and should therefore have a molecular clock of similar light sensitivity (Peschel et al., 2006). For simplicity, we will use "cry^{01}" for "$w^{1118};;cry^{01}$" and "control" for the "w^{1118}" strain throughout the article.

The flies were reared under LD 12:12 cycles on *Drosophila* medium (0.8% agar, 2.2% sugar-beet syrup, 8.0% malt extract, 1.8% yeast, 1.0% soy flour, 8.0% corn flour, and 0.3% hydroxybenzoic acid) at either 20 °C or 25 °C. Only male flies at an age of 3 to 6 days were taken for the experiments.

Recording the Locomotor Activity of Flies

Locomotor activity of individual male flies was recorded photoelectrically as described previously (Helfrich-Förster, 1998; Rieger et al., 2007). Briefly, the flies were confined to photometer cuvettes that were placed with one end in an infrared light beam. On the opposite end, they had access to water and sugar. Activity was monitored during consecutive 1-minute intervals. Light was provided by white LEDs (Lumitronix LED-Technik GmbH, Jungingen, Germany). The recording units were placed in a temperature-controlled room or an incubator (I-36NL, Percival Scientific Inc., Perry, IA). The temperature was kept constant at 20 °C throughout all experiments.

For determining the shifting behavior of the flies, these were monitored under LD cycles (12:12) for 7 days either at 100, 1000, or 10,000 lux (19 µW/cm^2, 150 µW/cm^2, or 1300 µW/cm^2, respectively), and then, the LD cycle was phase-delayed by 8 hours. Intensity was controlled with neutral density filters and by changing the voltage/current.

For monitoring PRCs, the flies were entrained to LD cycles (12:12) for 5 days (100 lux or 19 µW/cm2) and then transferred to DD and recorded for at least a further 10 days under DD. One group consisting of 59 control and 27 cry^{01} flies was recorded without any disturbance to assess mean period and initial phase of the free-running rhythms (Fig. 1 and below). The other flies received a light pulse of 1-hour duration and a light intensity of 1000 lux (150 µW/cm2) during the first day of DD at different circadian times

Table 1. Phase responses of control and *cry*^{01} flies to a 60-minute light pulse at different times of day.

CT	01	03	05	07	09	11	13	15	17	19	21	23
Control												
Phase shift, h	1.35 ±0.44	0.57 ±0.25	0.52 ±0.18	–0.11 ±0.22	0.15 ±0.13	0.18 ±0.25	–0.45 ±0.33	–4.05 ±0.18[a]	–3.48 ±0.45[a]	1.17 ±0.30[a]	2.75 ±0.20[a]	1.34 ±0.18[a]
cry^{01}												
Phase shift, h	0.31 ±0.19	0.31 ±0.25	0.38 ±0.26	–0.14 ±0.21	0.03 ±0.14	–0.57 ±0.19	–0.92 ±0.28	–0.97 ±0.21[a]	–0.11 ±0.15	–0.27 ±0.17	1.05 ±0.27[a]	1.05 ±0.21[a]

Values are shown as mean ± SEM.
a. The phase shift was statistically significant compared with nonpulsed flies.

Table 2. Phase responses of control and *cry*^{01} flies to light pulses with various durations at CT15 and CT21.

Duration	15 min		60 min		180 min		360 min	
CT	15	21	15	21	15	21	15	21
Control								
Phase shift, h	–3.91 ±0.22[a]	1.91 ±0.28[a]	–4.05 ±0.18[a]	2.75 ±0.20[a]	–5.27 ±0.23[a]	2.98 ±0.28[a]	–10.73 ±0.36[a]	5.73 ±0.32[a]
cry^{01}								
Phase shift, h	–1.06 ±0.28[a]	0.40 ±0.26	–0.97 ±0.21[a]	1.05 ±0.27[a]	–1.37 ±0.26[a]	0.46 ±0.19	0.86 ±0.19[a]	1.69 ±0.22[a]

Values are shown as mean ± SEM.
a. The phase shift was statistically significant compared with nonpulsed flies.

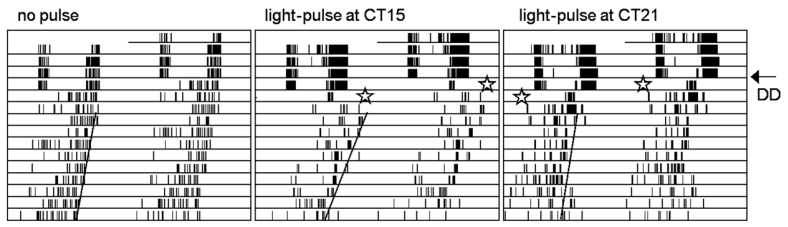

Figure 1. Method of administering light pulses and determining consecutive phase shifts in an anchored phase response curve. The light pulses (indicated by stars) were given either at CT15 or CT21 during the first day after the flies were released from 12:12 LD cycles. A line was drawn through the offset of the free-running activity and extrapolated back to determine the phase shift in comparison to unpulsed controls (detailed description in "Materials and Methods").

(CT1 to CT23 with 2-hour intervals). The given CT indicated the beginning of the 1-hour light pulse. CT0 was defined as the subjective beginning of the day and CT12 as the subjective beginning of the night. Thus, CT0 to CT24 is the duration of one endogenous cycle (period, τ). The actual CT of the light pulse was calculated by multiplying the real hour by 24 h/τ for each individual fly (Johnson, 1992). Similarly, the phase shifts were indicated as circadian hours (actual hours were multiplied by 24 h/τ). PRCs were calculated for control flies and *cry*^{01} mutants as indicated under "Data Analysis".

To determine the dose response characteristics of phase shifts in respect to light pulse duration, we administered light pulses of the same intensity (1000 lux) for 15, 60, 180, and 360 minutes at either CT15 or CT21 and, in a second experiment, 60-minute light pulses of 10,000 lux.

Data Analysis

The raw data of individual flies were displayed as actograms using the program El Temps (v. 1.228, Antoni Diez-Noguera; http://www.el-temps.com/). The time needed for resynchronization to an 8-hour shift of the LD cycle was determined in each single fly by one experienced person who was blind to the genotype and the irradiance. Average values were calculated for the 2 genotypes at the 3 irradiances, and averaged actograms were plotted to visualize the phase-shifting behavior.

For monitoring the responses to the light pulses, the phase of the rhythms was determined by the offset of the evening activity because this was more stable than the onset and the peak of activity under free-running conditions. First, we determined the activity offset of flies that had not received any light pulse on the first day in DD (59 control and 27 *cry*^{01} mutant flies) and calculated average phases for both genotypes. Those values were used as reference phases for the light-pulsed flies. To obtain the phase shift values for individual light-pulsed flies, their actual activity offset was determined on the actogram

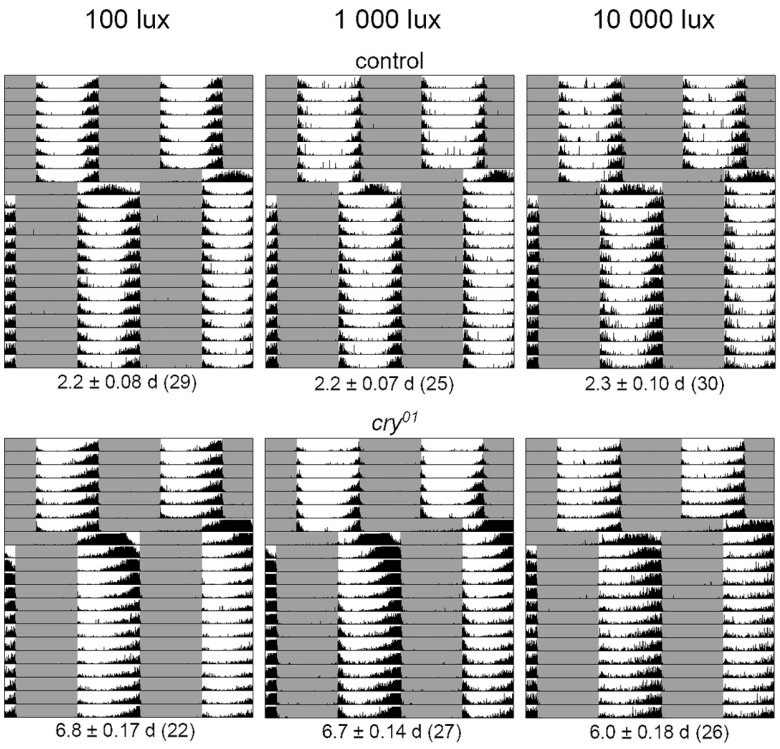

Figure 2. Average actograms of control and *cry*^{01} flies that were subjected to a phase delay of a 12:12 LD cycle by 8 hours (at 3 different light intensities). Below the average actograms, the number of days is given (± SEM) that the flies needed to re-entrain as well as the number of tested flies (in parentheses). Controls shifted their activity quickly and were completely adapted to the new light schedule on the second day after the shift regardless of the light intensity during the day (Kruskal-Wallis 1-way analysis showed that re-entrainment did not depend on irradiance: $F_{2,92} = 4.16$, $p = 0.125$). *cry*^{01} mutants needed 6 to 7 days until they reached their original phase relation to the LD cycle, meaning that they shifted 1.3 hours per day at maximum. The phase-shifting capabilities between control flies and *cry*^{01} mutants were significantly different (Kruskal-Wallis 1-way analysis at all irradiances: $p = < 0.00001$). Furthermore, in *cry*^{01} mutants, the speed of re-entrainment was faster at 10,000 lux than at 100 and 1000 lux (Kruskal-Wallis 1-way analysis revealed the re-entrainment depended on irradiance: $F_{2,73} = 12.85$, $p = 0.002$; the Wilcoxon post hoc test showed that re-entrainment was significantly faster at 10,000 lux as compared to the 2 lower irradiances: $p = 0.014$).

by drawing a line through all activity offsets and extrapolating it back to the day the phase shift occurred (Fig. 1). The determined activity offset was then subtracted by the calculated reference phase, and the conversion into circadian hours was done (see above). The calculated phase shifts of all individual flies were plotted against the CT of the light pulse in a scatter plot. Because the periods of control and *cry*^{01} flies were not significantly different and close to 24 hours ($^{t}cry^{01}$ = 23.79 ± 0.05 h; $^{t}control$ = 23.86 ± 0.06 h), we plotted the PRC also on the basis of real time (without calculating the individual CTs). This method allowed the calculation of average phase shifts and standard errors of the mean (SEM) for each time point and enabled a statistical comparison of the phase shift magnitude within and between the strains.

Statistics

The phase-shifting capabilities of controls and mutants to the 8-hour shift of the LD cycle were analyzed by the Kruskal-Wallis 1-way analysis followed by a Wilcoxon post hoc test (Systat 11, SPSS, Chicago, IL). Phase shifts after the light pulses were tested for a significant influence of time and genotype or duration of illumination and genotype using a 2-way ANOVA (Systat 11, SPSS). Few data sets were not normally distributed, as revealed by the Kolmogorov-Smirnov 1-sample test (Fig. 3). In these sets, p was adjusted according to Glaser (1978) by multiplication by 2. Values were regarded as significantly different at $p < 0.05$.

RESULTS

Re-entrainment experiments to 8-hour LD cycle delays showed that control flies re-entrain within approximately 2 days and this speed cannot be enhanced further by higher irradiances (Fig. 2). In contrast, *cry*^{01} mutants needed 6 to 7 days to re-entrain, and the time to re-entrainment was reduced by 0.8 days when irradiance was increased from 100 to 10,000 lux (Fig. 2). The phase-shifting behavior of *cry*^{01} mutants was very similar to that reported previously (Emery et al., 2000b); but in contrast to previous reports, we did not see any lights-on anticipation of morning activity. The latter can be explained by our recording system that misses small actions of the flies, such as movements between water and sugar, because the infrared light beam is on the opposite end of the cuvette (see Fig. 1 in Helfrich-Förster [1998]). If we monitor the activity of the flies with commercial *Drosophila* Activity Monitors (DAM, Trikinetics Inc., Waltham, MA), we see this morning anticipation (Yoshii and Helfrich-Förster, unpublished observations).

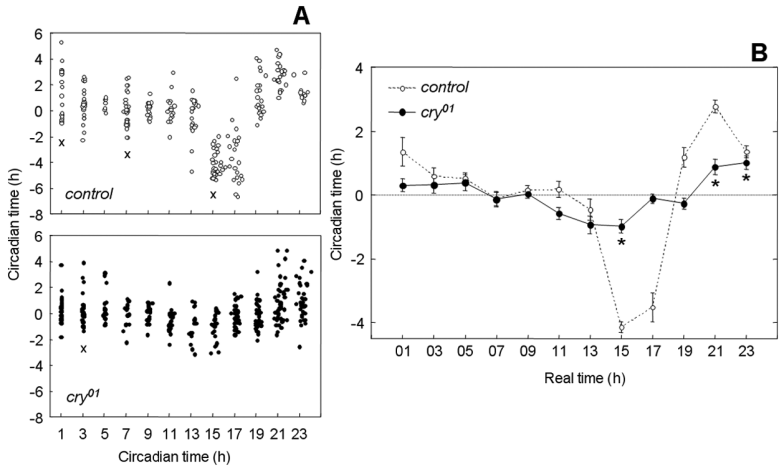

Figure 3. Phase response curves for control flies and *cry*^{01} mutants plotted in circadian time (CT) (A) and in real time (B). Flies were pulsed for 1 hour with white light (1000 lux) during the first subjective day of DD at the times indicated on the abscissa. Phase changes were calculated by comparing behavioral offsets of light-pulsed flies to the behavior of flies that did not receive a pulse. Phase delays and advances are plotted in circadian hours as negative and positive values, respectively. (A) The phase shifts of all light-pulsed individuals are shown as dots in CT. Crosses indicate the data sets that were not normally distributed. (B) Mean phase shifts (± SEM) are calculated out of the individual phase shifts of all flies pulsed at the same real time (shown as dots in A). Asterisks indicate the phase advances/delays in *cry*^{01} mutants that were significantly different from unpulsed flies. ANOVA revealed that the phase shifts were highly dependent on time in both strains (control: $F_{11,238} = 54.74$, $p < 0.001$; *cry*^{01} mutants: $F_{11,320} = 8.91$, $p < 0.001$) and that they depended additionally significantly on the strain ($F_{11,558} = 24.02$, $p < 0.001$).

Experiments giving entrained flies a 1-hour light pulse during the first day in DD revealed that *cry*^{01} mutants and control flies phase-shifted their activity, showing delays in the early night and advances in the late night and a dead zone in the middle of the subjective day. This pattern is evident in the scatter plot (Fig. 3A) and in the averaged PRC (Fig. 3B). ANOVA revealed that the phase shifts were highly dependent on time in both strains and that they depended additionally significantly on the strain. Control flies showed phase delays of up to approximately 4 hours and phase advances of approximately 2.5 hours, whereas *cry*^{01} mutants showed reduced phase changes of approximately 1 hour for both advances and delays (Fig. 3B). In both strains, maximal phase delays occurred at approximately CT15 and maximal phase advances at approximately CT21, but the shape of the PRC was different at its transition region: the control flies showed the expected rapid transition between delays and advances, but *cry*^{01} revealed a second small "dead zone" between the switch. As a consequence, the phase advance started later in *cry*^{01} mutants at CT21 than in the control flies at CT19.

Next, we tested the dependence of phase shift magnitude on length of the light pulse, varying pulse lengths between 15 and 360 minutes. The light pulses were administered at the most sensitive parts of the clock in the delay (CT15) and advance (CT21) zones. After light pulses of 15 minutes, both strains showed significant phase delays, and control flies showed additionally significant phase advances (Fig. 4A). After longer light pulses, significant delays and advances were present in both strains, but *cry*^{01} mutants clearly behaved differently from control flies: Whereas delays and advances of controls increased significantly with increasing light pulse duration, this was not the case in *cry*^{01} mutants until a pulse duration of 180 minutes (3 hours). But when light pulse duration was increased to 6 hours, a significant change occurred: the light pulses at both time points provoked phase advances, and at CT21, these were slightly but significantly larger than the ones provoked by the shorter light pulses (Fig. 4A).

Next, we tested whether 1-hour light pulses of higher intensity could provoke larger phase shifts by light-pulsing control and *cry*^{01} mutants with 10,000 lux at CT15 or CT21. After this high intensity pulse, the majority of flies became inactive, especially after the CT21 pulse. At CT21, the small fraction of active flies phase-advanced their activity as expected, and there was a tendency to increase magnitude as compared to 1000-lux light pulses in *cry*^{01} mutants but not in control flies (Fig. 4B). Indeed, at 10,000 lux and CT21, the phase advances of *cry*^{01} mutants were not significantly different from the ones of control flies (ANOVA: $F_{1,7} = 0.17$, $p = 0.70$). At CT15, *cry*^{01} mutants did not phase-shift at all, whereas control flies showed no further increase in phase delays as compared to 1000 lux (Fig. 4B).

Our results demonstrate that the phase-shifting capability of wild-type but not of *cry*^{01} mutants can increase to extremely large values when time of the pulse is extended to 6 hours, indicating that a CRY-dependent mechanism must exist to allow large magnitude phase shifts from these long light pulses.

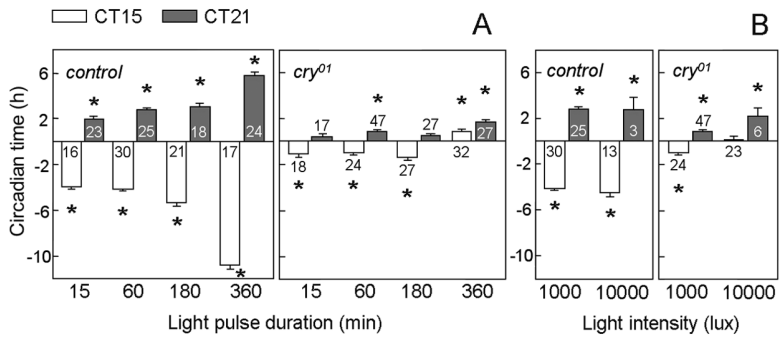

Figure 4. Phase shift responses to light pulses (1000 lux) of different duration (A) or intensity (B) applied either at CT15 or CT21 (± SEM). (A) In control flies, the magnitude of advances and delays was clearly dependent on the duration of the light pulse (ANOVA for advances: $F_{3,86} = 37.31$, $p < 0.001$; ANOVA for delays: $F_{3,80} = 159.92$, $p < 0.001$). In *cry*^{01} mutants, the magnitude of advances and delays did not increase with increasing duration of the light pulses until 180 minutes (3 hours) (ANOVA for advances: $F_{2,81} = 1.09$, $p = 0.34$; ANOVA for delays: $F_{2,66} = 0.76$, $p = 0.47$). However, after 360-minute (6-hour) light pulses, a slight but significant increase of phase advances occurred at CT21 ($p = 0.01$), and the light pulses at CT15 resulted in phase advances instead of phase delays. (B) We light-pulsed 36 controls and 48 *cry*^{01} mutants with 10,000 lux at CT15 and 37 controls and 34 *cry*^{01} mutants at CT21. Surprisingly, the majority of flies became inactive after the light pulse, especially after the one administered at CT21. At CT21, the remaining 3 controls and 6 mutant flies phase-advanced their activity as expected. In control flies, the increase of light intensity to 10,000 lux did not change the magnitude of phase advances or delays (ANOVA for advances: $F_{1,26} = 0.03$, $p = 0.86$; ANOVA for delays: $F_{1,41} = 2.21$, $p = 0.14$). In *cry*^{01} mutants, the magnitude of phase delays was significantly affected by light intensity for CT15 pulses (ANOVA for advances: $F_{1,51} = 2.28$, $p = 0.14$; ANOVA for delays: $F_{1,45} = 9.48$, $p = 0.003$). The number of tested flies is indicated in, above, or below the columns, respectively, and phase shifts that were significantly different from unpulsed controls are marked by a star.

The magnitude of a phase shift with a 1-hour pulse is saturated for intensity in control flies but not in *cry*^{01} mutants, suggesting that the mutants have a low circadian light sensitivity.

DISCUSSION

PRCs are powerful tools to characterize the general properties as well as the light sensitivity of circadian clocks. There are 2 main ways to record a PRC. 1) The light pulse is applied while the oscillator is stably free-running in DD (Dushay et al., 1990; Saunders et al., 1994), or 2) the light pulse is applied in a free-run shortly after release from entraining conditions (also called anchored PRC) (Levine et al., 1994; Emery et al., 1998; Rutila et al., 1998; Stanewsky et al., 1998; Suri et al., 1998). We used the anchored PRC because this is the easiest method to light-pulse many flies at the same time and because the PRC shape soon after release from entrainment should be more reflective of its shape during entrainment than after a long exposure to free-running conditions (Mrosovsky, 1996; Johnson, 1999).

Our anchored PRC results for control flies are almost identical to the results of Dushay et al. (1990), although the latter authors used light pulses of 2000 lux and 10-minute duration and applied the light pulses on the fourth day of free-run. This indicates that the 2 methods to monitor a PRC yield very similar results in *D. melanogaster*. The magnitudes of phase shifts were also very similar to the other PRCs recorded for wild-type flies (Saunders et al., 1994; Emery et al., 1998; Rutila et al., 1998; Stanewsky et al., 1998; Suri et al., 1998): approximately 4 hours for phase delays and 1 to 3 hours for phase advances. This indicates that magnitudes depend little on the used light intensity ranging from 300 to 2000 lux and pulse duration from 10 minutes to 1 hour. The most likely explanation for this similarity is that the response to brief light pulses (up to 1 hour) was already saturated. This idea gets support from the present study, in which we could not increase phase shift magnitude of control flies at CT15 and CT21 by increasing irradiance to 10,000 lux. The saturation hypothesis is further supported by a seminal study of Nelson and Takahashi (1991), who tested the phase-shifting effects of brief light pulses ranging from 3 seconds to 1 hour in hamsters and found that 5-minute pulses evoked nearly the same response as 1-hour stimuli. They concluded that saturation had occurred after a light pulse duration of 5 minutes. Furthermore, the lowest number of photons was needed to reach saturation at this light pulse duration. In flies, the number of photons emitted during 1 hour at 10,000 lux seems to be far beyond saturation. The strong light had an unexpected additional effect on the activity of the flies because the majority of flies stopped running permanently, especially when the light pulse was administered at CT21. This is consistent with the activity-inhibiting effect of high intensity light we observed previously (Rieger et al., 2007).

cry^{01} mutants also responded with significant phase shifts to 1-hour light pulses, although the magnitude of advances and delays was only about one quarter of the control flies. Shorter light pulses (15 minutes) only provoked significant phase delays, but not phase advances, indicating that *cry*^{01} mutants are already at the limit of their sensitivity. This is in accordance with a previous study that did not detect significant phase shifts in *cry*^{b} mutants to 10-minute light pulses of 1400 lux (Stanewsky et al., 1998). Without any doubt, *cry* mutants are much less light sensitive than wild-type flies. Nevertheless, the residual responses to light pulses (phase shifts of ~1 hour) can explain the rather normal entrainment of *cry*^{01} mutants to LD cycles that was shown in many previous studies (Stanewsky et al., 1998; Emery et al., 2000b; Helfrich-Förster et al., 2001; Rieger et al., 2003; Bachleitner et al., 2007). Phase shift magnitudes of 1 hour appear very small, but they are not unusual for mammals in response to brief light pulses (see PRC atlas of Johnson [1990]). In fact, the re-entrainment properties of *cry*^{01} mutants (Fig. 2) closely resemble the ones reported for mammalian species (Aschoff et al., 1975).

In contrast to control flies, the light responses of *cry*^{01} mutants seemed not to be saturated in respect to irradiance: 1) the mutants significantly changed their phase-shifting behavior after increasing irradiance of the 1-hour light pulses from 1000 lux to 10,000 lux, and 2) they accelerated re-entrainment to an 8-hour phase delay of the LD cycle by almost 1 day when irradiance was increased to 10,000 lux.

In nature, brief light pulses rarely occur. Therefore, PRCs to brief pulses may fail to predict the behavior under LD 12:12 entrainment conditions. This is because longer exposure to light not only instantaneously phase-shifts the clock (nonparametric entrainment) but also influences its speed (parametric entrainment) (Aschoff, 1979; Wever, 1966). Thus, the application of longer light pulses can help to better understand entrainment. Comas et al. (2006) systematically monitored PRCs for single light pulses of different duration (1, 3, 4, 6, 9, 12, and 18 hours) in mice. As expected, they found that longer light pulses caused a higher PRC amplitude, an effect that was also observed in other species including humans and flies (Gander and Lewis, 1983; Czeisler et al., 1989; Saunders et al., 1994). Here, we found that control flies increased phase delays to 11 hours (and phase advances to ~6 hours) when light pulse duration was extended to 6 hours, making understandable why fruit flies can entrain immediately to an 8-hour phase delay of the 12:12 LD cycle (Fig. 2). Comas et al. (2006) settled the strongest phase-shifting effect to the first half of the light pulse (the light action centered on average at 38% of the light pulse), possibly due to light adaptation of the circadian system and its photoreceptors. This might be also true for flies, at least for the controls.

The response of *cry*^{01} mutants to longer light pulses was fundamentally different from wild-type flies. No prominent increase in phase shift magnitude with increasing light pulse duration occurred in the mutants. Just when light pulse duration reached 6 hours, a small but significant increase of phase advances became evident. Therefore, the *cry*^{01} mutants are not so much disturbed in sensing light pulses than in collecting and integrating light input over time. The latter may be also reflected in the strange phase-shifting behavior of *cry*^{01} mutants after 6-hour light pulses at CT15. Instead of showing the expected delays, the flies exhibited phase advances (Fig. 4A). The reason for this behavior may lie in the fact that a 6-hour light pulse starting at CT15 will end at CT21, meaning that the end falls into the advance zone. Let us assume that *cry*^{01} mutants are not able to collect light properly over the 6 hours but instead sense mainly lights-on and lights-off. Then, very little phase shifts could be expected. If, for still unknown reasons, the light action is not centered on the first half of the light pulse but closer to lights-off, even small phase advances could result, and this is exactly what we observed. Nevertheless, this explanation can only partly explain the *cry* mutant results. We know already that *cry* mutants are not completely impaired in integrating light input over time. *cry*^{b} and *cry*^{01} mutants still show prominent period changes (parametric light effects) under LL (Helfrich-Förster et al., 2001; Yoshii et al., 2004; Rieger et al., 2006; Dolezelova et al., 2007), indicating that an essential part of the parametric light input is mediated by the eyes and still intact in *cry*^{01} mutants. Most interestingly, constant light sensed via the eyes changed the velocity differently in different clock neurons, meaning that the molecular clock of some neurons ran faster and in other neurons slower under LL (Rieger et al., 2006). Perhaps 6-hour light pulses are long enough to elicit differential velocity changes in the different clock neurons and, as a consequence, caused the observed unusual phase shifts. Modeling the "circadian integrated response characteristic" (CIRC), as was recently suggested by Roenneberg

et al. (2010), may help to explain the entrainment characteristics of CRY-less flies because this model makes no assumptions about how entrainment occurs (by phase shifts or velocity changes).

Leaving all speculation aside, there is one main difference between wild-type and CRY-deficient flies regarding parametric light effects: *cry* mutants do not become arrhythmic at LL, not even at high irradiances (Emery et al., 2000a; Helfrich-Förster et al., 2001; Yoshii et al., 2004; Rieger et al., 2006). In this respect, the clock of CRY-deficient flies appears similar to that of mammals because the clock of most mammalian species runs under constant dim light (Aschoff, 1979). On the molecular level, this difference is easy to understand because light-activated *Drosophila* CRY leads to degradation of TIM (Ceriani et al., 1999; Busza et al., 2004). After TIM has disappeared, PER cannot be stabilized, and as a consequence, the clock stops. Indeed, Saunders et al. (1994) noted that after 6-hour light pulses, the activity rhythm of wild-type flies always started with the same phase, suggesting that the clock had completely stopped and was restarted after lights-off. Mammalian-like CRY is not light sensitive, and thus, light will probably not completely stop the mammalian clock, at least not after light pulses of 6 hours. Only a longer light exposure will stop the clock, as recently reported in mice after a pulse longer than 15 hours (Chen et al., 2008).

The PRC for 12-hour light pulses shows that the clock of CRY-less flies is mainly light responsive at dawn and dusk. Such temporally restricted sensitivity must be sufficient for entrainment because dawn and dusk are the most important times at which a clock needs to respond to light (Bünning, 1969; Bachleitner et al., 2007). Because the light sensitivity of CRY-less flies is mediated by photoreceptor organs (as the compound eyes, the H-B eyelets, and possibly the ocelli), our results suggest that these organs transmit photic information to the clock only in the morning and evening. Thus, different photoreceptors may be responsible for the different parts of a PRC.

ACKNOWLEDGMENTS

The authors thank David Dolezel for the cry^{01} mutants and relevant control flies and Nicolai Peschel and Dirk Rieger for helpful discussions and comments on the article. This study was supported by the German Research Foundation (DFG; Fo207/11-3) and by the European Community (6th Framework Project EUCLOCK, no. 018741).

CONFLICT OF INTEREST STATEMENT

The author(s) have no potential conflicts of interest with respect to the research, authorship, and/or publication of this article.

REFERENCES

Aschoff J (1979) Circadian rhythms: influences of internal and external factors on the period measured in constant conditions. Z Tierpsychol 49:225-249.

Aschoff J, Hoffmann K, Pohl H, and Wever R (1975) Re-entrainment of circadian rhythms after phase-shifts of the zeitgeber. Chronobiologia 2:23-78.

Bachleitner W, Kempinger L, Wülbeck C, Rieger D, and Helfrich-Förster C (2007) Moonlight shifts the endogenous clock of *Drosophila melanogaster*. Proc Natl Acad Sci U S A 104:3538-3543.

Benito J, Houl JH, Roman GW, and Hardin PE (2008) The blue-light photoreceptor CRYPTOCHROME is expressed in a subset of circadian oscillator neurons in the *Drosophila* CNS. J Biol Rhythms 23:296-307.

Bünning E (1969) Die Bedeutung tagesperiodischer Blattbewegungen für die Präzision der Tageslängenmessung. Planta 86:209-217.

Busza A, Emery-Le M, Rosbash M, and Emery P (2004) Roles of the two *Drosophila* CRYPTOCHROME structural domains in circadian photoreception. Science 304:1503-1506.

Ceriani MF, Darlington TK, Staknis D, Mas P, Petti AA, Weitz CJ, and Kay SA (1999) Light-dependent sequestration of TIMELESS by CRYPTOCHROME. Science 285:553-556.

Chen R, Seo D, Bell E, von Gall C, and Lee C (2008) Strong resetting of the mammalian clock by constant light followed by constant darkness. J Neurosci 28:11839-11847.

Comas M, Beersma DGM, Spoelstra K, and Daan S (2006) Phase and period responses of the circadian system of mice (*Mus musculus*) to light stimuli of different duration. J Biol Rhythms 21:362-372.

Czeisler CA, Kronauer RE, Allan JS, Duffy JF, Jewett ME, Brown EN, and Ronda JM (1989) Bright light induction of strong (type 0) resetting of the human circadian pacemaker. Science 244:1328-1333.

Dolezelova E, Dolezel D, and Hall JC (2007) Rhythm defects caused by newly engineered null mutations in *Drosophila*'s *cryptochrome* gene. Genetics 177:329-345.

Dushay MS, Konopka RJ, Orr D, Greenacre ML, Kyriacou CP, Rosbash M, and Hall JC (1990) Phenotypic and genetic analysis of Clock, a new circadian rhythm mutant in *Drosophila melanogaster*. Genetics 125:557-578.

Emery P, So WV, Kaneko M, Hall JC, and Rosbash M (1998) CRY, a *Drosophila* clock and light-regulated cryptochrome, is a major contributor to circadian rhythm resetting and photosensitivity. Cell 95:669-679.

Emery P, Stanewsky R, Hall JC, and Rosbash M (2000a) A unique circadian-rhythm photoreceptor. Nature 404:456-457.

Emery P, Stanewsky R, Helfrich-Förster C, Emery-Le M, Hall JC, and Rosbash M (2000b) *Drosophila* CRY is a deep brain circadian photoreceptor. Neuron 26:493-504.

Gander PH and Lewis RD (1983) Phase-resetting action of light on the circadian activity rhythm of *Rattus exulans*. Am J Physiol 245:R10-R17.

Glaser WR (1978) *Varianzanalyse*. Stuttgart: Gustav Fischer Verlag.

Helfrich-Förster C (1998) Robust circadian rhythmicity of *Drosophila melanogaster* requires the presence of lateral neurons: a brain-behavioral study of *disconnected* mutants. J Comp Physiol A 182:435-453.

Helfrich-Förster C, Winter C, Hofbauer A, Hall JC, and Stanewsky R (2001) The circadian clock of fruit flies is blind after elimination of all known photoreceptors. Neuron 30:249-261.

Hirsh J, Riemensperger T, Coulom H, Iche M, Coupar J, and Birman S (2010) Roles of dopamine in circadian rhythmicity and extreme light sensitivity of circadian entrainment. Curr Biol 20:209-214.

Johnson CH (1990) *An Atlas of Phase Responses Curves for Circadian and Circatidal Rhythms*. Nashville: Department of Biology, Vanderbilt University. p 715.

Johnson CH (1999) Forty years of PRCs: what have we learned? Chronobiol Int 16:711-743.

Johnson CH (1992) Phase response curves: what can they tell us about circadian clocks? In *Circadian Clocks from Cell to Human*, Hiroshige T and Honma K, eds, pp 209-246. Sapporo: Hokkaido University Press.

Konopka RJ, Pittendrigh C, and Orr D (1989) Reciprocal behaviour associated with altered homeostasis and photosensitivity of *Drosophila* clock mutants. J Neurogenet 6:1-10.

Levine JD, Casey CL, Kalderon DD, and Jackson FR (1994) Altered circadian pacemaker functions and cyclic AMP rhythms in the *Drosophila* learning mutant *dunce*. Neuron 13:967-974.

Morin LP and Allen CN (2006) The circadian visual system. Brain Res Rev 51:1-60.

Mrosovsky N (1996) Methods of measuring phase shifts: why I continue to use an Aschoff type II procedure despite the skepticism of referees. Chronobiol Int 13:387-392.

Nelson DE and Takahashi JS (1991) Sensitivity and integration in a visual pathway for circadian entrainment in the hamster (*Mesocricetus auratus*). J Physiol 439:115-145.

Ohata K, Nishiyama H, and Tsukahara Y (1998) Action spectrum of the circadian clock photoreceptor in *Drosophila melanogaster*. In *Biological Clocks: Mechanisms and Applications*, Touitou Y, ed, pp 167-171. Amsterdam: Elsevier.

Peschel N, Veleri S, and Stanewsky R (2006) *Veela* defines a molecular link between Cryptochrome and Timeless in the light-input pathway to *Drosophila*'s circadian clock. Proc Natl Acad Sci U S A 103:17313-17318.

Rieger D, Fraunholz C, Popp J, Bichler D, Dittmann R, and Helfrich-Förster C (2007) The fruit fly *Drosophila melanogaster* favors dim light and times its activity peaks to early dawn and late dusk. J Biol Rhythms 22:387-399.

Rieger D, Shafer OT, Tomioka K, and Helfrich-Förster C (2006) Functional analysis of circadian pacemaker neurons in *Drosophila melanogaster*. J Neurosci 26:2531-2543.

Rieger D, Stanewsky R, and Helfrich-Förster C (2003) Cryptochrome, compound eyes, Hofbauer-Buchner eyelets, and ocelli play different roles in the entrainment and masking pathway of the locomotor activity rhythm in the fruit fly *Drosophila melanogaster*. J Biol Rhythms 18:377-391.

Roenneberg T, Remi J, and Merrow M (2010) Modeling a circadian surface. J Biol Rhythms 25:340-349.

Rutila JE, Maltseva O, and Rosbash M (1998) The *timSL* mutant affects a restricted portion of the *Drosophila melanogaster* circadian cycle. J Biol Rhythms 13:380-392.

Saunders DS, Gillanders SW, and Lewis RD (1994) Light-pulse phase response curves for the locomotor activity rhythm in *Period* mutants of *Drosophila melanogaster*. J Insect Physiol 40:957-968.

Stanewsky R, Kaneko M, Emery P, Beretta B, Wager-Smith K, Kay SA, Rosbash M, and Hall JC (1998) The *cry*^{b} mutation identifies *cryptochrome* as a circadian photoreceptor in *Drosophila*. Cell 95:681-692.

Suri V, Qian Z, Hall JC, and Rosbash M (1998) Evidence that the TIM light response is relevant to light-induced phase shifts in *Drosophila melanogaster*. Neuron 21: 225-234.

Veleri S, Brandes C, Helfrich-Förster C, Hall JC, and Stanewsky R (2003) A self-sustaining, light-entrainable circadian oscillator in the *Drosophila* brain. Curr Biol 13:1758-1767.

Veleri S, Rieger R, Helfrich-Förster C, and Stanewsky R (2007) Hofbauer-Buchner eyelet affects circadian photosensitivity and coordinates TIM and PER expression in *Drosophila* clock neurons. J Biol Rhythms 22:29-42.

Wegener C, Hamasaka Y, and Nässel DR (2004) Acetylcholine increases intracellular Ca^{2+} via nicotinic receptors in cultured PDF-containing clock neurons of *Drosophila*. J Neurophysiol 91:912-923.

Wever RA (1966) Ein mathematisches Modell für die circadiane Periodik. Zeitschrift für angewandte Mathematik und Mechanik 46:148-157.

Yoshii T, Funada Y, Ibuki-Ishibashi T, Matsumoto A, Tanimura T, and Tomioka K (2004) *Drosophila cry*^{b} mutation reveals two circadian clocks that drive locomotor rhythm and have different responsiveness to light. J Insect Physiol 50:479-488.

Yoshii T, Todo T, Wülbeck C, Stanewsky R, and Helfrich-Förster C (2008) Cryptochrome is present in the compound eyes and a subset of *Drosophila*'s clock neurons. J Comp Neurol 508:952-966.

3.2 Mapping of a *rh7* deletion

The first aim of my main project was to precisely characterize an *rh7* mutant strain which was generated within a previous PhD thesis by P-element based mutagenesis (Bachleitner, 2008). The original P element insertion line, y^1w^{67c23}*; P{EPgy2}EY13118*, was obtained from Bloomington Stock Center (Indiana University, Bloomington, IN, U.S.A.). It carried a P element in the 5'UTR of the *rh7* gene that clearly reduced the expression levels of *rh7*. Remobilization of the P element by crossing these flies to a *Δ2-3* "jumpstarter" strain resulted in a precise excision control ($rh7^{13}$), referred to as revertant, and in an imprecise excision line, referred to as $rh7^{47}$ mutant (Bachleitner, 2008). In homozygous $rh7^{47}$ mutant flies, no *rh7* transcripts were detected by qPCR, making it likely that the transcription start site was located within this deletion. The expression of the downstream located gene, CG9760, stayed unaffected by the mutation, but the exact breakpoints of the deletion remained unknown.

In the present thesis, the deletion was further characterized on the molecular level by DNA breakpoint determination (Fig. 15). PCR reactions were performed using special sets of primers in order to narrow the deletion breakpoint down to a short genomic region. Finally, a ~1.4 kb genomic DNA sequence containing the breakpoint was cloned into the pGEM-T Easy vector and sequenced. In detail, the sequenced DNA fragment of 1363 bp size was composed of P element DNA (565 bp in total), DNA of micropia {2987}, a natural transposable element (480 bp), and *rh7* DNA (318 bp of the noncoding region of exon 4). This data revealed that the deletion comprises ~10.35 kb and extends over the entire *rh7* coding sequence. Consequently, the $rh7^{47}$ mutant is a true knockout mutant and will be called $rh7^0$ in the following. Together with its isogenic control (the revertant) it allowed to investigate the biological functions of Rh7.

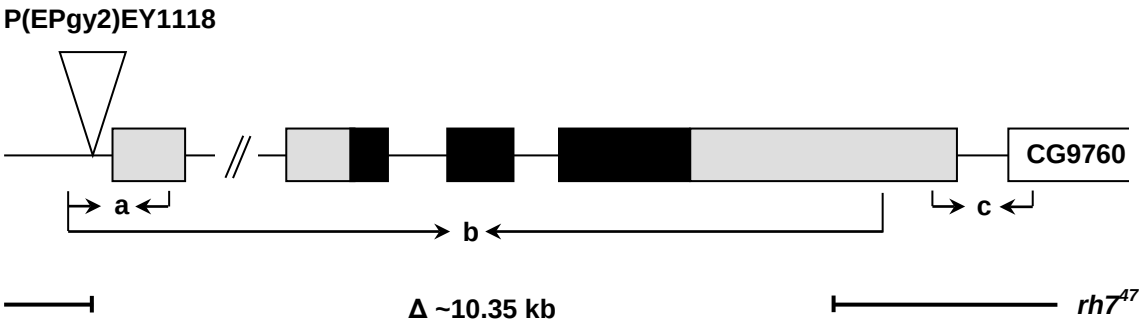

Figure 15: Genomic organization of the wild-type and mutant *rh7* locus (not to scale).
Boxes represent the four exons; black color indicates coding, gray color noncoding regions. Black arrows indicate primer positions for transcript detection (a) and breakpoint determination, respectively (b and c). The line below refers to the mutant allele, $rh7^{47}$ ($rh7^0$) and the extent of the deletion.

3.3 Generation of UAS-*rh7* transgenic fly lines

In the next step, we generated UAS-*rh7* lines to later manipulate *rh7* expression with help of the GAL/UAS binary expression system.

For this purpose, full-length *rh7* cDNA was amplified by PCR from pOT2 vector of a commercially available cDNA clone, GH14208, using a primer pair creating restriction enzyme sites (EcoRI / KpnI). After restriction enzyme digestion and amplification, the purified PCR product (1.8 kb) was first ligated into the pGEM-T Easy vector and then further subcloned into the pUAST expression vector using EcoRI restriction sites. The cDNA insert was confirmed by sequencing after the “in sense” direction was verified by digestion with XhoI.

To create transgenic fly lines, the 10.8 kb pUAS-*rh7* construct was microinjected into embryos, as described in section 2.2.1. Almost 40% of the eggs developed to larvae and, after crossing back to w^{1118}, ten independent stable lines were established from transformant male progeny (Table 15).

Table 15: Established w[*]; P{w[+mC]=UAS-rh7} lines.

$w^{[*]}$; *P{*$w^{[+mC]}$*=UAS-rh7}* (strain number)	Insertion (chromosome)	Properties
3	III	Homozygous viable
4	III	Homozygous viable
8	III	Homozygous viable
9	III	Homozygous lethal
10.2	III	Homozygous lethal
10.3	II	Homozygous viable
11	III	Homozygous viable
16	III	Homozygous viable
20	II	Homozygous lethal
21	II	Homozygous lethal

Four homozygous viable lines (4, 8, 10.3 and 20) were tested for *rh7* expression by driving the construct under the control of the ubiquitous driver *actin*-GAL4. *GMR*-GAL4, a photoreceptor-specific driver, was additionally crossed to strain #10.3. As a control, we crossed w^{1118} flies to both GAL4 driver lines. Based on qPCR results, lines number 8 and 10.3 were chosen for further experiments, because they showed a 14.3-fold and 12.5-fold increased relative expression level of *rh7*, respectively.

3.4 Expression of Rh7 in *Drosophila*

My next goal was to determine in detail to which level and in which tissues wild-type fruit flies express *rh7*. Since all so far known rhodopsins are exclusively expressed in photoreceptor cells, strong emphasis was laid on the analysis of the compound eyes.

3.4.1 Levels of *rh7* mRNA expression in the adult fly brain and retina

We used qPCR to analyze the relative expression levels of *rh7* mRNA in brains and retinas of CS wild-type flies, of $rh7^{0}$ and $ninaE^{17}$ (a Rh1 null mutant and *ninaE* in the following) mutants and of flies that express *rh7* under the control of the *rh1*-promotor, either in addition to, or instead of *rh1*. All transgenic lines were compared with their isogenic controls. For each genotype, total RNA was isolated from preparations of a single brain and three retinas (including the laminar layers), reversely transcribed into cDNA and tested by qPCR, as described in 2.3.1.13. The resulting data (Fig. 16A-C) revealed that Rh7 expression is present in both brain and retina at an approximately equal level in fly lines carrying the wild-type *rh7* allele (underlined genotypes).

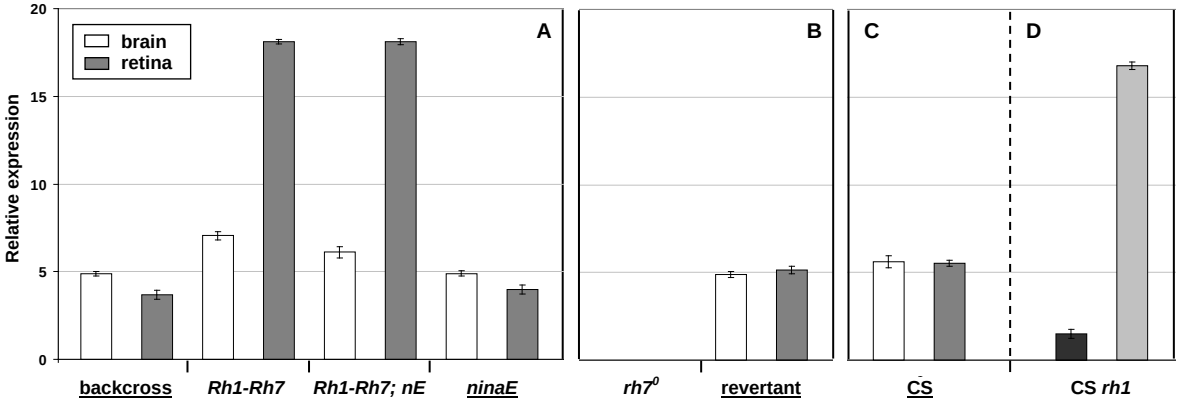

Figure 16: Relative expression levels of *rh7* (A-C) and *rh1* (D) in adult brain and retina.

A-C: Open bars represent relative expression levels of *rh7* in the brain, filled bars in the retina, respectively. Underlined genotypes carry the wild-type *rh7* allele.

A: *Rh1-Rh7* promotor construct lines and corresponding controls; *nE* = *ninaE*.

B: *Rh7* null mutant and precise excision control.

C: Wild-type CS.

D: Relative expression levels of *rh1* in the brain (dark gray bar) and in the retina (light gray bar) of CS flies.

Error bars represent ± SEM. For details, see text.

Transgenic lines expressing *rh7* under the control of the *rh1* promotor showed almost 5x higher expression in the retina in comparison to their controls, backcross and *ninaE*, and the level of *rh7* expression in the brain was significantly elevated, too ($p < 0.01$). The data of the control lines (backcross and *ninaE*) was similar in both tissues (A). As expected, no transcripts could be detected in the *rh7* null mutant (B).

In addition, we tested the relative expression of *rh1* in CS wild-type flies (D) in order to compare our results to a well-described control. Unlike *rh7* (C), the relative expression of *rh1* was low in CS brains compared to retinas and, furthermore, significantly lower in CS retinas in comparison to the retinal expression of the *rh1* promoter-driven *rh7* expression in the two promotor construct lines shown in A ($p \leq 0.001$).

In *ninaE* mutant flies, outer photoreceptors R1-R6 degenerate in an age-dependent manner (e.g., Leonard et al., 1992; Kurada and O´Tousa, 1995; Bentrop et al., 1997) and, we did not detect any *rh1* expression in *ninaE* brains or retinas in the experiment shown above. For this reason, it was hard to understand why retinal levels of *rh7* mRNA were similar to that of wild-type flies. To test whether *rh7* levels depend on the age of *ninaE* flies, we compared the expression of *rh7* between very young (~1-day-old) and aged (> 21-day-old) mutants (Fig. 17). We did not observe a decreased relative expression level neither in brains (A) nor in retinas (B) in elderly *ninaE* flies. In fact, retinal expression of *rh7* was rather increased in aged mutants ($p = 0.001$).

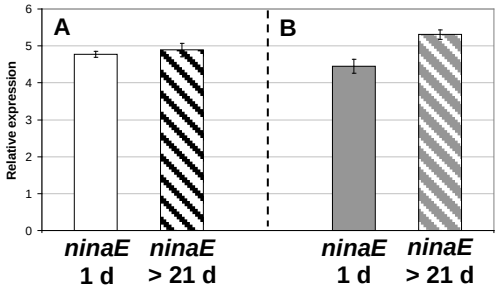

Figure 17: Relative expression levels of *rh7* in young and aged *ninaE* mutant flies.
Relative expression levels of *rh7* in *ninaE* brains (A) and retinas (B). Solid bars represent data from 1-day-old, dashed bars data from > 21-day-old flies. Relative expression levels of *rh7* do not decrease with age in *ninaE* mutants. Error bars represent ± SEM.

3.4.2 Rh7 expression in eyes and antennae by UAS-reporter lines

A Japanese research group (N. Fuse, Kyoto University, Kyoto) reported strong GAL4-mediated expression of *rh7* in Johnston's organ (JO) using a commercially available enhancer trap line (BL #12787) carrying a transposon insertion in the 3' UTR of the *rh7* gene (Maeda, 2011). They could confirm their observations by RT-PCR experiments and suggested a role for Rh7 in the auditory signaling pathway (Fuse, personal communication).

For this reason, we chose two of our *rh7*-GAL4 lines, #5 and #9 carrying the construct on the third chromosome (from Bleyl, 2008) and the enhancer trap line (used by the Japanese group) to study reporter gene expression in the eyes and in JO, which is located in the second antennal segment. We crossed these lines to two different UAS-EYFP lines, to one UAS-GFP and one UAS-myr-mRFP line and analyzed heads of the progeny using fluorescent microscopy. Only with UAS-myr-mRFP, a clear staining of antennal neurons could be observed in the offspring of all crosses, as exemplarily

shown for *UAS-myr-mRFP; rh7-GAL4#9* in Figure 18A. In this individual experiment, the enhancer trap-derived reporter gene expression pattern included photoreceptors of the ocelli (B) and, in dissected samples, a broad signal in the lamina (C) and a weak signal in the retina (D) was detected.

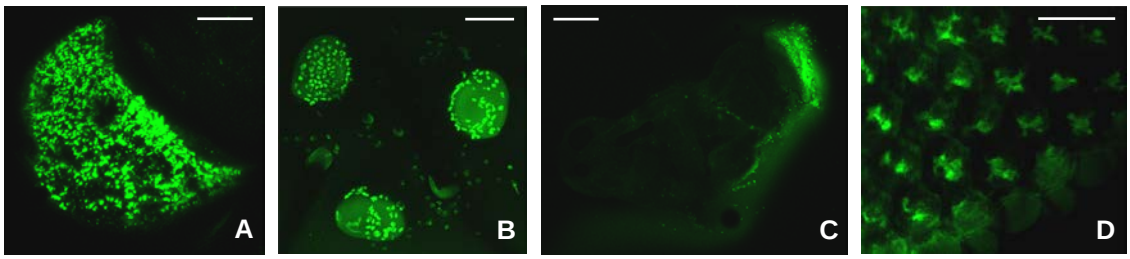

Figure 18: Reporter gene expression pattern (membrane tethered UAS-myr-mRFP) resulting from crosses to a *rh7*-GAL4#9 driver (A) and an enhancer trap line (B-D).

A: In *UAS-myr-mRFP; rh7-GAL4#9* flies, *rh7* is expressed in JO neurons located in the second antennal segment.

B-D: Enhancer trap-derived expression pattern. The signal is present in photoreceptors of the ocelli (B), in the lamina (C) and the proximal area of the retina (D).

Scale bars: A, B, D = 25 µm; C = 100 µm.

We confirmed *rh7* expression in the second antennal segment in our experiments, but we were not able to unequivocally assign gene expression to a certain subset of JO neurons, perhaps partly due to a lack of experience. As mentioned above, such a staining pattern could not be achieved with any other non-membrane-tethered GFP or EYFP lines. Using one of the latter, it would have been easier to identify subgroups of auditory neurons (Senthilan, personal communication).

3.4.3 Expression of Rh7 on the protein level

In the following step, I used immunohistochemistry (IHC) to investigate whether Rh7 is also expressed on the protein level. This item was already addressed by Bachleitner (2008), but the results were ambiguous. Bachleitner (2008) used an Rh7 antibody directed against a C-terminal 20-mer peptide of Rh7 and found staining in the retina and the ocelli. This staining was significantly reduced in *rh7* knockout mutants, but not completely absent. Presumably, sequence similarities among the seven members of the rhodopsin gene family prevented specific recognition of Rh7. For this reason, we repeated IHC including different techniques. Furthermore, new peptide antibodies were raised in rabbits and in guinea pigs. These antibodies, directed against an N-terminal extracellular domain of Rh7 and without any sequence homology to the other rhodopsins, were tested on western blots and in IHC.

3.4.3.1 Characterization of the new antibodies on western blots

We performed western blot analysis using head extracts of adult *Rh1-Rh7; ninaE* flies expressing high levels of *rh7* mRNA compared to wild-type flies (see Fig. 16A). As negative controls for non-specific binding, we used preimmune sera instead of specific antisera and tested $rh7^0$ mutants. In addition, we compared antisera from different collection time points (collected in 30-day intervals after the initial immunization) as well as final antibodies before and after the affinity purification. To test simultaneously and under the same conditions, membranes were cut into stripes after the blocking step and then either incubated in one of the four primary antibodies (2x rabbit, 2x guinea pig) or in the corresponding preimmune serum. After the secondary antibody incubation, pieces of membrane were placed together on the scanning surface of the imaging system for fluorescent signal detection.

The specificity of the new peptide antibodies was tested and confirmed using a simple dot blot analysis (see section 2.3.2.5). As exemplarily shown in Figure 19, the guinea pig-derived antibodies recognized the purified peptide and no signals were detected using the preimmune sera.

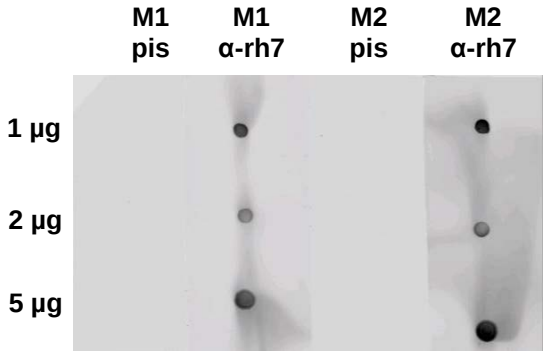

Figure 19: Dot blot analysis of new anti-Rh7 antibodies.

Dot blot analysis demonstrates the specificity of the new anti-Rh7 antibodies obtained from guinea pig (M1 and M2, serum collection day 150, 1:5000). Incubation with corresponding preimmune sera did not produce any signals. Peptide concentration is indicated on the left.

In the representative western blot shown in Figure 20A, rabbit 1 preimmune serum was tested in comparison to serum samples collected 61, 90 and 120 days after the initial immunization. Like in dot blot analysis, no or only weak background staining was present in the area in which the Rh7 signal would have been expected when treated with preimmune serum. Unfortunately, antibodies did not recognize any consistent prominent bands in this region either. Instead, all serum samples produced multiple unspecific bands, even at higher dilutions, and we did not observe any potential Rh7 signal at the expected size of ~53.7 kDa increasing in intensity in consecutive serum samples.

Direct comparisons between *Rh1-Rh7; ninaE* flies and *rh7* knockout mutants generally resulted in similar band patterns, as exemplarily shown in Figure 20B. Therefore, we

concluded that the antibodies are not able to detect Rh7 in western blots, at least not after the present treatment conditions.

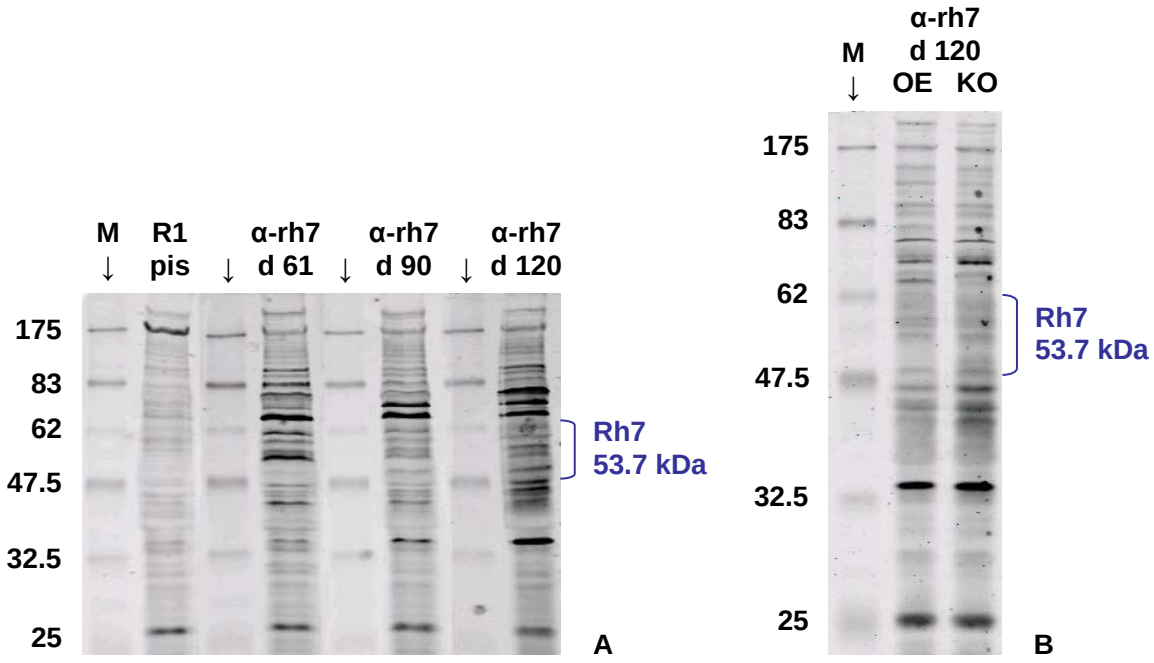

Figure 20: Detection of Rh7 by western blot analysis using different serum samples (A) and the knockout mutant (B) for controls.

A: Rabbit 1 (R1) preimmune serum (pis) and antisera from different serum collections (61, 90 and 120 days after the initial boost; 1:5000) were tested using head extracts of *Rh1-Rh7; ninaE* flies.

B: Direct comparison of *Rh1-Rh7; ninaE* (OE) and $rh7^0$ (KO) head extracts using rabbit 1 anti-Rh7 antibody from collection day 120 (1:5000).

In both images, the blue bracket labels the area in which the Rh7 signal would have been expected due to its molecular size of 53.7 kDa. M: Prestained Protein Marker. For details, see text.

Then, we tested the supernatant of the homogenate with (standard procedure) and without the heat denaturation step prior to SDS-PAGE as well as the resuspended pellet (Fig. 21). The antibody (R1, collection day 150, affinity purified) produced the same staining patterns for *Rh1-Rh7; ninaE* and $rh7^0$ flies under all conditions and, apparently, did not specifically recognize Rh7. The other antibodies were tested in the same way and gave equivalent results. To increase protein levels, we overexpressed Rh7 in all photoreceptor cells using *GMR-GAL4; UAS-rh7#8* flies but could not detect Rh7 in western blotting either.

In a last attempt, we used affinity purified antibodies. The affinity purification generally resulted in a strong reduction in non-specific banding but, nevertheless, no differences between *Rh1-Rh7; ninaE* flies and *rh7* null mutants could be observed. As previously mentioned, each of the four antibodies detected the purified peptide (1 µg) in dot blot analysis. Taken all these results together, we concluded that the new antibodies were not suited to detect Rh7 in western blot analysis.

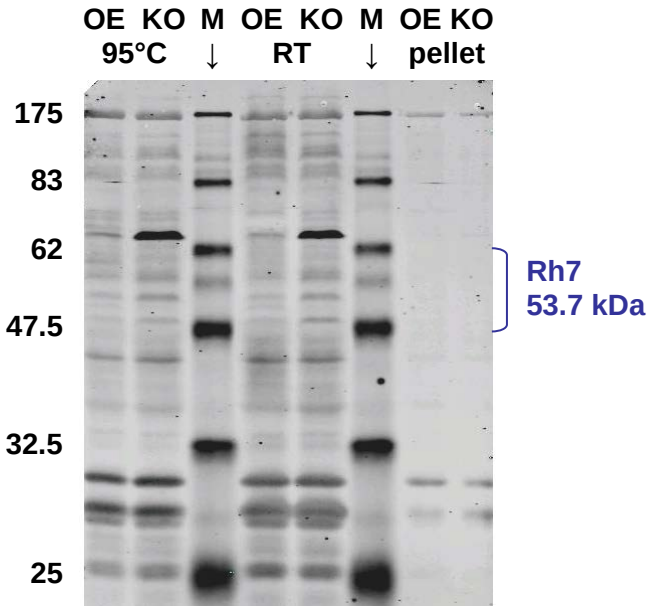

Figure 21: Comparison of different sample preparation treatments for the detection of Rh7 by western blot analysis.

Before SDS-PAGE, supernatants from *Rh1-Rh7; ninaE* (OE) and *rh7*^{0} (KO) head extracts were either denatured (3', 95°C) or left untreated (RT) and tested together with the resuspended pellet (3', 95°C) in western blotting using affinity purified rabbit 1 anti-Rh7 antibody (collection day 150, 1:500).

The blue bracket labels the area in which the Rh7 signal would have been expected due to its molecular size.

M: Prestained Protein Marker.

For details, see text.

3.4.3.2 Rh7 immunohistochemistry on fly heads and brains

Next, we used IHC to test for the presence and the location of Rh7 in whole mounts of adult brains and retinas, on cryosections and paraffin sections of fly heads. For these stainings, we used a previously generated anti-Rh7 antibody and the newly generated antibodies.

3.4.3.2.1 Whole mount antibody staining of adult brains and retinas

Brains were dissected as described in section 2.3.3.1, but ocelli were kept attached to them if possible. First, we tested the previously generated anti-Rh7 antibody ("Rh7:E") which is directed against a C-terminal intracellular peptide (Bachleitner, 2008).

To visualize putative Rh7 labeling in respect to photoreceptor cells or clock neurons, double-labeling experiments were carried out using either anti-Rh7 antibody combined with anti-chaoptin or, alternatively, with nb33 (anti-PDF precursor) antibody.

First, we stained wild-type control (revertant) brains in comparison to *rh7*^{0} brains which served as a negative control. To make sure that the antibody really recognizes Rh7, we overexpressed Rh7 in specific cells. For this purpose, we used two independent UAS-*rh7* lines (#8 and #10.3) to express Rh7 1) in all neurons by crossing to *elav*-GAL4 2) in all clock neurons by crossing to *tim*(UAS)-GAL4 3) in a subset of clock neurons, the LN_vs, by crossing to *Pdf*-GAL4 and 4) specifically by crossing to a *rh7*-GAL4 line. Moreover, we tested the antibody on brains of *glass* mutant flies because their *rh7* mRNA levels were shown to be strongly elevated by qPCR (Bleyl, 2008). Samples were analyzed by confocal laser scanning microscopy. All experiments gave consistent results: Chaoptin staining was present in the projections sent from retinal

photoreceptor cells into the medulla and in the ocellar photoreceptors. However, we observed no Rh7 staining in brains of *rh7* knockout mutants, revertant controls and *glass* mutants. Furthermore, Rh7 could neither be detected in the LN_vs (labeled by anti-nb33) nor in any other neurons in which its expression was driven according to the respective GAL4 line (images not shown).

Completely independent from the genotype tested, the antibody recognized the ocelli, as exemplarily shown in Figure 22 for *Pdf-GAL4*; *UAS-rh7#8* flies.

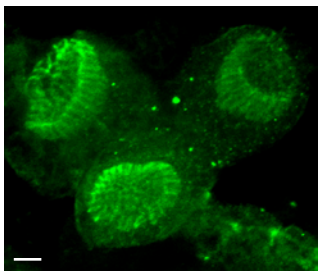

Figure 22: Localization of Rh7 in the ocelli.
Rh7:E anti-Rh7 antibody (1:1000) stains ocellar photoreceptors in *Pdf-GAL4*; *UAS-rh7#8* flies, although *Pdf*-GAL4 does not drive gene expression there.
Scale bar = 10 µm.

In general, all new peptide antibodies (see 2.2.6) stained the ocelli only prior to affinity purification, but the staining intensity was comparable in $rh7^0$ mutants, *Rh1-Rh7* and control flies, as observed with the previous Rh7:E anti-Rh7 antibody. The same was true for the brains of these three genotypes in which no cells were labeled at all.

Interestingly, Rh7 could be detected in the retinal photoreceptors (in the whole mount preparations in which the retina stayed attached to the brain), as exemplarily shown in Figure 23 for *Rh1-Rh7*. In general, the staining was weaker using guinea pig-obtained antibodies, but it was otherwise independent from the date of serum collection and the affinity purification. On the other hand, no difference in signal strength between $rh7^0$ and control flies could be observed. In both genotypes, retinal staining was present at higher (1:100) and equally weak or absent at lower antibody concentrations (1:1000). Control staining experiments with preimmune sera were negative.

We made exactly the same experiences with staining of cryosections. For this reason, no extra section will be devoted to these experiments.

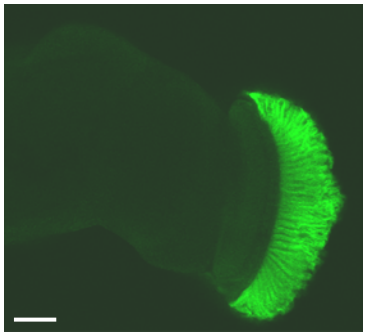

Figure 23: Detection of Rh7 in the retina of *Rh1-Rh7* flies.
Rabbit 1 anti-Rh7 antibody (serum sample day 150, affinity purified, 1:1000) labels the brain-attached retina in *Rh1-Rh7* flies.
Scale bar = 50 µm.

Subsequently, to specify the antibody labeling in the retina, we stained whole mount retina preparations with affinity purified antibodies from final serum sample collection (day 180 for guinea pig, day 240 for rabbit), hereinafter referred to as “final” antibodies. Higher magnification image scanning (using the 63x oil objective and up to 12x optical zoom) allowed for a detailed view of the retinal staining pattern in *Rh1-Rh7* flies. The promotor construct causes additional expression of Rh7 in the outer photoreceptors R1-R6 of the ommatidia in this fly strain.

In contrast to the first results we got of staining with earlier collected serum samples (from day 120 and 150) and lower magnification images, Rh7 could only be definitely detected in R1-R6 rhabdomeres by the final anti-Rh7 antibodies obtained either from rabbit 2 (Fig. 24A) or guinea pig 2 serum, whereas other final antibodies stained surrounding retinal tissue (C). Double labeling with anti-Rh1 antibody allowed for clear identification of R1-R6 rhabdomeres (B).

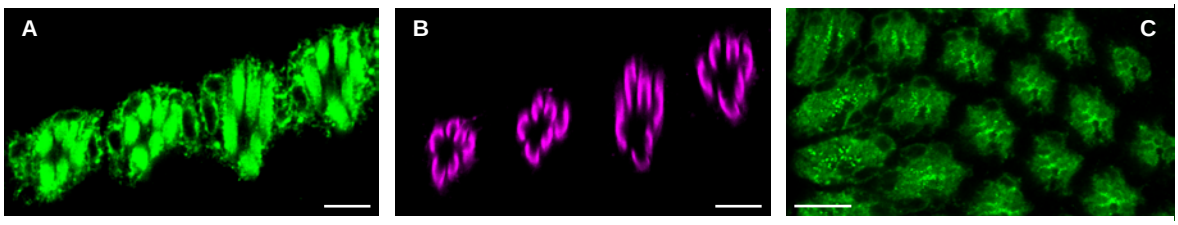

Figure 24: Detection of Rh7 in the rhabdomeres of R1-R6 in *Rh1-Rh7* retinas.

A: Rabbit 2 anti-Rh7 antibody (day 240, affinity purified, 1:500) labels the rhabdomeres of the outer photoreceptors R1-R6.

B: 4C5 anti-Rh1 antibody (1:100) specifically recognizes R1-R6 rhabdomeres.

C: Guinea pig 1 anti-Rh7 antibody (day 210, affinity purified, 1:1000) labels tissue that surrounds the rhabdomeres.

Scale bars: A+B = 10 µm; C = 50 µm.

Final rabbit 2 anti-Rh7 antibody specifically and reproducibly recognized Rh7 and was thus chosen for the following experiments in which we aimed to detect Rh7 in retinas of wild-type and control flies (CS, ALA and revertant) using *rh7* knockout tissue as negative control. As exemplarily shown for ALA ommatidia in Figure 25A, the staining was located to the interior side of all rhabdomeral photoreceptor membranes or to the borders of the interrhabdomeral space, possibly depending on the scanning position of the single ommatidium. However, Rh7 did not colocalize with Rh1 (B) in the outer rhabdomeres; the overlapping signals in the merged image (C) resulted from high staining intensity. An increased number of analyzed samples strengthened our opinion that the two proteins are not present in the same part of the retinal tissue but rather complementary to each other (D-F). Like Rh1, the Rh7 antibody staining extended through the whole depth of the retina (G).

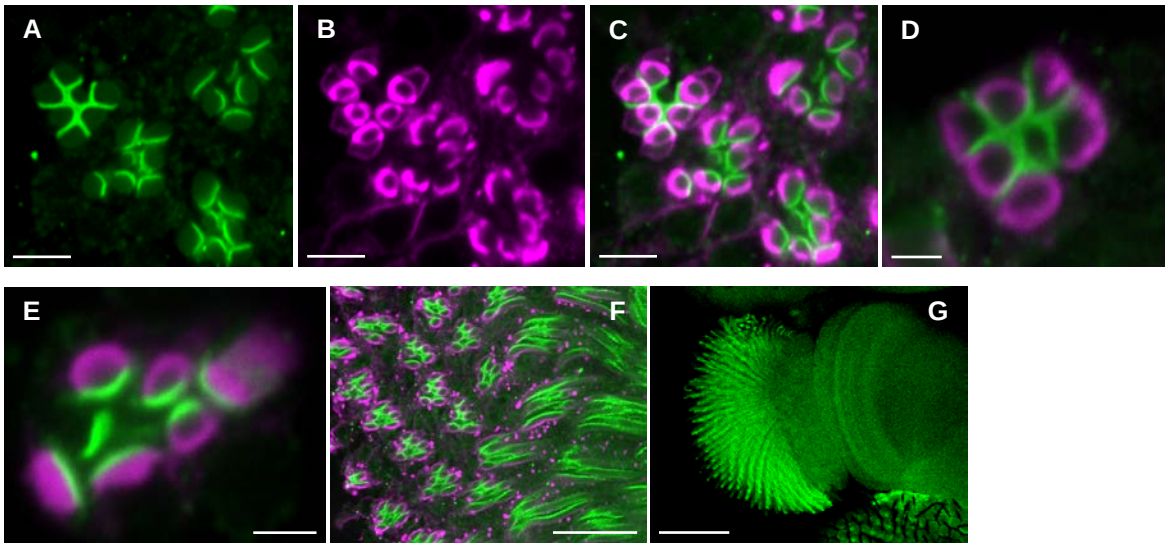

Figure 25: Localization of Rh7 in wild-type ALA retinas.

A: Rabbit 2 anti-Rh7 antibody (day 240, affinity purified, 1:100) labels all interior photoreceptor membranes and the borders of the interrhabdomeral space in wild-type ALA ommatidia.

B: 4C5 anti-Rh1 antibody (1:100) specifically recognizes R1-R6 rhabdomeres.

C-E: Rh1 and Rh7 do not colocalize in R1-R6 rhabdomeres but show a rather complementary staining pattern.

G: Anti-Rh7 antibody (see A) stains the entire depth of the retina.

Scale bars: A-C = 5 µm; E+D = 2 µm; F = 20 µm; G = 100 µm.

Unfortunately, comparisons between knockout mutant and revertant retinas showed that this distinct Rh7 antibody staining is present in both genotypes and therefore not specific. Because of the results obtained by deletion mapping and qPCR (section 3.2 and 3.4.1), we were sure that Rh7 synthesis is completely abolished in *rh7*^{0} mutants. Nevertheless, retinas of other Rh7 mutant strains, “Dark-fly” and “Df RC3”, which were kindly provided by a Japanese research group, were tested using final rabbit 2 anti-Rh7 antibody. In both mutants, we observed the same retinal staining pattern as in *rh7*^{0} and revertant flies before, and there was also no difference between Df RC3 and the corresponding control line (Fig. 26A-C).

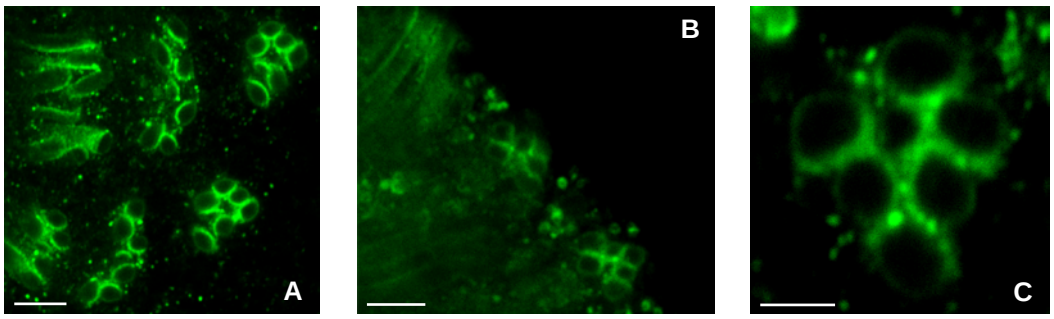

Figure 26: Identical staining patterns in Rh7 mutant and control flies.

The rhabdomeral antibody staining pattern does not differ between Rh7 mutant (A: Dark fly, B: Df RC3) and control flies (C: Control for B). Antibody: Rabbit 2 anti-Rh7 antibody (day 240, affinity purified, 1:100). Scale bars: A+B = 5 µm; C = 2 µm.

From these results we concluded that the final rabbit 2 anti-Rh7 antibody is only able to detect high amounts of Rh7, as shown for R1-R6 rhabdomeres of *Rh1-Rh7* retinas. The interrhabdomeral or interior membrane staining observed in wild-type ommatidia was present in different Rh7 mutant strains as well, and was therefore regarded as a non-specific signal.

3.4.3.2.2 Antibody staining of paraffin embedded head sections

Paraffin sections of adult fly heads were prepared and samples were deparaffinized and rehydrated prior to the antibody staining procedure as described in section 2.3.3.2. Because of the antibody staining results from whole mount preparations, we focused on the affinity purified anti-Rh7 antibodies (2x rabbit, 2x guinea pig) and tested them in different dilutions (1:100, 1:200, 1:300).

In contrast to whole mount antibody staining, all four primary antibodies stained the lamina in addition to the retina in frontal head sections of *Rh1-Rh7* flies (Fig. 27A). Retinas were stained broadly independent from antibody concentrations and we were not able to distinguish exactly between single photoreceptors and rhabdomeres (A'). In flies carrying the wild-type *rh7* allele, a weak antibody staining was usually present, extending through the entire depth of the retina (B). On the other hand, no clear differences could be observed in comparison to *rh7* knockout mutants (C), although, the staining of the outer retinal area did not look exactly the same in higher magnification images (B' and C').

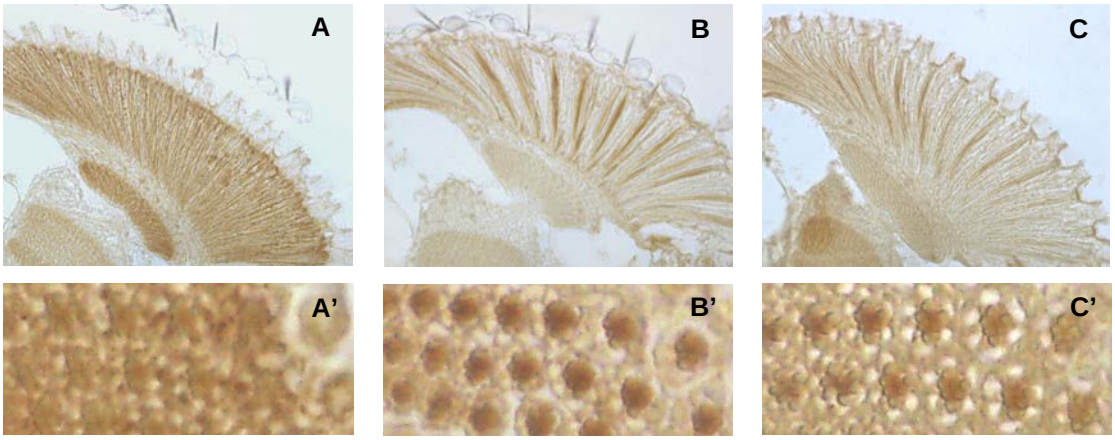

Figure 27: Detection of Rh7 on paraffin embedded head sections.

A-C: Rabbit 2 anti-Rh7 antibody staining (day 240, affinity purified) of adult head sections.

A'-C': Higher magnification view of the respective retinal staining.

A: Anti-Rh7 antibody (1:200) stains the retina and the lamina in sections of *Rh1-Rh7* fly heads.

B: Anti-Rh7 antibody (1:300) labels certain areas of the retina in sections of controls carrying the wild-type *rh7* allele (*GMR*-GAL4).

C: Anti-Rh7 antibody (1:300) labels certain areas of the retina in sections of $rh7^{0}$ flies.

An exception was guinea pig 1-obtained anti-Rh7 antibody that exclusively stained the lamina in control and *rh7*^{0} flies. Besides difficulties in tissue preservation, variable antibody staining intensities on the same microscope slide made it generally difficult to reproduce and evaluate the results.

In summary, we were not able to support the *rh7* mRNA expression data at the protein level using immunohistochemical approaches. Newly generated peptide antibodies were not suitable for western blotting technique and although they detected Rh7 at high concentrations in IHC, they additionally showed strong unspecific labeling in the interrhabdomeric space. In wild-type tissue, Rh7 expression seemed too weak to be detected by the antibodies. Thus, the question of Rh7 localization remained largely unanswered.

3.5 Functional characterization of Rh7

In 2000, when the *Drosophila* genome sequencing project was basically completed (Adams et al., 2000), the annotated gene CG5638 was denominated Rhodopsin 7 based on sequence similarities to the six known rhodopsins, even though a potential photoreceptive function had not been demonstrated yet.

However, previous results from our group showed that expression of Rh7 in place of Rh1 (ommatidal R1-R6 photoreceptors) is able to rescue the wild-type eye structure and the electroretinogram (ERG) response in the compound eyes of *ninaE* mutant flies (Bachleitner, 2008; Grebler, 2010). In order to complement these results and to further investigate a possible role of Rh7 in photoreception, we conducted misexpression experiments and studied the *rh7* knockout mutant and different transgenic lines at the histological (by analyzing the eye morphology) and behavioral levels.

3.5.1 Role of Rh7 in photoreceptor development

As already mentioned in the introduction, proper maturation, transport and localization of Rh1 are crucial for normal photoreceptor development and maintenance (Colley et al., 1995; Kumar and Ready, 1995; Kurada and O´Tousa, 1995).

Ectopic expression of Rh7 in photoreceptors R1-R6 using *Rh1-GAL4; UAS-rh7#8* did not produce a phenotype in the adult compound eye. The arrangement of ommatidal photoreceptors seemed unaffected and no other structural differences in comparison to the driver or to the effector line could be observed in toluidine blue-stained paraffin sections. The same was true for the expression of Rh7 in all photoreceptor cells which was analyzed in semithin sections of *GMR-GAL4; UAS-rh7#10.3* heads. In both cases, the actual presence of Rh7 could unfortunately not be confirmed by IHC. In contrast,

the size of the retinal and the laminar layer was reduced in paraffin head sections of *GMR-GAL4; UAS-rh7#8* flies, but this was also observed in about half of the sectioned *GMR*-GAL4 controls. Therefore, we repeated the misexpression experiment crossing this UAS line to *longGMR*-GAL4 (*lGMR*) flies for which a longer glass site was used, and that was reported to be more photoreceptor-specific than the normal *GMR*-GAL4 (Wernet et al., 2003). Nevertheless, the results from paraffin head sections of *lGMR-GAL4; UAS-rh7#8* and the corresponding control flies were ambiguous: Already the driver line alone, which was homozygous for the construct, displayed degenerative eye phenotypes to some extent, as described for *GMR*-GAL4, and, as exemplarily shown in Figure 28A. As expected, the eye structure in UAS-*rh7#8* was not affected by the presence of the UAS construct (B). Anyway, *lGMR-GAL4; UAS-rh7#8* sections were similar to *lGMR*-GAL4 and we observed phenotypes ranging from perfectly normal (C) to clearly degenerated (D). However, the most severely affected eye structures in *lGMR-GAL4; UAS-rh7#8* flies looked still better than the worst ones in *lGMR*-GAL4 controls. Thus, cause and effect relationships could not be determined. Consequently, misexpression experiments did not promote characterization of Rh7.

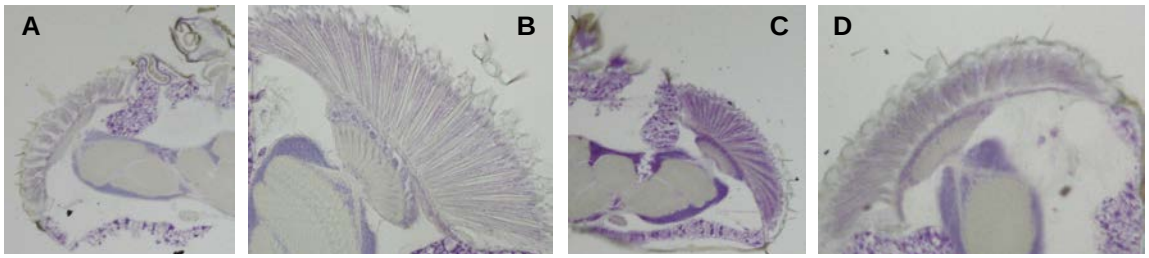

Figure 28: *GMR*-GAL4 and *GMR-GAL4; UAS-rh7#8* partly show degenerative eye phenotypes.
A-D: Toluidine blue staining of adult horizontal head sections.
A: Retina and lamina are severely reduced in thickness and the ommatidal arrangement seems clearly disturbed in the homozygous *GMR*-GAL4 driver line.
B: UAS-*rh7#8* flies show an intact, control-like structured retinal and laminar layer.
C+D: The eye phenotype in *GMR-GAL4; UAS-rh7#8* ranges from normal (C) to degenerated (D).

Additionally, we checked head sections of genotypes that were frequently used in our experiments. Overview images of control strains, revertant and backcross, but also of *rh7*^{0} mutants showed intact eye structures of usual size and composition. Independent from *ninaE* background, the retinal morphology seemed slightly altered in *Rh1-Rh7* in a way that the ommatidal arrangement was not always as regular as in the control. Accordingly, small gaps between retinal photoreceptor cells have been observed from time to time in semithin sections (Bachleitner, 2008).

Degeneration of R1-R6 rhabdomeres – or rather the resulting structural disturbance in the arrangement of the retinal photoreceptors – which is present in mutant flies lacking the visual pigment Rh1 (*ninaE*) could be visualized in paraffin sections (Fig. 29A, A').

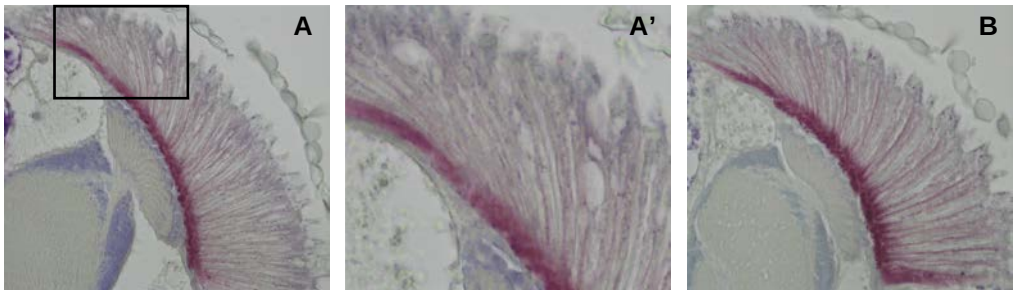

Figure 29: Expression of Rh7 in R1-R6 prevents retinal degeneration of photoreceptors in *Rh1-Rh7; ninaE* flies.

A+B: Toluidine blue staining of adult horizontal head sections.

A: The retinal pattern is disturbed and, as shown in the magnification of the selected area aside (A'), gaps are present in the retina of *ninaE* mutants.

B: Expression of Rh7 in place of Rh1 (R1-R6) is able to rescue the *ninaE* phenotype.

Expression of Rh7 in place of Rh1 principally rescued the mutant phenotype in *Rh1-Rh7; ninaE* retinas. (B). Therefore, Rh7 seems indeed able to functionally replace Rh1 in morphogenesis and maintenance of R1-R6 rhabdomeres.

3.5.2 Behavioral characterization of Rh7

Rh7 knockout flies did not display any obvious morphological phenotype, thus making it difficult to propose a function in photoreception. Nevertheless, $rh7^{0}$ mutants showed altered photoreceptor sensitivity in the ERG, suggesting that Rh7 might be expressed in ommatidal photoreceptors R1-R6 (Grebler, 2010).

Therefore, we tested $rh7^{0}$ mutants for motion detection, which is mediated by these outer photoreceptors (Yamaguchi et al., 2008) as well as for circadian photoreception, which is dependent on the retinal photoreceptors and CRY.

3.5.2.1 Motion vision

Motion vision was investigated by determination of the optomotor response (OR) in a rather simple setup, based on a striped cylinder with a plexiglass arena located at its center (see 2.3.4.4). The absence of Rh7 did not affect motion vision. In fact, *rh7* null mutants performed like revertant controls (Fig. 30A).

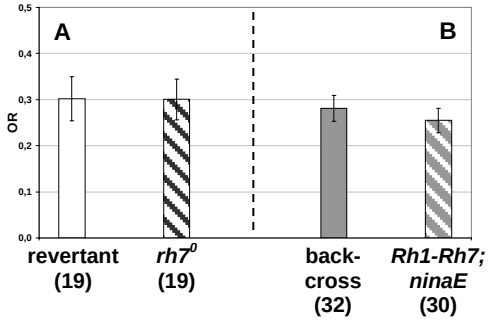

Figure 30: Optomotor response (OR) in *rh7^0* (A) and *Rh1-Rh7; ninaE* (B) flies in comparison to respective controls.

A: The loss of Rh7 in *rh7^0* does not affect the OR.

B: The presence of Rh7 in R1-R6 is able to mediate the OR in *Rh1-Rh7; ninaE* flies.

In parenthesis: No. of flies tested.

Next, we tested *Rh1-Rh7; ninaE* flies to find out if Rh7 is able to overtake the function of Rh1 in motion detection and indeed, the averaged response scores did not differ significantly from control values (B). Thus, Rh7 must somehow be able to initiate the downstream motion vision signaling pathway of Rh1.

3.5.2.2 Circadian photoreception

3.5.2.2.1 Blue-light shift experiments

An action spectrum originating from ERG dose-response curves to colored light of distinct wavelengths showed that *Rh1-Rh7; ninaE* flies are most sensitive to blue light of ~470 nm and have a second peak in the UV (< 370 nm; Grebler, unpublished data). Altogether, the progression of the curve is very similar to the action spectrum obtained from backcross controls, which basically reflects the sensitivity of Rh1 as the major photoreceptor in *Drosophila*. The blue-light photoreceptor CRY and six well-described rhodopsins with different spectral sensitivity contribute to photic circadian entrainment. For this reason, it is rather difficult to investigate a possible effect of the loss of Rh7 on the circadian clock and only specific light conditions might allow for detection of subtle differences. The locomotor activity is a robust behavioral output of the circadian clock and easy to record (see 2.3.4.1), and was thus used to address this topic. Due to their high light sensitivity, wild-type flies are able to immediately resynchronize their activity rhythms to a shifted LD cycle. As described in section 2.3.4.3, shift experiments were carried out under extremely low irradiances to decelerate entrainment and at monochromatic light of ~470 nm and ~400 nm, because only at these two wavelengths little differences in the shape of the action spectra were present between Rh1 and Rh7 expressing flies (v. s.). We tested *Rh1-Rh7* flies which were more light-sensitive in ERG dose-response curve recordings than controls due to the additional presence of Rh7 in R1-R6 rhabdomeres (Grebler, unpublished data) and *rh7^0* mutants.

As exemplarily shown in representative actograms of individual flies (Fig. 31), the two genotypes, revertant and *rh7*^{0}, require a different number of days to re-entrain their activity rhythms to the 6 h shifted – in this case delayed – LD 12:12 cycle.

Figure 31: Resynchronization of activity rhythms to a 6 h delay of the blue LD 12:12 cycle.

The locomotor activity rhythm of two representative, individual flies, revertant control and *rh7*^{0}, is displayed in a double-plotted actogram. After 6 days of entrainment, a 6 h delay of the blue LD 12:12 cycle was introduced as indicated by the blue background pattern.

The control fly re-entrains to the shifted LD cycle within ~3 days, whereas the *rh7*^{0} mutant needs ~7 days.

The number of days the flies needed for entrainment was visually determined from single-fly actograms, averaged and plotted for the different genotypes and conditions tested. At 470 nm (Fig 32B), *rh7* null mutants needed significantly longer to re-entrain to both the 6 h advanced and 6 h delayed LD 12:12 cycle. At 400 nm (A), the same tendency could be observed and re-entrainment was slower in comparison to the longer wavelength condition. In general, flies tended to resynchronize slightly faster to shift advances than to delays. This is in accordance with the period lengths of these genotypes which ranged between 23.1 h and 23.4 h and were therefore shorter than 24 h.

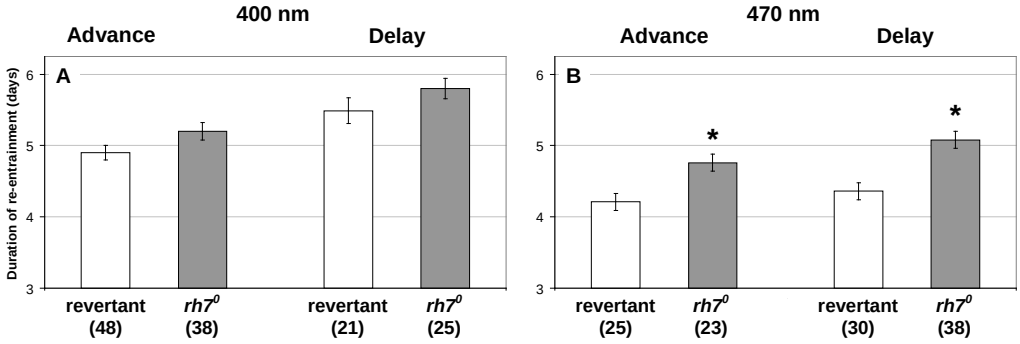

Figure 32: Re-entrainment duration in *rh7*^{0} and control flies under blue LD 12:12 cycles of low intensity.

Control and *rh7*^{0} flies required a different number of days to resynchronize their locomotor activity rhythm to a 6 h shift – either advance or delay – of the blue LD 12:12 cycle.

Under blue LD 12:12 cycles of 470 nm and low light intensity (0.0006 µW/cm^2), resynchronization took significantly longer in *rh7*^{0} mutants ($p < 0.01$) independent from the shifting direction (B). Under UV conditions (400 nm; 0.0004 µW/cm^2), the same tendency could be observed (A).

In parenthesis: No. of flies tested. Error bars represent ± SEM.

Next, we tested and analyzed *Rh1-Rh7* flies under the same conditions. As shown in Figure 33, the re-entrainment duration was different in comparison to control flies at

470 nm (B) but not at 400 nm (A). Surprisingly, additional expression of Rh7 in R1-R6 resulted in a slower resynchronization of the activity rhythm to both advances and delays instead of the expected acceleration.

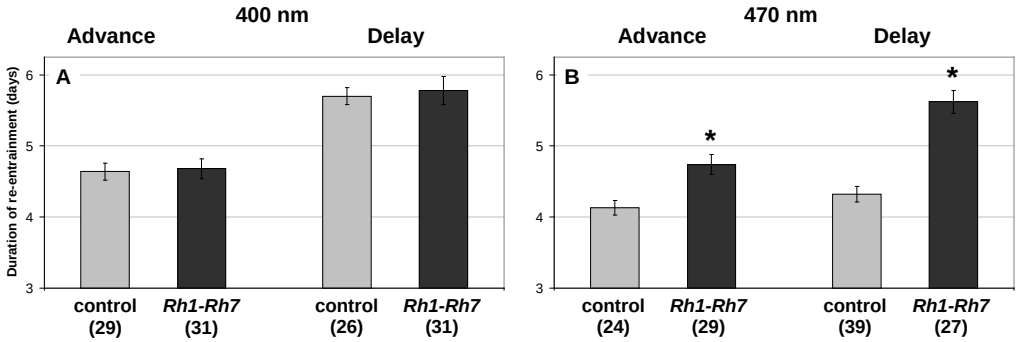

Figure 33: Re-entrainment duration in *Rh1-Rh7* and control flies under blue LD 12:12 cycles of low intensity.

Under blue LD 12:12 cycles of 400 nm and low irradiance (0.0004 µW/cm^2), the average speed of resynchronization to 6 h shifts – either advance or delay – was similar in control (backcross) and *Rh1-Rh7* flies (A). At longer wavelength conditions (470 nm; 0.0006 µW/cm ^{2}), resynchronization took significantly longer in *Rh1-Rh7* ($p < 0.01$) independent from the shifting direction (B).

In parenthesis: No. of flies tested. Error bars represent ± SEM.

To give an overview over the results, experimental data was summarized in Table 16.

Table 16: Re-entrainment duration in *rh7^0*, *Rh1-Rh7* and respective controls (revertant and backcross) after 6-h advances or delays of the blue (400 nm and 470 nm) LD 12:12 cycle.

Values in bold are significantly different ($p < 0.01$) from respective control values. For details, see legends of previous figures.

Genotype	Average re-entrainment duration at ~400 nm (days ± SEM)		Average re-entrainment duration at ~470 nm (days ± SEM)	
	6-h advance	6-h delay	6-h advance	6-h delay
Revertant	4.9 ± 0.10	5.5 ± 0.18	4.2 ± 0.12	4.4 ± 0.12
Rh7^0	5.2 ± 0.12	5.8 ± 0.14	**4.8 ± 0.12**	**5.1 ± 0.12**
Backcross	4.6 ± 0.12	5.7 ± 0.12	3.1 ± 0.10	4.3 ± 0.11
Rh1-Rh7	4.7 ± 0.14	5.8 ± 0.20	**4.7 ± 0.14**	**5.6 ± 0.16**

Thus, Rh7 seems to somehow be able to contribute to the light input into the circadian clock, although extreme conditions (monochromatic light of low intensity) were chosen to reveal these effects.

3.5.2.2.2 Entrainment in *rh7^0* mutants

To collect further information about a circadian photoreceptive function of Rh7 in wild-type flies, we investigated locomotor activity rhythms of *rh7* null mutants under various standard conditions. For this purpose, we used both a home-made activity recording system, referred to as cuvette system and a commercially available system, referred to

as DAM System in the following (for details see 2.3.4.1). At first, we applied LD 12:12 cycles of different light intensities, ranging from 10 lux up to 1000 lux, provided by computer-controlled white-light LEDs. The recorded locomotor activity was initially displayed in a double-plotted actogram for each single fly and then plotted in an average daily activity profile (hereinafter also referred to as daily average) for each genotype including data of several days, flies and experiments (see section 2.3.4.2.1).

3.5.2.2.2.1 Entrainment to LD and LM cycles

Under LD 12:12 conditions and independent from the irradiance, *rh7*^{0} flies showed a typical, wild-type-like bimodal activity pattern comprising morning and evening activity peaks separated by low activity levels around midday and during the night (Fig. 34). The midday trough was more prominent in *rh7*^{0} flies under all three light intensities. In comparison to control flies (revertant), the prolongation of this “siesta” seemed to be caused by an overall reduction of morning activity (MA) levels and an earlier decrease of activity.

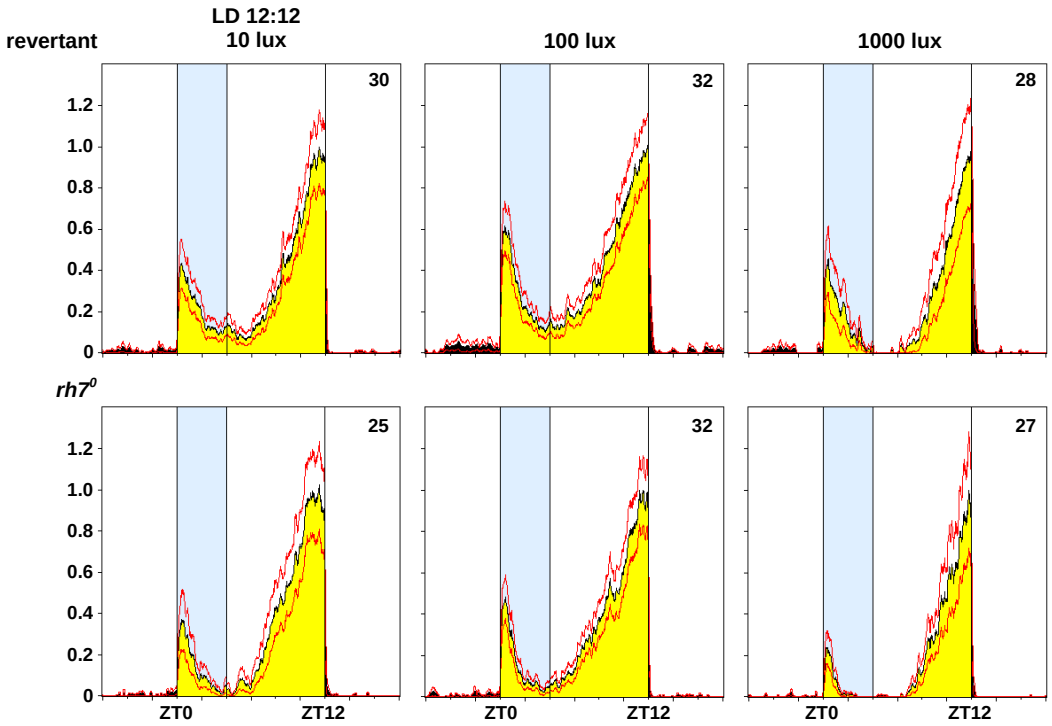

Figure 34: Cuvette system recording-based daily averages of *rh7*^{0} and revertant flies under LD 12:12 cycles of different light intensities.

Mutant and control flies were monitored under LD 12:12 cycles at irradiances of 10, 100 and 1000 lux. Infrared light beam crosses were recorded in 1-min bins and daily averages calculated as described under 2.3.4.2.1. Two vertical lines label lights-on (ZT0) and lights-off (ZT12), respectively. The blue background indicates the 4-h interval subsequent to lights-on (ZT0-ZT4) used for calculation of MA levels.

Numbers: No. of flies tested. Red curves represent ± SEM. For details, see text**.**

To quantify these effects, we calculated average MA levels (number of light beam crosses) within a 4-h interval subsequent to lights-on (ZT0-ZT4) and the offset of MA, as described in 2.3.4.2.2 and 2.3.4.2.3. In *rh7* null mutants, the MA was significantly reduced at 10 and 100 lux ($p < 0.05$), and the same tendency could be observed at 1000 lux irradiance (Table 17 and Fig. 36). The MA offset was significantly advanced (by 1.2 h) in *rh7*^{0} under 1000 lux conditions ($p < 0.001$; see Table 19). Unfortunately, the activity levels during midday were too high at lower irradiances in the majority of flies (especially in the controls) to reliably determine the offset of MA.

Experiments carried out under LD 12:12 conditions of ~1000 lux light intensity with a different activity recording system, the DAM System, revealed another effect on the MA bout (Fig. 35). In contrast to revertants, activity in *rh7*^{0} started to rise ~2.5 h before lights-on, resulting in a significantly higher ($p < 0.05$) average activity level within a preceding 3-h interval (ZT21-ZT0).

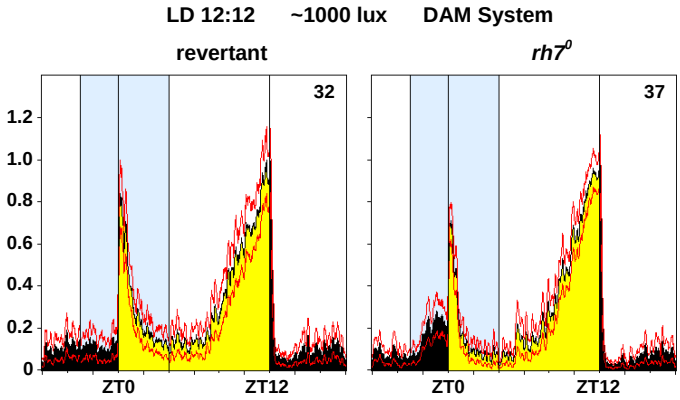

Figure 35: DAM System recording-based daily averages of *rh7*^{0} and revertant flies.

Mutant and control flies were monitored under LD 12:12 cycles of ~1000 lux intensity. Infrared light beam crosses were recorded in 1-min bins and daily averages calculated as described in section under 2.3.4.2.1. Two vertical lines label lights-on (ZT0) and lights-off (ZT12), respectively. The blue background extends over the intervals – 3 h before (ZT21-ZT0) and 4 h after (ZT0-4) lights-on – used for calculation of MA levels.

Numbers: No. of flies tested. Red curves represent ± SEM. For details, see text.

To allow for a direct comparison and to confirm our daily average-based statements, calculations of MA levels were summarized in Table 17 and plotted in Figure 36 for both recording systems.

Table 17: Relative average morning activity (MA) levels in *rh7*^{0} and revertant flies under LD 12:12 conditions.

Mutant and control flies were monitored under LD 12:12 cycles and increasing light intensities of 10, 100 and 1000 lux. Daily averages were determined and MA levels calculated within a 4-h interval subsequent to lights-on (ZT0-ZT4).

DAM: DAM System-based recording. For this data, the average MA level is additionally shown for a 3-h period prior to lights-on (ZT21-ZT0).

Values in bold are significantly different ($p < 0.05$) from respective control values.

Genotype	Light intensity LD 12:12	MA levels (average sum of beam crosses ± SEM)	
		4-h interval after lights-on (ZT0-ZT4)	
Revertant (n = 30)	**10 lux**	1637 ± 284	
Rh7^0 **(n = 25)**		**840 ± 215**	
Revertant (n = 32)	**100 lux**	2614 ± 242	
Rh7^0 **(n = 32)**		**1351 ± 151**	
Revertant (n = 28)	**1000 lux**	909 ± 196	
Rh7^0 **(n = 27)**		395 ± 69	
DAM System		**4-h interval after lights-on (ZT0-ZT4)**	**3-h interval before lights-on (ZT21-ZT0)**
Revertant (n = 32)	**1000 lux**	1375 ± 96	377 ± 35
Rh7^0 **(n = 37)**		1189 ± 89	**822 ± 126**

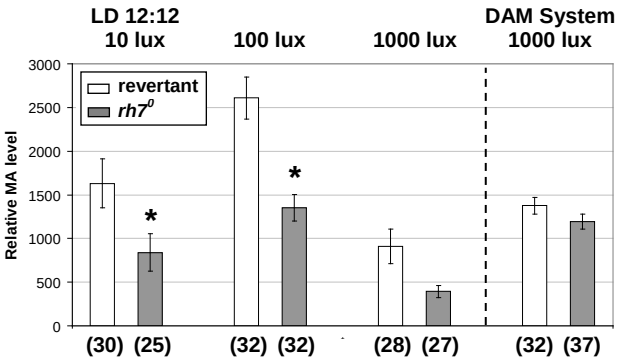

Figure 36: Relative average MA levels of *rh7^0* and revertant flies under LD 12:12 cycles of different light intensities.

Mutant and control flies were monitored under LD 12:12 cycles of 10, 100 and 1000 lux intensity and daily averages generated. MA levels were plotted within a 4-h interval subsequent to lights-on (ZT0-ZT4). Separated by a dashed line, MA levels calculated from DAM System-based daily averages (~1000 lux) are shown to the right in comparison. In *rh7^0*, MA levels are significantly reduced at 10 ($p = 0.01$) and 100 lux ($p < 0.001$) conditions, and the same tendency is present at 1000 lux in the data from both recording systems.

In parenthesis: No. of flies tested. Error bars represent ± SEM.

To further investigate these effects, we repeated the experiments under “moonlight” (M) conditions and entrained the flies to LM 12:12 cycles applying nocturnal dim light of 0.01 lux intensity. Low light intensities during the night have previously been shown to advance the morning and to delay the evening activity into the moonlight phase (Bachleitner et al., 2007). In general, we observed this shifting behavior in *rh7^0* flies,

although, like under LD conditions, levels of MA and the following midday break were different from revertant controls (Fig. 37).

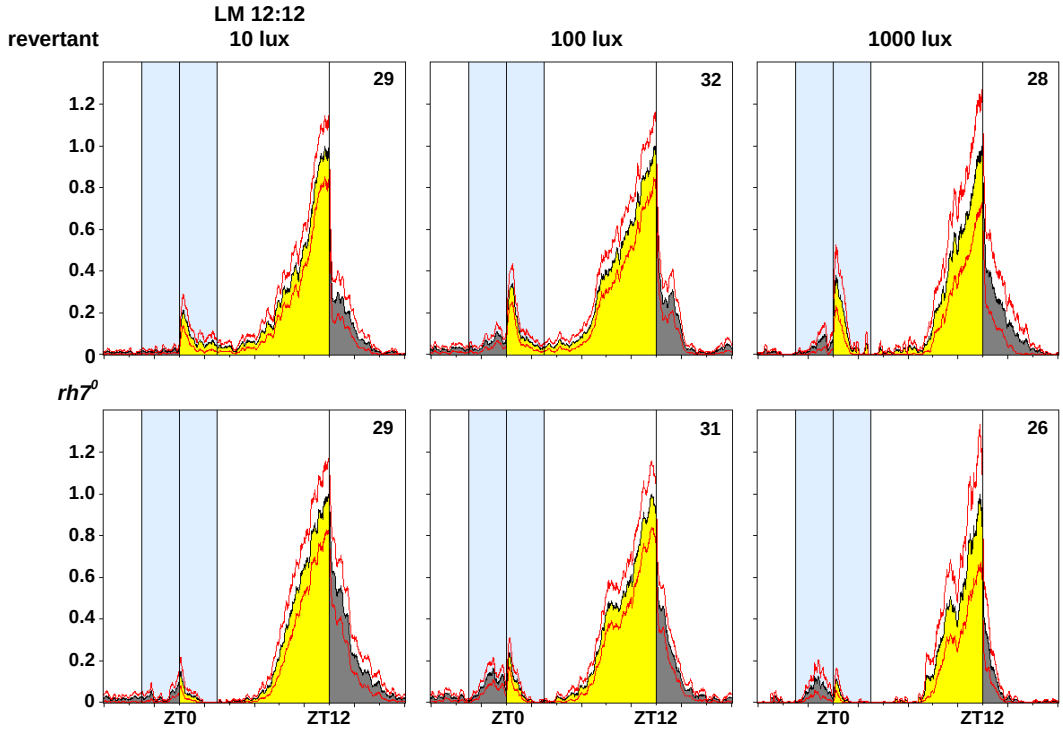

Figure 37: Cuvette system recording-based daily averages of *rh7*^{0} and revertant flies under LM 12:12 cycles of different light intensities.

Mutant and control flies were monitored under LM 12:12 cycles at irradiances of 10, 100 and 1000 lux during the light and 0.01 lux during the moonlight phase. Infrared light beam crosses were recorded in 1-min bins and daily averages calculated as described under 2.3.4.2.1. Two vertical lines label lights-on (ZT0) and lights-off (ZT12), respectively. The blue background covering ZT21-ZT0 and ZT0-ZT3 indicates the two 3-h intervals used for calculation of MA levels.

Numbers: No. of flies tested. Red curves represent ± SEM. For details, see text.

We determined and plotted average MA levels within a 6-h period composed of a 3-h interval preceding (ZT21-ZT0) and following (ZT0-ZT3) lights-on (Table 18 and Fig. 38). By trend, the total MA (ZT21-ZT3) was reduced in the mutants in comparison to controls ($p = 0.5$ at 10 lux). Remarkably, their level of activity was significantly lower after lights-on under all irradiances ($p < 0.05$), whereas the activity prior to lights-on tended to be elevated. We previously showed daily averages from DAM System recording for LD conditions. Interestingly, the level of MA was similarly affected in this experiment and therefore, data was included in the summary table (Table 18).

Table 18: Relative average MA levels in *rh7*^{0} and revertant flies under LM 12:12 conditions.

Mutant and control flies were monitored under LM 12:12 cycles of 10, 100 and 1000 lux during the light and 0.01 lux during the moonlight phase. Daily averages were determined and MA levels calculated within a 6-h period comprising a 3-h interval before (ZT21-ZT0) and after (ZT0-ZT3) lights-on. MA levels calculated from DAM System recordings (LD, 1000 lux) were incorporated.

Values in bold are significantly different ($p < 0.05$) from respective control values.

Genotype	Light intensity LD 12:12	MA levels (average sum of beam crosses ± SEM)		
		3-h interval before lights-on (ZT21-ZT0)	3-h interval after lights-on (ZT0-ZT3)	total 6-h interval (ZT21-ZT3)
Revertant (n = 29)	**10 lux**	102 ± 29	505 ± 159	607 ± 172
***Rh7*^{0} (n = 29)**		140 ± 44	**135 ± 50**	**275 ± 86**
Revertant (n = 32)	**100 lux**	358 ± 62	817 ± 131	1175 ± 168
***Rh7*^{0} (n = 31)**		587 ± 103	**439 ± 93**	1026 ± 166
Revertant (n = 28)	**1000 lux**	122 ± 35	373 ± 85	494 ± 114
***Rh7*^{0} (n = 26)**		257 ± 71	**110 ± 34**	367 ± 95
Revertant (n = 32)	**DAM 1000 lux**	377 ± 35	1221 ± 89	1598 ± 94
***Rh7*^{0} (n = 37)**		**822 ± 126**	1090 ± 87	1913 ± 168

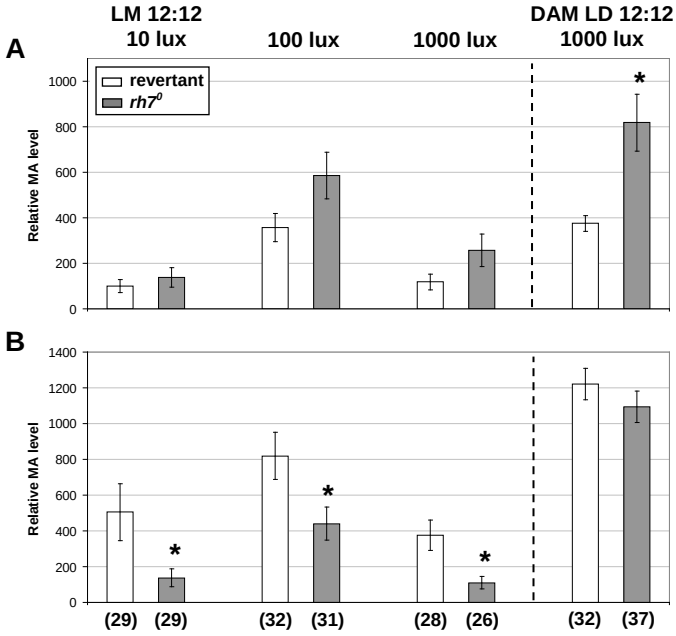

Figure 38: Relative average MA levels within a 3-h interval (A) before (ZT21-ZT0) and (B) after (ZT0-ZT3) lights-on.

Mutant and control flies were monitored under LM 12:12 cycles of 10, 100 and 1000 lux intensity during the light and 0.01 lux during the moonlight phase. We calculated average MA levels from daily averages within two 3-h intervals. By tendency, *rh7*^{0} flies increased their MA before lights-on (A). On the contrary, they showed significantly reduced MA levels ($p \leq 0.01$) subsequent to lights-on (B).

Histograms separated by dashed lines: Similar effects on the MA level were observed under LD 12:12 cycles of ~1000 lux intensity in DAM System-based recordings.

In parenthesis: No. of flies tested. Error bars represent ± SEM.

Furthermore, the MA offset was significantly advanced in *rh7*^{0} mutants – up to 1.2 h in comparison to controls – independent from the irradiance ($p < 0.01$), as summarized in Table 19 and plotted in Figure 39 (including the evaluable 1000-lux LD experiment).

Table 19: Average MA offset in *rh7*^{0} and revertant flies under LM 12:12 conditions.

Mutant and control flies were monitored under LM 12:12 cycles of increasing light intensities (10, 100 and 1000 lux) during the light and 0.01 lux during the moonlight phase. Average MA offsets were calculated as described under 2.3.4.2.3. In addition, offsets from the 1000-lux LD 12:12 experiment are shown.

Values in bold are significantly different ($p < 0.01$) from respective control values.

Genotype	Light program	Average MA offset (ZT ± SEM)	Difference (h)
Revertant (n = 25)	**LM 12:12 10 lux**	1.70 ± 0.20	0.96
***Rh7*^{0} (n = 20)**		**0.75 ± 0.25**	
Revertant (n = 31)	**LM 12:12 100 lux**	2.07 ± 0.13	0.85
***Rh7*^{0} (n = 30)**		**1.22 ± 0.12**	
Revertant (n =24)	**LM 12:12 1000 lux**	1.22 ± 0.12	0.60
***Rh7*^{0} (n = 18)**		**0.62 ± 0.13**	
Revertant (n = 28)	**LD 12:12 1000 lux**	2.80 ± 0.18	1.23
***Rh7*^{0} (n = 26)**		**1.57 ± 0.13**	

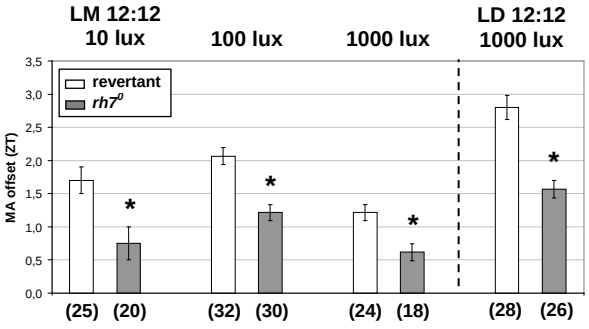

Figure 39: Average MA offset in *rh7*^{0} and revertant flies under LM 12:12 conditions.

Mutant and control flies were monitored under LM 12:12 cycles of 10, 100 and 1000 lux intensity during the light and 0.01 lux during the moonlight phase. Average MA offsets were calculated from single fly activity profiles, averaged and plotted in reference to lights-on (ZT0). Independent from the irradiance, the MA offset occurred significantly earlier in *rh7*^{0} ($p < 0.01$) with advances ranging from 0.6 to 0.95 h.

An even stronger effect on the MA offset in *rh7*^{0} (1.2 h advance) was present under LD cycles of 1000 lux intensity (see histograms separated by dashed lines).

In parenthesis: No. of flies tested. Error bars represent ± SEM.

Despite the presence of all other circadian photoreceptors, *rh7*^{0} mutants unexpectedly displayed differences in their locomotor activity rhythms under both LD and LM 12:12 conditions. In LD, the average MA in *rh7*^{0} was significantly decreased, causing a more pronounced siesta. Under LM cycles, *rh7* null mutants shifted their average MA further into the moonlight phase than control flies. As a consequence, the level of MA was significantly reduced subsequent to lights-on and the offset of activity was significantly advanced, resulting in a more prominent midday trough and thereby confirming our LD results.

3.5.2.2.3 Entrainment in *rh7*^{0} *cry*^{01} double mutants

To further investigate the role of Rh7 in light entrainment, we created *rh7*^{0} *cry*^{01} double mutants by recombination (see section 2.2.4), thereby additionally eliminating CRY, a blue-light photopigment regarded to be the main circadian photoreceptor in *Drosophila*. Unless stated otherwise, activity monitoring was carried out applying light intensities of 1000 lux during the experimental day, because all genotypes showed higher and thus easier to analyze activity levels under this irradiance. In general, the activity pattern of the obtained recombinant strains (*rh7*^{0} *cry*^{01}#39 and #112) was highly similar under the investigated conditions. Therefore, data was pooled for calculation of average daily activity profiles prior to normalization and smoothing.

3.5.2.2.3.1 Entrainment to LD and LM cycles

Under LD 12:12 conditions (Fig. 40), average locomotor activity levels were low both in *cry*^{01} and *rh7*^{0} *cry*^{01} mutants at the beginning of the light phase. The timing and the shape of the MA peak strongly resembled those of *rh7*^{0} mutants. Nevertheless, the average MA within a 4-h interval following lights-on (ZT0-ZT4) was further reduced in the double mutant ($p < 0.01$) and the average MA offset (ZT1.0) occurred significantly earlier ($p < 0.05$) in comparison to both single mutants (*cry*^{01}: ZT1.3 and *rh7*^{0}: ZT1.6). The latter did not differ significantly neither in their average MA level nor in their offset of activity (Fig. 41A and B).

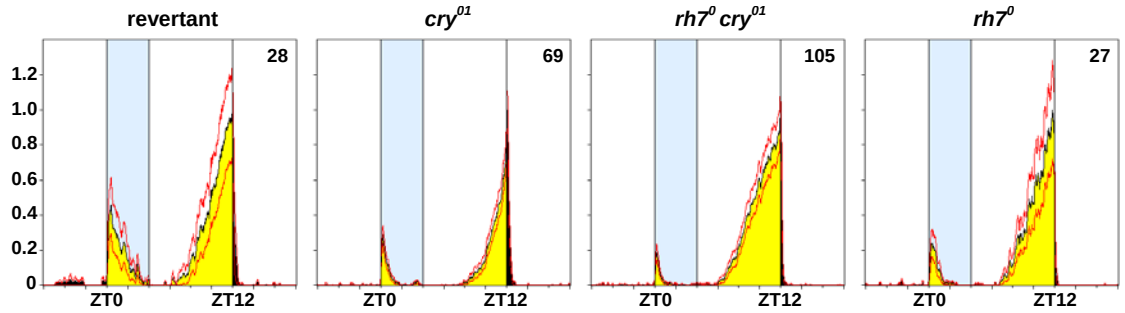

Figure 40: Cuvette system recording-based daily averages of revertant, *rh7⁰*, *cry⁰¹* and *rh7⁰ cry⁰¹* flies under LD 12:12 conditions.

Flies were monitored under LD 12:12 cycles of 1000 lux intensity. Infrared light beam crosses were recorded in 1-min bins and daily averages calculated as described under 2.3.4.2.1. Two vertical lines label lights-on (ZT0) and lights-off (ZT12), respectively. The blue background indicates the 4-h interval subsequent to lights-on (ZT0-ZT4) used for calculation of MA levels.

Numbers: No. of flies tested. Red curves represent ± SEM. For details, see text.

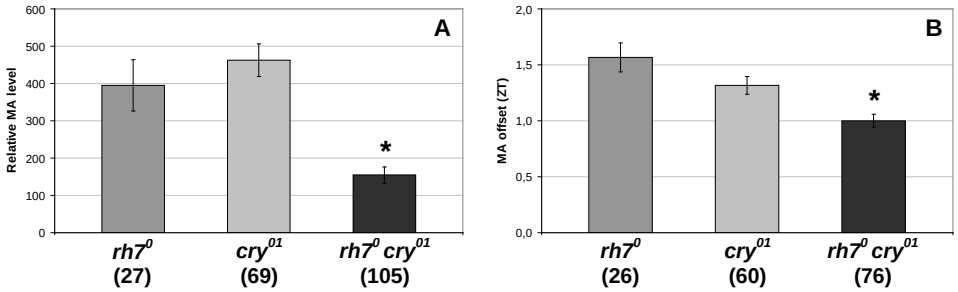

Figure 41: Relative average MA levels (A) and average MA offset (B) in *rh7⁰*, *cry⁰¹* and *rh7⁰ cry⁰¹* mutants.

Flies were monitored under LD 12:12 cycles of 1000 lux intensity. Average MA levels (A) were calculated and plotted within a 4-h interval subsequent to lights-on (ZT0-ZT4). The MA offset (B) was determined from single-fly activity profiles, averaged and transferred into ZT in reference to lights-on (ZT0). In comparison to both single mutants, MA levels were further reduced ($p < 0.01$) and the offset of activity was further advanced ($p < 0.05$) in *rh7⁰ cry⁰¹* double mutants.

In parenthesis: No. of flies tested. Error bars represent ± SEM.

Cry⁺ control flies for *cry⁰¹* mutants (Dolezelova et al., 2007) were additionally tested, but showed a revertant-similar average MA level (941 ± 176) and MA offset (2.5 ± 0.1). For this reason, revertant flies served as controls for *cry⁰¹* in all following experiments to reduce the number of test genotypes. In the current LD experiment, the level of MA was reduced in *cry⁰¹* mutants in comparison to *cry⁺* and revertant controls and their offset of activity was significantly advanced ($p < 0.001$).

Like in *rh7⁰* mutants, we analyzed the MA in DAM System recording-derived daily average activity profiles by calculation of average activity levels prior (ZT21-ZT0) and subsequent (ZT0-ZT3) to lights-on (Fig. 42).

Except for an increased MA ($p = 0.01$) after lights-on, activity levels in *cry⁰¹* and *rh7⁰* were similar and elevated in both genotypes before lights-on. Interestingly, *rh7⁰ cry⁰¹*

lacked this increase in activity and thus showed less MA within the corresponding 3-h period. In comparison to *cry*^{01} (but not to *rh7*^{0}), the level of activity was significantly decreased in the recombinants ($p \leq 0.001$) in all investigated intervals (Fig. 43A, Table 20).

In contrast to the previous calculation (4-h interval), MA following lights-on was not significantly reduced in *cry*^{01} in comparison to revertant controls resulting – mainly due to increased activity levels before lights-on – in a higher total (6-h) activity ($p < 0.001$).

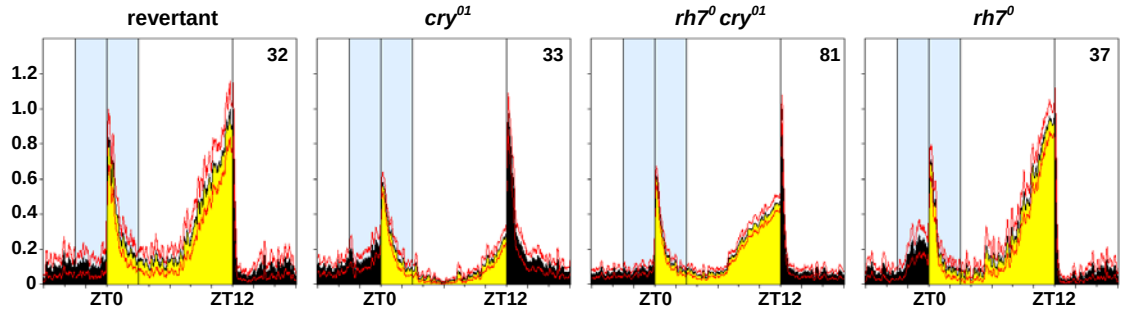

Figure 42: DAM System recording-based daily averages of revertant, *rh7*^{0}, *cry*^{01} and *rh7*^{0} *cry*^{01} flies under LD 12:12 conditions.

Flies were monitored under LD 12:12 cycles of ~1000 lux intensity. Infrared light beam crosses were recorded in 1-min bins and daily averages calculated as described under 2.3.4.2.1. Two vertical lines label lights-on (ZT0) and lights-off (ZT12), respectively. The blue background indicates the intervals used for calculation of MA levels – 3 h before (ZT21-ZT0) and after (ZT0-3) lights-on.

Numbers: No. of flies tested. Red curves represent ± SEM. For details, see text.

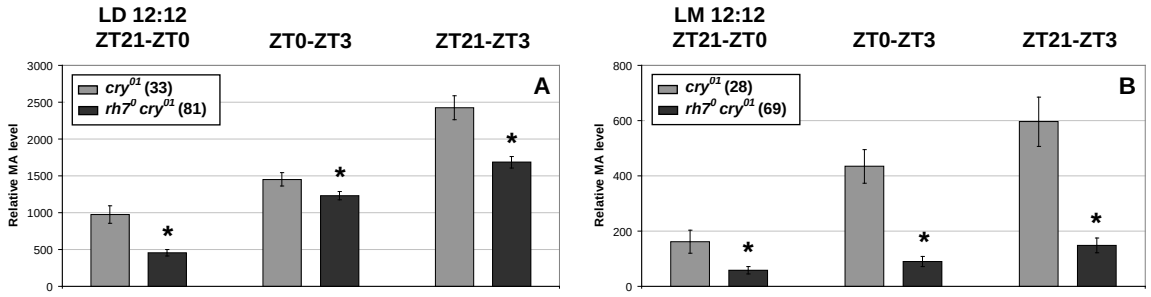

Figure 43: Relative average MA levels in *cry*^{01} and *rh7*^{0} *cry*^{01} mutants under LD and LM 12:12 conditions.

Flies were monitored under LD (A) or LM (B) 12:12 cycles of 1000 lux intensity during the light and (in B) 0.01 lux during the moonlight phase. Average MA levels were calculated from single-fly daily averages within three intervals – 3 h before (ZT21-ZT0) and after lights-on (ZT0-ZT3) and the total 6-h interval (ZT21-ZT3). Under both conditions and within all intervals, rh70 cry01 showed significantly reduced average MA levels in direct comparison to cry01 ($p < 0.05$).

In parenthesis: No. of flies tested. Error bars represent ± SEM.

Corresponding experiments under LM cycles (Fig. 44) largely confirmed our previous results. In comparison to single mutants, especially to *cry*^{01} ($p < 0.05$), average levels of MA were further reduced in the intervals of interest in *rh7*^{0} *cry*^{01} (Fig. 43B, Table 20).

However, their offset of activity (ZT0.8) was not affected by the reduction of MA levels and lay in between the offsets determined for *rh7*^{0} (ZT0.62) and *cry*^{01} (ZT0.95).

As observed under LD conditions (DAM System), average activity levels in *cry*^{01} were significantly elevated ($p < 0.001$) subsequent to lights-on (ZT0-ZT3), but otherwise similar to *rh7*^{0} including the MA offset (cuvette system).

Although the same tendencies like in LD were present, the MA was not significantly increased in *cry*^{01} mutants under LM conditions and also the offset of activity was not significantly advanced compared to revertant controls.

Present experimental data (average MA levels and offsets) is summarized in Table 20 and Table 21.

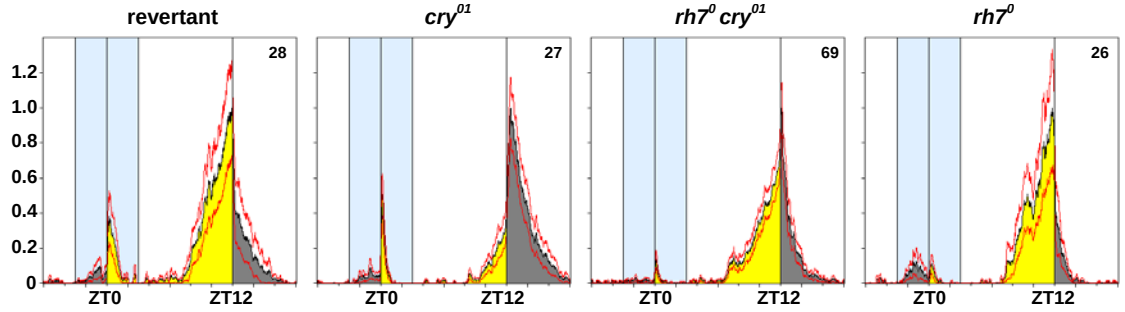

Figure 44: Cuvette system recording-based daily averages of revertant, *rh7*^{0}, *cry*^{01} and *rh7*^{0} *cry*^{01} flies under LM 12:12 conditions.

Flies were monitored under LM 12:12 cycles of 1000 lux intensity during the light and 0.01 lux during the moonlight phase. Infrared light beam crosses were recorded in 1-min bins and daily averages calculated as described under 2.3.4.2.1. Vertical lines label lights-on (ZT0) and lights-off (ZT12), respectively.

Numbers: No. of flies tested. Red curves represent ± SEM. For details, see text.

Table 20: Relative average MA levels in revertant, *rh7*^{0}, *cry*^{01} and *rh7*^{0} *cry*^{01} flies under LD and LM 12:12 conditions.

Flies were monitored under LD and LM 12:12 cycles of 1000 lux intensity during the light and (in LM) 0.01 lux during the moonlight phase. Daily averages were determined and MA levels calculated within a 6-h interval comprising a 3-h interval before (ZT21-ZT0) and after (ZT0-ZT3) lights-on.

Values in bold are significantly different ($p < 0.001$) from respective control values (*rh7*^{0} and *cry*^{01} mutants served as controls for recombinants and revertant as control for *cry*^{01}).

Genotype	Light program	MA levels (average sum of beam crosses ± SEM)		
		3-h interval before lights-on (ZT21-ZT0)	3-h interval after lights-on (ZT0-ZT3)	total 6-h interval (ZT21-ZT3)
Revertant (n = 32)	**DAM LD 12:12 1000 lux**	377 ± 35	1221 ± 89	1598 ± 94
***Rh7*^{0} (n = 37)**		822 ± 126	1090 ± 87	1913 ± 168
***Cry*^{01} (n = 33)**		**975 ± 118**	1447 ± 91	**2422 ± 164**
***Rh7*^{0} *cry*^{01} (n = 81)**		457 ± 43	1228 ± 57	1685 ± 76

Revertant (n = 28)	**LM 12:12 1000 lux / 0.01 lux**	119 ± 34	376 ± 85	494 ± 114
***Rh7*^{0} (n = 26)**		257 ± 71	111 ± 34	367 ± 95
***Cry*^{01} (n = 28)**		162 ± 42	435 ± 61	596 ± 89
***Rh7*^{0} *cry*^{01} (n = 26)**		59 ± 13	90 ± 19	149 ± 27

Table 21: Average MA offset in revertant, *rh7*^{0}, *cry*^{01} and *rh7*^{0} *cry*^{01} flies under LD and LM 12:12 conditions.

Flies were monitored under LD and LM 12:12 cycles of 1000 lux during the light and (in LM) 0.01 lux during the moonlight phase. Average MA offsets were calculated as described in 2.3.4.2.3.

Values in bold are significantly different ($p \leq 0.01$) from respective control values (*rh7*^{0} and *cry*^{01} mutants served as controls for recombinants and revertant as control for *cry*^{01}).

Genotype	Light program	Average MA offset (ZT ± SEM)
Revertant (n = 28)	**LD 12:12 1000 lux**	2.80 ± 0.18
***Rh7*^{0} (n = 26)**		1.57 ± 0.13
***Cry*^{01} (n = 60)**		**1.32 ± 0.08**
***Rh7*^{0} *cry*^{01} (n = 76)**		**1.00 ± 0.06**
Revertant (n =24)	**LM 12:12 1000 lux**	1.22 ± 0.12
***Rh7*^{0} (n = 18)**		0.62 ± 0.13
***Cry*^{01} (n = 26)**		0.95 ± 0.08
***Rh7*^{0} *cry*^{01} (n = 35)**		0.78 ± 0.06

However, the additional loss of CRY apparently affected the evening activity (EA), too, most prominently under LD 12:12 conditions. In contrast to *cry*^{01}, the activity started to increase around midday (~ZT6) and rose immediately in *rh7*^{0} *cry*^{01}, thereby causing an advanced onset of EA and, accordingly, more activity before and less activity after lights-off (ZT12).

To verify this effect, we determined the average EA onset based on single-fly activity profiles, as described in section 2.3.4.2.3. In comparison to *cry*^{01} flies, the onset of activity was significantly advanced in the double mutants ($p < 0.001$) under both LD and LM conditions (Table 22, Fig. 45A). *Rh7*^{0} mutants showed an average EA onset lying closer to the time points determined for *rh7*^{0} *cry*^{01} and also tended to advance their EA onset compared to revertants (Fig. 45B). The opposite was true for *cry*^{01} flies

in which the onset of activity was significantly delayed – by ~0.7 h under LD and ~0.6 h under LM cycles – in comparison to revertant controls ($p < 0.01$).

Table 22: Average EA onset in *cry*^{01}, *rh7*^{0} *cry*^{01}, *rh7*^{0} and revertants under LD and LM 12:12 conditions.

Flies were monitored under LD and LM 12:12 cycles of 1000 lux intensity during the light and (in LM) 0.01 lux during the moonlight phase. Average EA onsets were calculated from single-fly daily averages.

Values in bold are significantly different ($p < 0.001$) from respective control values.

Genotype	Light program	Average EA onset (ZT ± SEM)	Difference (h)
***Cry*^{01} (n = 69)**	**LD 12:12 1000 lux**	9.62 ± 0.13	1.88
***Rh7*^{0} *cry*^{01} (n = 105)**		**7.73 ± 0.12**	
***Cry*^{01} (n = 27)**	**LM 12:12 1000 lux**	9.33 ± 0.25	0.93
***Rh7*^{0} *cry*^{01} (n = 69)**		**8.40 ± 0.17**	
Revertant (n =28)	**LD 12:12 1000 lux**	8.53 ± 0.25	0.43
***Rh7*^{0} (n = 27)**		8.10 ± 0.18	
Revertant (n = 28)	**LM 12:12 1000 lux**	8.73 ± 0.25	0.26
***Rh7*^{0} (n = 26)**		8.47 ± 0.18	

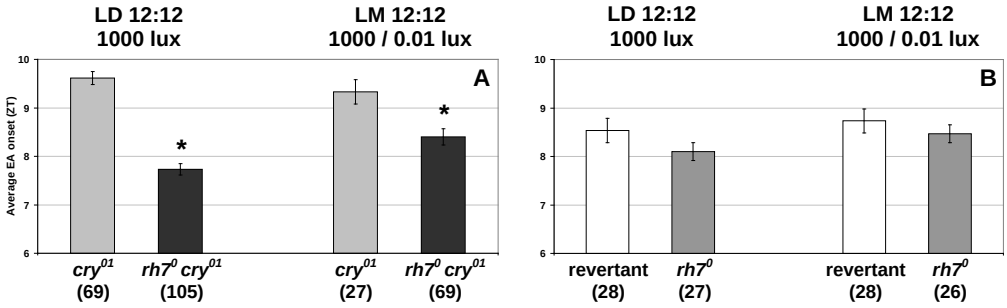

Figure 45: Average EA onset in *cry*^{01} and *rh7*^{0} *cry*^{01} (A) and in revertant and *rh7*^{0} flies (B) under LD and LM 12:12 conditions.

Flies were monitored under LD and LM 12:12 cycles of 1000 lux intensity during the light and (in LM) 0.01 lux during the moonlight phase. Average EA onsets were determined from activity profiles. Under both conditions, *rh7*^{0} *cry*^{01} mutants significantly advanced their EA onset in comparison to *cry*^{01} controls ($p < 0.001$). Compared to revertants, the same tendency was present in *rh7*^{0} mutants.

In parenthesis: No. of flies tested. Error bars represent ± SEM.

Like previously conducted for the MA, we calculated average EA levels under LD and LM 12:12 cycles (see 2.3.4.2.2). Therefore, activity was determined from average daily activity profiles within a 6-h interval preceding (ZT6-ZT12) and 1-h interval following

lights-off (ZT12-ZT13) for standard LD conditions. Taking the shift of the evening activity peak into account, EA levels were calculated within a 6-h period preceding (ZT6-ZT12) and following lights-off (ZT12-ZT18) in LD DAM System and LM recordings.

In all three experiments (Fig. 46, Table 23) average EA levels of *rh7*^{0} *cry*^{01} flies were increased prior to lights-off and significantly decreased subsequent to lights-off in direct comparison to *cry*^{01} mutants ($p < 0.001$). Besides, their overall average EA was significantly increased ($p < 0.05$) in both LD experiments (7 h / 12 h) and, by trend, also under LM conditions (data not shown). Comparing *rh7*^{0} to revertant flies, we found the same tendency with significant differences in the average level of EA only within two certain intervals (see Table 23).

In contrast, EA levels were generally – and, for the most part, significantly – reduced before and elevated after lights-off comparing *rh7*^{0} *cry*^{01} to *rh7*^{0}*.*

In reference to Rh7, the absence of CRY had an opposing effect on the EA. Under all conditions, the level of activity was decreased in the interval prior to and significantly increased in the interval subsequent to lights-off ($p < 0.001$) in comparison to revertant controls (see Figure 46, Table 23).

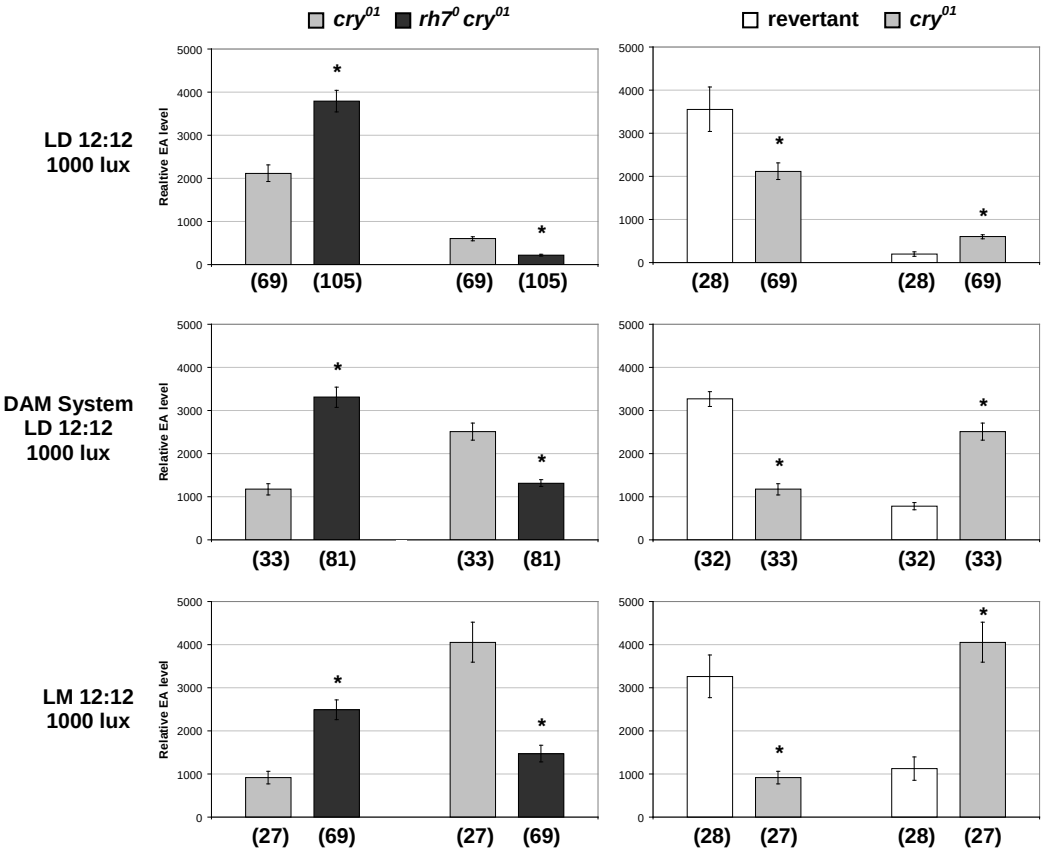

Figure 46: Relative average EA levels in *cry*^{01} and *rh7*^{01} *cry*^{01} (left column) and in revertant and *cry*^{01} flies (right column) under different recording conditions.

Flies were monitored under LD (home-made and DAM recording system) or LM 12:12 cycles of 1000 lux intensity during the light and (in LM) 0.01 lux during the moonlight phase. Average EA levels were calculated from average daily activity profiles within the following intervals: LD: 6 h before (ZT6-ZT12) and 1 h after lights-off (ZT12-ZT13); LD DAM System and LM: 6 h before and after lights-off (ZT12-ZT18).

Under all investigated conditions, EA levels of $rh7^{01}$ cry^{01} flies were significantly elevated before (ZT6-ZT12) and decreased after lights-off (ZT12-ZT13 / ZT12-ZT18) in direct comparison to cry^{01} ($p < 0.001$). We observed the opposite effect comparing cry^{01} mutants to revertant flies ($p < 0.001$).

In parenthesis: No. of flies tested. Error bars represent ± SEM.

Table 23: Relative average EA levels in revertant, $rh7^0$, cry^{01} and $rh7^0$ cry^{01} flies under LD and LM 12:12 conditions.

Values in bold are significantly different ($p < 0.05$) from respective control values ($rh7^0$ and cry^{01} mutants served as controls for recombinants and revertant as control for cry^{01}). For details, see legend of figure above.

Genotype	Light program	EA levels (average sum of beam crosses ± SEM)	
		6-h interval before lights-off (ZT6-ZT12)	1-h interval after lights-off (ZT12-ZT13)
Revertant (n = 28)	**LD 12:12 1000 lux**	3555 ± 516	198 ± 57
***Rh7*^{0} (n = 27)**		3857 ± 428	**58 ± 20**
***Cry*^{01} (n = 69)**		**2119 ± 190**	**602 ± 46**
***Rh7*^{0} *cry*^{01} (n = 105)**		3795 ± 251	**223 ± 22**
		6-h interval before lights-off (ZT6-ZT12)	6-h interval after lights-off (ZT12-ZT18)
Revertant (n = 32)	**DAM LD 12:12 1000 lux**	3266 ± 175	782 ± 82
***Rh7*^{0} (n = 37)**		**4484 ± 230**	813 ± 75
***Cry*^{01} (n = 33)**		**1173 ± 134**	**2511 ± 199**
***Rh7*^{0} *cry*^{01} (n = 81)**		**3309 ± 234**	**1317 ± 78**
Revertant (n = 28)	**LM 12:12 1000 lux**	3262 ± 495	1122 ± 269
***Rh7*^{0} (n = 26)**		3611 ± 440	801 ± 173
***Cry*^{01} (n = 27)**		**920 ± 146**	**4054 ± 463**
***Rh7*^{0} *cry*^{01} (n = 69)**		**2489 ± 227**	1469 ± 193

The main effects on the MA observed in $rh7^0$ single mutants persisted and were even enhanced in $rh7^0$ cry^{01} double mutants. Moreover, additional loss of CRY affected the

timing and the level of EA under LD and LM 12:12 conditions. In comparison to *cry*^{01}, the EA peak was advanced in recombinants, confirmed by an earlier onset of activity and higher activity levels previous to lights-off (ZT12). Regarding the effects on the EA, *rh7*^{0} mutants showed the same tendency compared to revertant controls.

3.5.2.2.4 Entrainment to different photoperiods

To investigate MA and EA in more detail, we monitored locomotor activity rhythms of *rh7*^{0} and *cry*^{01} single mutants, the corresponding double mutant and revertant controls under different photoperiods initially by application of LD 08:16 and LD 16:08 cycles of 1000 lux light intensity. Wild-type flies are known to entrain their activity rhythms to these short and long day conditions (Rieger et al., 2003). The daily average activity profiles of the investigated genotypes and photoperiods are compiled in Figure 47 including equinox (LD 12:12) daily averages. In general, all genotypes were able to entrain to the different photoperiods and displayed the usual bimodal activity pattern. Under short days of 08:16, controls were already active before lights-on (ZT0) and still active after lights-off (ZT8). In LD 12:12, morning and evening activity came along with lights-on and lights-off, respectively. Under long days of 16:08, the MA occurred after lights-on and the EA peaked clearly before (~2 h) lights-off (ZT16). Besides, the MA was more pronounced under short day conditions and the EA, on the contrary, under long days.

The same was basically true for *rh7*^{0} mutants. Notably, they shifted their EA further into the night under short days and spent 49% of their total average activity during this period, whereas it was only 26% in case of the controls. However, we did not observe this effect under short days of lower (10 or 100 lux) irradiances (data not shown).

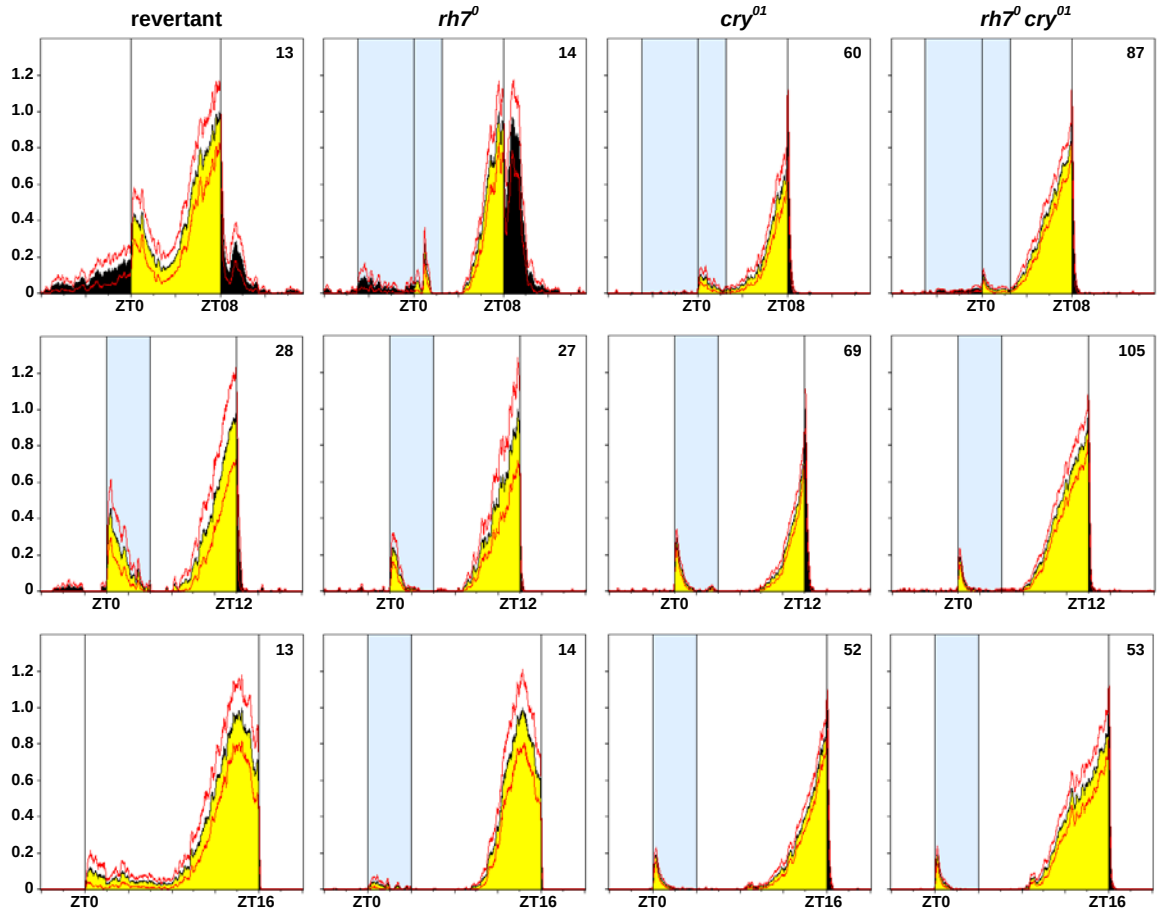

Figure 47: Cuvette system recording-based daily averages of revertant, *rh7*^{0}, *cry*^{01} and *rh7*^{0} *cry*^{01} flies under different photoperiods.

Flies were monitored under LD 08:16 (top row), 12:12 (middle row) or 16:08 cycles (bottom row) of 1000 lux intensity. Infrared light beam crosses were recorded in 1-min bins and daily averages calculated as described under 2.3.4.2.1. Two vertical lines label lights-on (ZT0) and lights-off (depending on the photoperiod), respectively. The blue background indicates the respective intervals used for calculation of MA levels.

Numbers: No. of flies tested. Red curves represent ± SEM. For details, see text.

Although we could not directly determine and compare average MA levels and offsets, mainly due to a broad morning peak in revertant flies, *rh7*^{0} showed definitely less MA and a more prominent midday trough under both LD 08:16 and 16:08 conditions, as previously confirmed for LD 12:12 cycles (section 3.5.2.2.2.1).

In contrast to revertant and *rh7*^{0}, *cry*^{01} and *rh7*^{0} *cry*^{01} flies kept their activity bouts close to lights-on and lights-off. They squeezed most of their activity into the 8-h day (86% in *cry*^{01} and 90% in *rh7*^{0} *cry*^{01}), and, under long days (16 h), their EA increased steadily until (and did not peak before) lights-off (ZT16). Only under even shorter photoperiods (LD 04:20), both genotypes advanced their MA (20% of total activity is shifted into the dark phase in *cry*^{01} and 33% in *rh7*^{0} *cry*^{01}), whereas under longer days (20:04), both activity peaks still followed lights-on and lights-off, respectively (Fig. 48).

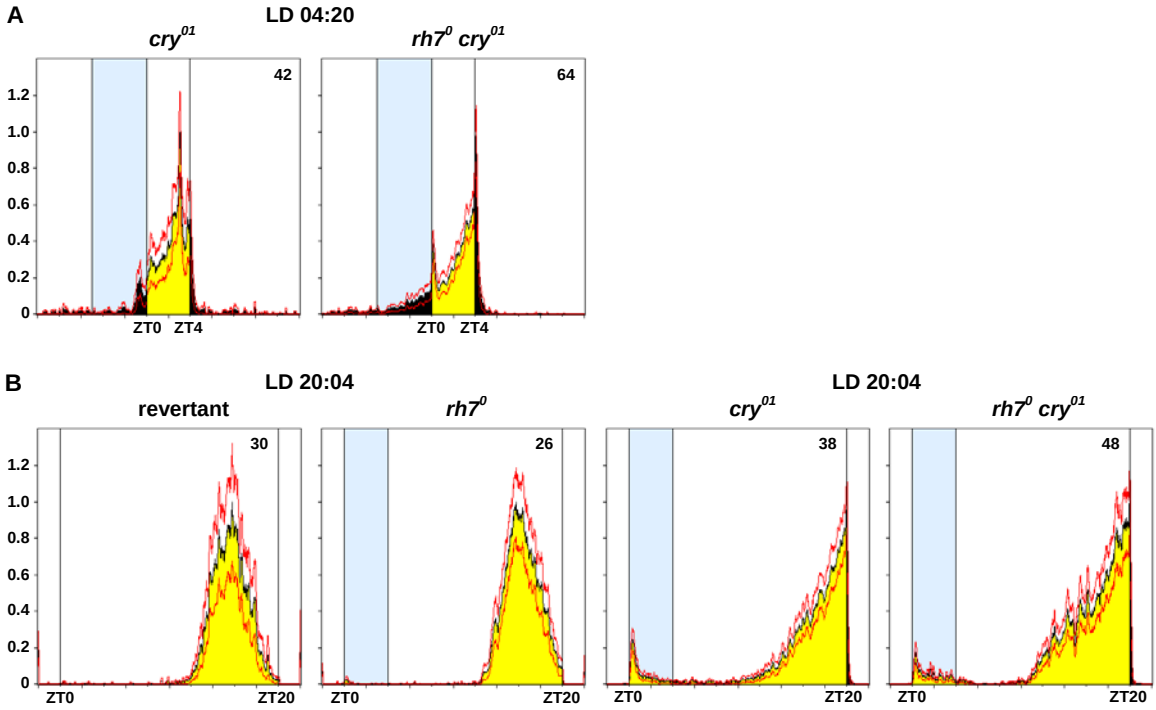

Figure 48: Cuvette system recording-based daily averages of revertant, *rh7*^{0}, *cry*^{01} and *rh7*^{0} *cry*^{01} flies under short (04:20) and long days (20:04).

Cry^{01} and *rh7*^{0} *cry*^{01} were monitored under LD 04:20 (A) and, together with revertant and *rh7*^{0} flies, under 20:04 cycles (B) of 1000 lux intensity. Infrared light beam crosses were recorded in 1-min bins and daily averages calculated as described under 2.3.4.2.1. Two vertical lines label lights-on (ZT0) and lights-off (ZT4 in A; ZT20 in B), respectively. The blue background indicates the respective intervals (5 h in A; 4 h in B) used for calculation of average MA levels.

Numbers: No. of flies tested. Red curves represent ± SEM. For details, see text.

To statistically compare the average activity profiles under different photoperiods, we calculated average MA levels and determined the average EA onset. Under short day conditions, the average MA was either analyzed within a 7.5-h interval composed of a 5-h period prior to and a 2.5-h period subsequent to lights-on (08:16) or exclusively within the former 5-h period (04:20). Under long photoperiods (16:08 and 20:04), we defined a 4-h interval following lights-on to determine MA levels (see daily averages).

Under long days, MA levels were lowest in *rh7*^{0} mutants within the 4-h period and the MA was also significantly decreased in *rh7*^{0} *cry*^{01} recombinants ($p < 0.05$) in direct comparison to *cry*^{01} mutants (Fig. 49, Table 24). As shown in Table 24, the opposite was true for LD 08:16 cycles under which the MA was decreased in *cry*^{01} and *rh7*^{0} *cry*^{01} within all intervals in comparison to *rh7*^{0}. In detail, recombinants tended to be more active than *cry*^{01} under short days prior to lights-on, but showed similar activity levels subsequent to lights-on (08:16) resulting in slightly increased levels of activity within the total 7.5-h period.

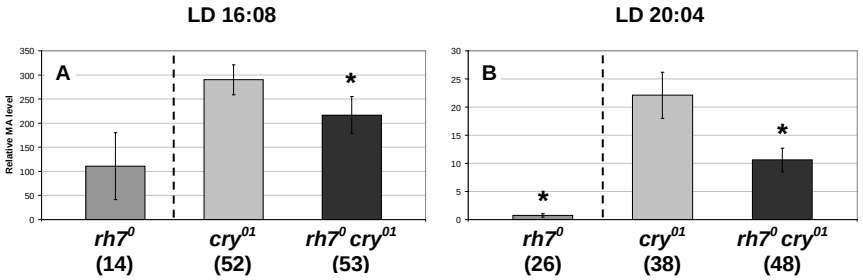

Figure 49: Relative average MA levels in *rh7^0*, *cry^{01}* and *rh7^0 cry^{01}* mutants under long days.

Flies were monitored under LD 16:08 (A) and 20:04 (B) cycles of 1000 lux intensity. Average MA levels were calculated from individual activity profiles within a 4-h interval subsequent to lights-on (ZT0-ZT4). Under both conditions, recombinant flies showed significantly reduced average MA levels in direct comparison to *cry^{01}* ($p < 0.05$), and the MA was further reduced in *rh7^0* mutants (B: $p < 0.001$).

In parenthesis: No. of flies tested. Error bars represent ± SEM.

Table 24: Relative average MA levels in *rh7^0*, *cry^{01}* and *rh7^0 cry^{01}* mutants under long and short day conditions.

Flies were monitored under long (16:08; 20:04) and short days (08:16; 04:20) of 1000 lux intensity. Daily averages were determined and MA levels calculated within a 4-h period subsequent to lights-on for long days and within a 7.5-h period comprising a 5-h interval before (ZT19-ZT0) and 2.5-h interval after (ZT0-ZT2.5) lights-on for short day conditions. Under 04:20, MA levels were not determined after lights-on because the EA would have been partly included in the calculation.

Values in bold are significantly different ($p < 0.01$) from respective control values.

Genotype	Light program	MA levels (average sum of beam crosses ± SEM)		
		4-h interval after lights-on (ZT0-ZT4)		
Rh7^0 **(n = 14)**	**LD 16:08 1000 lux**	111 ± 69		
Cry^{01} **(n = 52)**		290 ± 31		
Rh7^0 cry^{01} **(n = 53)**		217 ± 38		
Rh7^0 **(n = 26)**	**LD 20:04 1000 lux**	**0.7 ± 0.3**		
Cry^{01} **(n = 38)**		22.1 ± 4.1		
Rh7^0 cry^{01} **(n = 48)**		10.6 ± 2.1		
		MA levels (average sum of beam crosses ± SEM)		
		5-h interval before lights-on (ZT19-ZT0)	2.5-h interval after lights-on (ZT0-ZT2.5)	total 7.5-h interval (ZT19-ZT2.5)
Rh7^0 **(n = 14)**	**LD 08:16 1000 lux**	**385 ± 102**	297 ± 67	**682 ± 132**
Cry^{01} **(n = 60)**		9 ± 3	167 ± 34	176 ± 34
Rh7^0 cry^{01} **(n = 87)**		69 ± 24	134 ± 25	203 ± 37

***Cry*^{0} (n = 42)**	**LD 04:20 1000 lux**	211 ± 43	
***Rh7*^{0} *cry*^{01} (n = 64)**		420 ± 125	

As previously carried out for LD 12:12 cycles, we calculated average EA onsets under short (08:16) and long days (16:08 and 20:04). In accordance with the daily averages, the onset of activity occurred generally earlier under short and later under long day conditions. In comparison to the corresponding controls, the onset was significantly advanced in *rh7*^{0} *cry*^{01} ($p \leq 0.1$) and significantly delayed in *rh7*^{0} ($p < 0.001$) mutants under all three photoperiods (Fig. 50, Table 25). By trend, the onset of activity in the double mutants was also advanced in comparison to *rh7*^{0} mutants ($p < 0.01$ at 20:04). Moreover, the EA onset was significantly delayed in *cry*^{01} compared to revertant flies ($p < 0.01$) except for LD 20:04 ($p = 0.7$).

Comparing LD 16:08 to 20:04, we found a further delay of the EA onset for revertant and *rh7*^{0} flies, whereas the determined time points (in ZT) for *cry*^{01} and *rh7*^{0} *cry*^{01} did not change with increasing day length. The results (including previous LD 12:12 data) are summarized in Table 25 and Figure 50.

Table 25: Average EA onset in *rh7*^{0} *cry*^{01} and *cry*^{01} and in *rh7*^{0} and revertant controls under different photoperiods.

Flies were monitored under different photoperiods ranging from LD 08:16 to 20:04 using 1000 lux light intensity. Average EA onsets were determined from daily averages and calculated in relation to lights-on (always defined as ZT0).

Values in bold are significantly different ($p \leq 0.01$) from respective control values.

Genotype	Light program	Average EA onset (ZT ± SEM)	Difference (h)
***Cry*^{01} (n = 59)**	**LD 08:16 1000 lux**	5.42 ± 0.17	1.17
***Rh7*^{0} *cry*^{01} (n = 86)**		**4.25 ± 0.12**	
***Cry*^{01} (n = 69)**	**LD 12:12 1000 lux**	9.62 ± 0.13	1.88
***Rh7*^{0} *cry*^{01} (n = 105)**		**7.73 ± 0.12**	
***Cry*^{01} (n = 52)**	**LD 16:8 1000 lux**	10.88 ± 0.32	0.98
***Rh7*^{0} *cry*^{01} (n = 53)**		**9.90 ± 0.17**	
***Cry*^{01} (n = 38)**	**LD 20:04 1000 lux**	12.87 ± 0.28	0.87
***Rh7*^{0} *cry*^{01} (n = 48)**		**12.00 ± 0.23**	

Revertant (n = 13)	**LD 08:16 1000 lux**	3.67 ± 0.23	1.50
***Rh7*^{0} (n = 14)**		**5.17 ± 0.15**	
Revertant (n = 28)	**LD 12:12 1000 lux**	8.53 ± 0.25	0.43
***Rh7*^{0} (n = 27)**		8.10 ± 0.18	
Revertant (n = 13)	**LD 16:08 1000 lux**	8.93 ± 0.32	1.72
***Rh7*^{0} (n = 26)**		**10.65 ± 0.13**	
Revertant (n = 30)	**LD 20:04 1000 lux**	12.45 ± 0.16	0.83
***Rh7*^{0} (n = 26)**		**13.28 ± 0.15**	

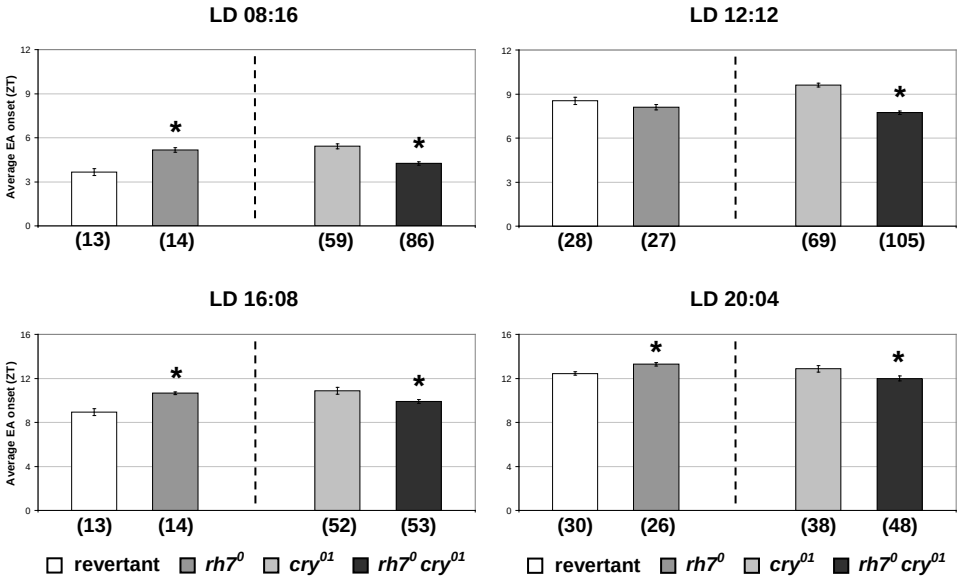

Figure 50: Average EA onset in *rh7*^{0} and revertant controls and in *rh7*^{0} *cry*^{01} and *cry*^{01} under different photoperiods.

Flies were monitored under short days (LD 08:16), equinox (LD 12:12) and long days (LD 16:08; 20:04) at 1000 lux irradiance. Average EA onsets were determined from daily averages and plotted in relation to lights-on (defined as ZT0) for each day length. Under all three photoperiods, the onset of activity was delayed in *rh7*^{0} and advanced in *rh7*^{0} *cry*^{01} in direct comparison to their respective controls.

In parenthesis: No. of flies tested. Error bars represent ± SEM.

Finally, we calculated the average maximum of the EA bout under long day conditions in relation to lights-on (ZT0). In general, the peak occurred significantly later ($p < 0.01$) in the absence of CRY (in *cry*^{01} and *rh7*^{0} *cry*^{01} mutants) compared to control and *rh7*^{0} flies, especially under LD 20:04 (> 3 h). Comparing LD 16:08 to 20:04, the maximum was significantly delayed within each genotype ($p < 0.05$). In contrast to

16:08 cycles, the maximum was significantly delayed in *rh7*^{0} ($p < 0.05$) and significantly advanced in *rh7*^{0} *cry*^{01} ($p < 0.001$) flies under 20:04 conditions in comparison to the corresponding controls, revertant and *cry*^{01} flies, respectively (Figure 51 and Table 26).

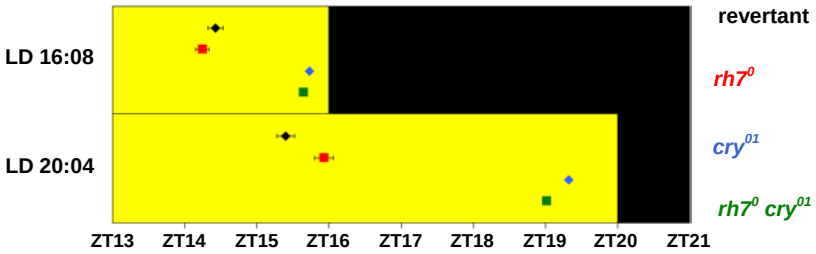

Figure 51: Average EA maximum in revertant controls, *rh7*^{0}, *cry*^{01} and *rh7*^{0} *cry*^{01} mutants under long day conditions.

The peak of EA was determined in single flies for LD 16:08 and 20:04 conditions and the average maxima plotted in relation to lights-on (ZT0). Background color indicates the respective LD cycle. In all genotypes, the peak depended on the photoperiod ($p < 0.05$), but mutants lacking CRY delayed their maximum closer to lights-off under longer photoperiods than *rh7*^{0} and revertant. In LD 20:04, *rh7*^{0} delayed the EA maximum ($p < 0.05$), whereas *rh7*^{0} *cry*^{01} advanced their peak ($p < 0.001$) in comparison to the corresponding controls.

Table 26: Average EA maximum in revertant controls, *rh7*^{0}, *cry*^{01} and *rh7*^{0} *cry*^{01} mutants under long photoperiods.

Flies were monitored under long days (LD 16:08 and 20:04) of 1000 lux light intensity. EA maxima were determined from individual daily activity profiles, averaged and calculated in relation to lights-on (ZT0).

Values in bold are significantly different ($p \leq 0.05$) from respective control values.

Genotype	Light program	Average EA maximum (ZT ± SEM)	Difference (h)
Revertant (n = 13)	**LD 16:08 1000 lux**	14.43 ± 0.11	0.20
***Rh7*^{0} (n = 14)**		14.25 ± 0.10	
***Cry*^{01} (n = 52)**	**LD 16:08 1000 lux**	15.73 ± 0.03	0.08
***Rh7*^{0} *cry*^{01} (n = 53)**		15.65 ± 0.05	
Revertant (n = 30)	**LD 20:04 1000 lux**	15.40 ± 0.13	0.55
***Rh7*^{0} (n = 26)**		**15.93 ± 0.13**	
***Cry*^{01} (n = 32)**	**LD 20:04 1000 lux**	19.32 ± 0.03	0.30
***Rh7*^{0} *cry*^{01} (n = 43)**		**19.02 ± 0.03**	

Briefly summarized, the *rh7* null mutation caused a reduction and an earlier offset of MA under equinox conditions which apparently persisted under the investigated photoperiods. In addition, we observed an effect on the EA onset: The onset of activity was significantly delayed in $rh7^0$ mutants under both short and long days and reflected in a delayed activity peak under LD 20:04 cycles.

In general, the average activity pattern of $rh7^0$ cry^{01} strongly resembled that of cry^{01} mutants. Nevertheless, their EA onset occurred significantly earlier in comparison to cry^{01} and, by tendency, earlier compared to $rh7^0$ under all photoperiods. Effects on the MA were rather complex and will be taken up in the discussion.

3.5.2.2.5 Activity rhythms under constant conditions

In addition to light entrainment, we studied locomotor activity rhythms under constant conditions, either constant darkness (DD) or constant light of 1000 lux intensity (LL). In DD, wild-type flies exhibit robust free-running rhythms with an endogenous period (τ) of ~24 h, whereas LL usually causes arrythmic behavior (Konopka et al., 1989) and disrupts the molecular clock (see section 1.9). Mutant flies lacking functional CRY are rhythmic under LL conditions (2000a), but show two dissociating components at high irradiances (Yoshii et al, 2004; Dolezelova et al., 2007).

On the basis of our previous LD experiments, revertant, $rh7^0$, cry^{01} and $rh7^0$ cry^{01} flies were entrained to LD 12:12 cycles of 1000 lux irradiance for five days prior to transfer into DD. All determined average period lengths (2.3.4.2.1) were in the normal range and varied from 23.5 h (revertant) to 24 h (cry^{01}). Remarkably, free-running rhythms were less robust in $rh7^0$ cry^{01} double mutants (mainly #39) and thus, the period length could only be definitely determined in half of the flies analyzed in total. The resulting data is summarized in Table 27. For example actograms see Figure 52.

Table 27: Mean free-running locomotor activity rhythms of revertant controls, $rh7^0$, cry^{01} and $rh7^0$ cry^{01} mutants.

Flies were entrained to LD 12:12 cycles of 1000 lux intensity and then released into DD. Locomotor activity was monitored for 11 days and the period length (τ) was determined in individual flies using chi square periodogram analysis. Tested genotypes display normal average period lengths ranging from 23.5 to 24.0 h. Rhythmicity was reduced in $rh7^0$ cry^{01}*#39*. Statistically, cry^{01} mutants showed a significantly longer period in comparison to all other phenotypes ($p < 0.01$), but their period length is in accordance with the 23.9 h period of their isogenic controls, cry^+ (data from Dolezelova et al., 2007; comparable recording conditions). N: No. of flies tested.

Genotype	n	n rhythmic (%)	Mean τ (h) ± SEM
Revertant	29	86	23.5 ± 0.06
Rh7^0	30	70	23.6 ± 0.05
Cry^{01}	30	73	24.0 ± 0.04
Rh7^0 cry^{01}	31	55	23.6 ± 0.09

Rh7^{0} cry^{01}#39	15	33	23.8 ± 0.16
Rh7^{0} cry^{01}#112	16	75	23.5 ± 0.09

Upon direct transfer from DD into LL conditions, revertant and *rh7^{0}* flies basically lost rhythmicity, whereas about half of the *cry^{01}* mutants and all *rh7^{0} cry^{01}* recombinants, irrespective from the line (#39 or #112), displayed rhythmic behavior. In detail, ~40% of *cry^{01}* mutants (11 flies in total) showed a free-running rhythm with a single activity component. In two rhythmic flies, a short component of 21.4 h (± 0.1) was detected, whereas a long component of 25.4 h (± 0.15) was present in seven animals. Activity rhythms of another two flies dissociated and showed both activity components with period lengths comparable to those of the single components. In contrast, *rh7^{0} cry^{01}* double mutants (16 flies in total) displayed robust activity rhythms with one periodic component of 25.5 h (± 0.12) that corresponds to the long period component of *cry^{01}* single mutants. Thus, the average period lengthened by almost 2 h in *rh7^{0} cry^{01}* flies in comparison to the previous DD conditions.

Representative individual actograms are shown in Figure 52. However, the majority of *cry^{01}* mutants died before monitoring in LL was finished and thus, the number of tested flies was too low for proper data analysis.

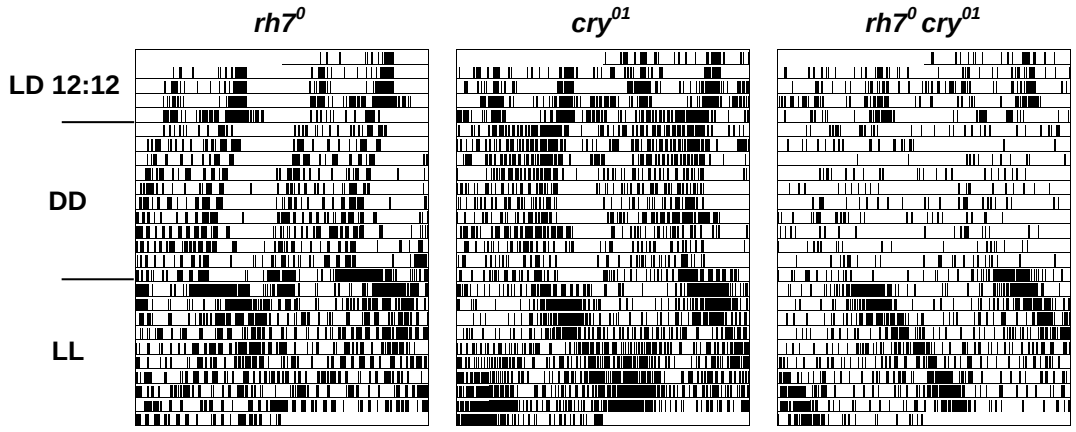

Figure 52: Representative double-plotted actograms of *rh7^{0}*, *cry^{01}* and *rh7^{0} cry^{01}* mutants.

Flies were entrained to LD 12:12 cycles of 1000 lux intensity prior to release into DD. After 11 days, flies were directly transferred into LL and recorded for further 10 days. Representative locomotor activity rhythms of individual flies are displayed in actograms. Period lengths (τ) were determined using chi square periodogram analysis.

Rh7^{0} mutants exhibited robust activity rhythms of ~23.6 h in DD conditions. Upon transfer into LL, a spontaneous burst of activity was observed before flies became arrythmic. The same was true for revertant controls. *Cry^{01}* mutants showed ~24 h rhythms in DD and rhythmic behavior in LL with either a short or a long periodic component or, as shown above, both components (τ_{short} = 22.3 h and τ_{long} 25.5 h in this example). *Rh7^{0} cry^{01}* double mutants displayed week rhythms of ~23.6 h under DD conditions, but showed free-running rhythms of ~25.4 h in LL (example: #112).

Interestingly, we found also differences in the average daily activity levels between DD and LL conditions. The total activity was significantly elevated in LL in revertant, $rh7^{0}$ and $rh7^{0}$ cry^{01} flies ($p < 0.01$). Only cry^{01} mutants, which tended to be less active under DD conditions, did not show any increase in locomotor activity upon transfer into LL. As a consequence, their average activity levels were significantly reduced under LL conditions compared to all other genotypes ($p < 0.01$).

4 Discussion

4.1 Expression of Rh7

4.1.1 Detection of Rh7 using qPCR and western blot

One of the major aims of this thesis was to investigate the expression of Rh7 in detail, first of all on the levels of mRNA. The expression of all so far characterized *Drosophila* rhodopsin pigments is limited to photoreceptor cells, but the blue-light photoreceptor CRY is also present in the majority of clock neurons in the brain. Thus, we isolated fly brains and retinas to study *rh7* expression in these tissues using real-time qPCR.

In fly strains carrying the wild-type *rh7* allele, relative expression of *rh7* was detected in both tissues at similar levels, whereas cDNA amplification from *rh7* knockout mutant samples failed. In comparison to *rh1*, levels of *rh7* mRNA were increased in the brain (~3.7-fold) and decreased in the retina (~3-fold) in *CS* wild-type flies. Both results are basically in accordance with the data obtained from the *Drosophila* anatomical gene expression atlas (Chintapalli et al., 2007). These studies detected *rh7* mRNA in the brain and in the retina and, moreover, confirmed low levels of *rh1* expression in the brain (http://flyatlas.org/). According to their data, retinal *rh1* expression could have been much more elevated in comparison to *rh7* in our experiments (more than 50-fold). However, mRNA levels differ by a factor of ~45 between the two data sets provided for *rh7* expression, and thus might not be well-suited for a direct comparison (for data sheets, see appendix 7.1.2).

We also determined *rh7* mRNA levels in flies that additionally expressed *rh7* under the promotor of *rh1* either in presence of (*Rh1-Rh7*) or in place of Rh1 (*Rh1-Rh7; ninaE*). We found that *rh7* expression in brain and retina samples of both genotypes was now even higher than *rh1* expression in the corresponding wild-type tissues (CS). This surplus can be explained by endogenous *rh7* expression which should not be affected by the Rh1-driven expression of *rh7*, as shown for Rh6 when overexpressed in R1-R6 (Salcedo et al., 1999).

In *ninaE* mutant flies, which lack Rh1 expression in R1-R6 photoreceptors, *rh7* mRNA levels were in the range of the other control strains (backcross, *CS* and revertant) in both tissues. Since loss of Rh1 directly affects the photoreceptor structure and results in a progressive retinal degeneration (Colley et al., 1995; Kumar and Ready, 1995; Kurada and O´Tousa, 1995), we compared 1-day-old to more than 21-day-old *ninaE* mutants, but we did not detect a reduction in relative expression of *rh7*. In the brain, mRNA levels were similar, whereas aged *ninaE* mutants even showed elevated *rh7*

expression in the retina. Thus, *rh7*-expressing cells are either not affected by R1-R6 degeneration or expression of *rh7* is still possible in the degenerating photoreceptors. However, an actual increase of *rh7* mRNA in elderly flies seems rather unlikely, but variations in *rh7* expression could be caused, for example, by differences in sample preparation and in homogenization efficiency. Furthermore, large individual difference in relative expression levels of *rh7* could be observed for both brains and retinas, mainly between different biological replicates. These differences are reflected in high standard deviations from average relative expression levels, as exemplarily shown in Figure 53. This histogram directly compares *rh7* mRNA levels in young, elderly and *ninaE* brains and retinas of unknown age (initial samples). In our experimental data, biological and technical replicates were summarized in order to calculate average relative expression levels. This approach results in a high number of total replicates, thereby generating low standard errors, but might not be completely justified. However, a higher number of biological replicates in combination with an alternative analysis of the present data should be considered to substantiate our results.

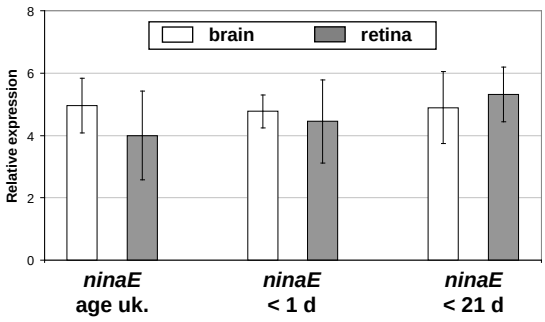

Figure 53: Relative rh7 expression levels in *ninaE* mutant brains and retinas.

Average *rh7* mRNA levels are plotted for *ninaE* mutant flies of different age. Expression levels vary strongly within the single replicates for each genotype, as indicated by the error bars representing standard variations.

In the original data set, the age of the analyzed flies was unknown (uk.).

Apart from that, our qPCR results are supported by previous reporter gene expression studies using three different *rh7*-GAL4 promotor constructs (Veleri, 2005; Bachleitner, 2008; Bleyl, 2008). In whole mount preparations, expression of GFP was reported in a series of different non-clock brain neurons in all cases, and Bleyl (2008) found (i. a.) additional staining in the laminar and retinal layer using anti-LacZ antibody labeling on cryosections of wild-type heads. Using two of these GAL4 lines and a commercially available enhancer trap line, we found reporter gene expression not only in the lamina and the retina, but as well in the ocelli (GAL4 enhancer trap line only) and the second antennal segment (all driver lines).

Antennae-specific expression of *rh7* was initially discussed by Japanese researchers since they found labeling of Johnston's organ (JO) AB neurons with this enhancer trap strain (Maeda et al., 2011). However, they did not detect any other signals driving reporter gene expression with this fly line and thus considered the possibility of *rh7*

expression in the compound eyes as rather unlikely. On the one hand, they confirmed their results by qPCR experiments (Fuse, personal communication), but on the other hand, *rh7* mRNA was not detected in the second antennal segment in a genetic screen for deafness genes in a cDNA microarray-based study (Senthilan, 2010).
In our experiments, staining of antennal cells could exclusively be achieved by driving *rh7* expression with a UAS-myr-mRFP reporter line. We failed to reproduce our results with other UAS-reporters, which were previously used by Senthilan (2010) and would thus have allowed identification of different subgroups of JO neurons.
Nevertheless, our results are further supported by qPCR experiments analyzing *rh7* mRNA levels in fly heads of eye mutants lacking either only the compound eyes or additional visual input (e.g., via the ocelli or CRY). The loss of the compound eyes resulted in a reduction of *rh7* expression in comparison to wild-type controls (~50%), indicating retinal and/or laminar expression of *rh7*, whereas the presence or absence of the ocelli did not significantly affect *rh7* transcript levels (Bleyl, 2008).

In a second approach, we investigated the Rh7 protein expression pattern using IHC. Since qPCR experiments strongly suggested *rh7* transcription in brain and retina, we first investigated protein expression in adult fly heads using western blot analysis.
To increase *rh7* expression and facilitate protein detection, we tested head extracts of *Rh1-Rh7; ninaE* flies using newly generated peptide antibodies directed against an extracellular domain of Rh7. For each of the four antibodies, different serum samples and affinity purified antibodies were available. All antibodies produced multiple bands, and some of them were also present after incubation with preimmune sera (in place of primary antibodies) and thus unspecific. In theory, an increase in the specific signal would have been expected with an increasing number of donor immunizations. This was not the case and, moreover, we could not see any difference in the band pattern comparing *Rh1-Rh7; ninaE* to $rh7^{0}$ flies. Western blot analysis usually includes a heat denaturation step prior to SDS-PAGE. To rule out the possibility that our peptide antibodies are not able to detect the denatured Rh7 protein, we skipped this step. Furthermore, we tested the membrane fraction of total head extracts as a control for insufficient homogenization, but detection failed under both experimental conditions.
Nevertheless, our protocol including solutions and experimental conditions for protein extraction, SDS-PAGE, blotting and signal detection was successfully used to detect 1D4-tagged Rh1 protein in our laboratory. Therefore, the protocol appears suitable to detect membrane-bound proteins like rhodopsins. Since we took the higher molecular weight of Rh7 into account, we considered experimental problems to be rather unlikely

and concluded that none of the new peptide antibodies was suited to detect Rh7 in western blot analysis.

A different anti-Rh7 antibody (Rh7:E), that recognizes an intracellular region of the protein, was previously tested in western blotting, but could not reproducibly detect the overexpressed protein in *Rh1-Rh7* head extracts either (Bachleitner, 2008). For this reason and also due to the low amount of residual antibody, Rh7:E was not reused in this application.

4.1.2 Immunohistochemistry on brains, retinas and head sections

We initially performed antibody staining of wild-type and *rh7*^{0} whole mount brains and retinas using anti-Rh7 (Rh7:E) combined with anti-chaoptin antibody for photoreceptor labeling. We found double-labeling in the ocelli but no staining in the brain. The ocellar staining was also present in *rh7* null mutants and was of equal intensity. Interestingly, the same was true for new peptide antibodies prior to affinity purification. It is unlikely that the previous or new peptide antibodies specifically bound to ocellar Rh2 instead of Rh7, since the amino acid sequences that should be recognized are both not even partially present in Rh2. Therefore, it remains unclear which protein these antibodies actually detected in ocellar photoreceptors of *rh7*^{0} mutants. Nevertheless, none of the purified antibodies produced any signal suggesting that Rh7 is not present in wild-type ocelli. At the protein level, another peptide antibody would be helpful to clarify ocellar expression of Rh7. At the level of *rh7* mRNA expression, qPCR of ocelli may help to solve this question, though it is technically challenging.

Revealing rh7 expression in the brain and in the retina was similarly difficult as in the ocelli. Although we could amplify *rh7* cDNA from individual wild-type brains, and *rh7*-GAL4-mediated reporter gene expression resulted in labeling of different neurons and their projections (Veleri, 2005; Bleyl, 2008), we did not observe cellular antibody staining in whole mount brains of adult wild-type flies. In agreement with our qPCR results, new antibodies (especially purified rabbit 2 anti-Rh7 antibody) were able to localize Rh7 in wild-type retina (see Fig. 25G). The observed staining was present in the interrhabdomeral space along and between the rhabdomeres of R1-6 (Fig. 25A), which may explain why qPCR still revealed *rh7* expression in *ninaE* mutants with degenerating photoreceptor cells R1-6 (see above). Unfortunately, retinas of *rh7* null mutants – our mutant and two other *rh7* mutants (Maeda et al., 2011) – were broadly and similarly stained as well, thereby putting the specificity of the antibody staining again into question. On the other hand, co-labeling with anti-Rh1 antibody showed that R1-R6 rhabdomeres are reliably recognized in ommatidia of *Rh1-Rh7* retinas (see Fig.

24A, B). Thus, new anti-Rh7 antibodies do not seem to be totally unspecific, but might rather not be able to detect small amounts of wild-type Rh7 protein putatively present in the retina.

Similar problems in terms of antibody specificity occurred in a previous study testing Rh7:E antibody on head cryosections (Bachleitner, 2008). Fluorescent labeling was also detected in *rh7*^{0} photoreceptors there, but the staining intensity was significantly reduced in comparison to wild-type rhabdomeres on the one hand, and *Rh1-Rh7* flies showed a clear increase in staining intensity on the other hand. Although we could not quantify our retinal staining pattern, signal strength was not evidently reduced in *rh7*^{0} retinas, and colleagues, who were blind for the genotype, were not able to distinguish between the different mutant and wild-type genotypes. The same applied to paraffin sections, and we could not differentiate between *rh7*^{0} and control staining patterns, although retinal antibody staining did not look exactly the same in microscope images of higher magnification (see Fig. 27B', C'). However, one has to be careful when interpreting this observation, since *GMR*-GAL4, which served as *rh7*$^{+}$ control in this case, sometimes shows an eye phenotype itself (see next section). This could have an effect on the antibody penetration and thus on the resulting staining, although we did not notice any structural abnormalities in this experiment.

Besides these generally ambiguous antibody staining results, we could not detect Rh7 after ectopic expression in non-photoreceptor cells, e.g., in the PDF-positive LN_v clock neurons. This might be rather due to inefficient mRNA translation (biosynthesis) or to defective processing in the following (maturation, translocation) than to lacking GAL4-directed transcriptional activation. Bleyl, for example, was able to detected *rh7* mRNA in non-photoreceptor cells using *engrailed-GAL4; UAS-rh7#8* embryos in order to test an in-situ hybridization probe for specific detection of *rh7* (personal communication). It would be interesting to see if expression of a different rhodopsin, which can reliably be detected by antibody staining (e.g., Rh1), in certain clock neurons would be possible.

Taken together, immunohistochemical results could not directly support our *rh7* mRNA expression data at the level of protein expression. If, nevertheless, localization of Rh7 in the compound eyes would be assumed, both rhabdomeral co-expression along with another rhodopsin as well as expression in photoreceptor-associated or postsynaptic cells would be conceivable possibilities. Due to our results from qPCR, co-expression of Rh7 along with Rh1 in R1-R6 seems less likely, since *rh7* mRNA levels were not decreased in *ninaE*, although their retina is characterized by massive degeneration in R1-R6 rhabdomeres. Moreover, as discussed in the following section, even only small amounts of rhodopsin in rhabdomeral membranes have been shown to prevent this

degenerative phenotype (Leonard et al., 1992; Kumar and Ready, 1995). On the other hand, transcription of *rh7* in the nuclei of R1-R6 photoreceptors might as well not be affected by the degeneration of rhabdomeres. Apart from that, expression of Rh7 only in the lamina could also explain the *ninaE* results. However, in the long term, there will be no way around specific antibodies to confirm localization of endogenous Rh7 in wild-type brain and retina.

4.2 Functional characterization of Rh7

4.2.1 Rh7 in photoreceptor development and the optomotor response

Apart from its role in motion and dim-light vision, Rh1 overtakes an important function in both normal development and maintenance of R1-R6 photoreceptors (Colley et al., 1995; Kumar and Ready, 1995; Kurada and O´Tousa, 1995) which is reflected by the *ninaE* eye phenotype (see Fig. 29A, A'). Paraffin sections of *Rh1-Rh7; ninaE* heads showed that expression of Rh7 in place of Rh1 (R1-R6) is able to restore the wild-type ommatidal structure, as previously observed in semithin sections (Bachleitner, 2008). On the contrary, loss of Rh7 did not have any structural effects; both retina and lamina looked revertant control-like in paraffin head sections of *rh7* knockout mutants.

These results might also contribute to the previous discussion about eye-specific Rh7 expression. Low levels of rhodopsin protein (~1-5% of the wild-type level) were shown to be sufficient to prevent rhabdomeral degeneration and to keep rhabdomeres intact for more than 6 weeks (Leonard et al., 1992; Kumar and Ready, 1995). Since Rh7 is able to locate to rhabdomeral membranes of R1-R6 photoreceptors in *Rh1-Rh7; ninaE* flies and to rescue the *ninaE* mutant phenotype, one might expect that low amounts of Rh7 – if indeed endogenously expressed in R1-R6 – should already prevent retinal degeneration in *ninaE* before it arises, which is not the case. Alternatively, Rh7 could be expressed below this threshold if, for example, it would be primarily or exclusively expressed in the lamina.

In order to see whether Rh7 is able to influence photoreceptor development and affect the normal eye phenotype, we ectopically expressed Rh7 using photoreceptor-specific drivers, either *GMR*-GAL4 (expression in all photoreceptors from early development on) or *rh1*-GAL4 (expression in R1-R6 photoreceptors from late pupal stage on), and analyzed the morphology of the compound eyes in paraffin and/or semithin sections of adult fly heads. *Rh1*-GAL4-mediated misexpression of Rh7 in R1-R6 produced normal control-like eye phenotypes, whereas both retina and lamina in *GMR-GAL4; UAS-rh7* head sections were clearly reduced in size. Although we did not observe a rough eye

phenotype in *GMR*-GAL4 homozygous flies under the dissection microscope, ~50% of them showed a *GMR-GAL4; UAS-rh7*-similar diminution of the retinal and the laminar layer. It has been shown that *GMR*-GAL4 causes developmental abnormalities in a dose-dependent manner including morphological defects, e.g., ommatidia of irregular size (Kramer and Staveley, 2003). Since there is no possibility to distinguish between *GMR*-GAL4-dependent and Rh7-induced effects, we repeated our experiment using the long*GMR*-GAL4 *(lGMR-GAL4)* driver, which was supposed to interfere with normal eye development to a much lesser extent. Nevertheless, we got similar results and observed unaffected as well as degenerated eye structures within both the driver and the *lGMR-GAL4; UAS-rh7* line and thus could not draw any final conclusion regarding the influence of Rh7 on the developing compound eye. However, later onset of Rh7 expression (*rh1*-GAL4) did not obviously alter the eye morphology, thereby indicating that additional localization of Rh7 to R1-R6 rhabdomeres does not disrupt the normal ommatidal pattern. Since the fine structure and arrangement of ommatidia cannot be investigated on paraffin sections, it might be helpful to examine these eye phenotypes by scanning electron microscopy, which allows to detect small structural differences and could therefore help to differentiate between misexpression- and GAL4-specific defects (as, for example, demonstrated in Anh et al., 2011).

Rh7 does not only work as a functional photoreceptor and compensate for the loss of Rh1 in photoreceptor development; but it is also able to restore motion vision in *Rh1-Rh7; ninaE* flies (Fig. 30B). Interestingly, this rescue experiment may allow for drawing conclusions about the Rh7 signaling pathway, since it showed that Rh7 has to be able to initiate the classical rhodopsin signaling cascade, and might thus generally use this pathway. I tried to confirm this assumption and aimed to interrupt rhodopsin signaling by generating *norpA; Rh1-Rh7; ninaE* triple mutants (which additionally lack PLCβ, a crucial enzyme in the visual transduction pathway) but, unfortunately, the required crosses were not viable. On the other hand, Rh7 does not seem to contribute to the OR in wild-type flies, since $rh7^0$ mutants were not impaired in this innate behavior but responded normally in our experiments. However, the OR in $rh7^0$ and control flies is currently investigated using a much more sophisticated setup that provides automated recording and allows changes in basic experimental parameters, e.g., pattern color or contrast. First results indeed indicated a reduced response in *rh7* knockout mutants to a bright achromatic stimulus (pattern of white stripes) of low luminance contrast (Schlichting, personal communication).

4.2.2 Rh7 in circadian photoreception

4.2.2.1 Blue-light shift experiments

The speed of re-entrainment to a shifted LD cycle generally reflects the sensitivity of a circadian oscillator or rather its photoreceptors to light. It was difficult to specifically address the function of Rh7 in photic entrainment because six other rhodopsins and the circadian photoreceptor CRY are expressed at comparatively high levels and are known to mediate light entrainment (see section 1.9). Nevertheless, re-synchronization was significantly slower for both 6 h phase advances and delays in *rh7* null mutants at a wavelength of ~470 nm, at which Rh7 presumably shows its maximum spectral sensitivity (Grebler, unpublished data). It is remarkable to see that Rh7 contributes to re-entrainment under these conditions, because both Rh1 (the major rhodopsin) and CRY (the main circadian photoreceptor) are highly sensitive to blue light either, and Rh1 was found to be expressed at normal levels in heads of $rh7^0$ mutants (Senthilan, personal communication). Unexpectedly, overexpression of Rh7 in *Rh1-Rh7* slowed down the process of re-entrainment as well – meaning that, under these conditions, not only the loss of Rh7 but also its additional presence in R1-R6 directly or indirectly reduced the sensitivity of the circadian clock. At ~400 nm conditions, we could only observe the same tendency in *rh7* null mutants, indicating that Rh7 has less impact at this shorter wavelength, whereas re-entrainment in *Rh1-Rh7* flies was not affected at all.

It is hard to understand why and how high levels of Rh7 expression should impair light entrainment, especially considering the fact that *Rh1-Rh7* flies showed an increased ERG response and thus a higher sensitivity to white light than their wild-type controls (Grebler, 2010). Since we found a reduction of circadian sensitivity in the absence of Rh7, it is even more puzzling that *rh7* knockout mutants themselves were shown to be not less sensitive but, on the contrary, even more sensitive to white light in the ERG (Grebler, unpublished data). However, one has to be aware that these results are not directly comparable. The ERG measures a physiological response to light, whereas our shift experiments investigate locomotor activity rhythms, a circadian behavioral output which is preceded and regulated by a wide range of processes within the entire circadian system. Nevertheless, these differences could also indicate that, despite its previously demonstrated photoreceptive qualities, Rh7 might not necessarily act as a photoreceptor *in vivo*, but could as well have the ability to affect the sensitivity of other photoreceptors. Although we will first focus on the role of Rh7 in circadian entrainment in the following, speculations about a more general function of Rh7 will be discussed in a later section.

4.2.2.2 Entrainment to LD and LM cycles

Since blue-light shift experiments provided some initial behavioral evidence that Rh7 is indeed involved in light entrainment, we investigated circadian photoreception in *rh7* null mutants by studying locomotor activity rhythms under LD and LM 12:12 cycles. In order to investigate a possible direct or indirect functional interaction between CRY and Rh7, we additionally analyzed cry^{01} flies and the corresponding $rh7^{0}$ cry^{01} double mutants.

In comparison to control flies, morning activity (MA) levels were generally decreased in $rh7^{0}$ mutants under both entrainment conditions. Furthermore, DAM System and LM monitoring revealed that this reduction in activity was accompanied by an advanced MA peak reflected by higher activity levels prior to lights-on and an earlier offset of MA. These effects did not directly depend on the irradiance and we obtained similar results with light intensities ranging from 10 lux up to 1000 lux. Nevertheless, most of the characteristics were more pronounced under lower light intensities when activity levels were higher in both genotypes, indicating that the general preference for low light intensities in wild-type flies (Rieger et al., 2007) persists in the absence of Rh7. Like in $rh7^{0}$, the offset of activity was advanced and the following siesta prolonged in cry^{01} mutants, although their MA levels were not significantly reduced. Interestingly, the corresponding $rh7^{0}$ cry^{01} double mutants mainly exhibited additive effects; their small MA bout was characterized by further reduction of MA levels and an even earlier offset of activity (see Fig. 41A, B). Since additive effects are often observed for two components that normally either operate in or affect the same pathway, these results could have provided a first hint that Rh7 and CRY act at different steps in a common light input pathway mediating circadian photoreception. Unfortunately, this finding did not hold true for the evening activity.

Whereas lack of either CRY or Rh7 affected the MA in the same way, the EA was completely different in the individual single mutants. In $rh7^{0}$ mutants, the EA peak was only slightly advanced and thus hardly affected under LD and LM cycles, whereas the onset of EA was significantly delayed in cry^{01} mutants. Cry^{01} mutants shifted their EA peak into the night, especially under moonlight conditions. As a consequence, EA levels were decreased prior to and increased subsequent to lights-off, respectively (Fig. 46, right column). The delay of the EA peak under nocturnal dim-light conditions is known to be mediated by the rhodopsin photoreceptors of the compound eye, and it has also been shown that *cry* mutant flies are able to shift their activity into moonlight under comparably high light intensities (Bachleitner et al., 2007).

However, the evening activity was differently affected in *rh7^{0} cry^{01}*, especially under LD conditions, and we observed opposite effects in comparison to *cry^{01}*: The EA onset occurred significantly earlier and activity levels were significantly increased prior to and decreased subsequent to lights-off provoking an advanced and generally more prominent EA peak (see Fig. 42). In contrast, the investigated parameters were hardly different from *rh7^{0}* flies and indicated only a slightly advanced EA in *rh7^{0} cry^{01}* double mutants. In summary, loss of both CRY and Rh7 restored the wild-type EA peak in *rh7^{0} cry^{01}*, except for an advanced EA onset in LD conditions. As previously indicated, a model in which CRY and Rh7 synergistically interact in the same linear entrainment pathway could not explain this complex result and thus different independent roles of these two proteins should rather be considered. To gain a better understanding of the three mutant phenotypes and to further investigate their behavioral characteristics, we monitored locomotor activity rhythms under different photoperiods.

4.2.2.3 Entrainment to different photoperiods

Although we could not calculate MA levels and the MA offset in revertant control flies under short (08:16) and long days (16:08), the MA peak was clearly reduced and advanced in *rh7^{0}* mutants, thereby confirming the previous LD 12:12 results (Fig. 47). Moreover, the prolongation of their midday trough was already present under 08:16 and became even more prominent under 16:08 cycles. In addition, the EA onset was significantly delayed in *rh7^{0}* under the different photoperiods and, under short days, the mutants even shifted their EA further into the night. Interestingly, the same effects are usually observed in wild-type flies when subjected to LD 12:12 cycles of high light intensities (Rieger et al., 2007). With increasing irradiance, the activity peaks move further apart (the MA advances, whereas the EA delays), resulting in a broad midday trough. In *rh7^{0}* mutants, this behavior could be caused by an increased sensitivity to light, which was indeed confirmed in the ERG both by adaptation experiments and by recording a dose-response curve (Grebler, unpublished data).

We found the same tendencies in *cry^{01}* mutants but, in contrast to revertant and *rh7^{0}*, their MA peak followed lights-on under 08:16 cycles, and it did not advance into the night until the day was further shortened to 04:20 conditions. The same applied to the EA peak which did not shift into the night under short days and followed lights-off even under long days of 20 h. Thus, *cry^{01}* activity was able to precisely track lights-on and -off transitions independent from the respective photoperiod. Remarkably, this tracking behavior has neither been observed in wild-type flies before nor in *cry^{b}* mutants under lower light intensities of a different source (Rieger et al., 2003; Rieger et al., 2012). In

the Northern Hemisphere, all organisms experience extreme photoperiods. Fruit flies are generally able to entrain their daily activity rhythms to these short and long day conditions, respectively. In this context, CRY has been shown to be mainly important for entrainment to short photoperiods (Rieger et al., 2003). Thus, the flexibility in the timing of the activity bouts in the absence of CRY might even explain why northern *Drosophila* species (e.g., *D. montana*), which are subjected to very long photoperiods during summer, showed a reduced number of CRY-positive clock neurons (Hermann et al., in press).

Both under short and long days, the activity profiles of $rh7^{0}$ cry^{01} mutants closely resembled those of cry^{01} flies (Fig. 47) except for the (slightly) advanced EA onset and the resulting broad EA bout that were already observed under equinox conditions. Nevertheless, $rh7^{0}$ cry^{01} mutants differed from cry^{01} flies in some of the investigated parameters, but these effects could not be explained by the characteristics of the $rh7^{0}$ mutant. However, activity monitoring under different photoperiods suggested that Rh7 and CRY play rather different roles and might have different functions in either short or long day conditions. This might be one reason why the activity pattern of $rh7^{0}$ cry^{01} double mutants appears difficult to explain. Analysis of clock protein oscillation might be the most appropriate way to investigate the mechanisms underlying the three mutant phenotypes. According to the dual oscillator model, morning (M) and evening (E) peak of the fly's bimodal activity pattern are thought to be controlled by certain subsets of clock neurons representing morning and evening oscillator (MO and EO), respectively. In a simplified model, the MA is under the control of the s-LN_v neurons, whereas the LN_ds together with the 5^{th} s-LN_v control the EA. The oscillators are coupled and their molecular oscillations (cycling of clock proteins) are in phase but respond differently to light (Grima et al., 2004; Stoleru et al., 2004; Rieger et al., 2006). Based on this model, it should be possible to show a correlation between the activity pattern, with regard to the timing of activity peaks, and the PER cycling in the corresponding oscillator cells. Since there are, for example, differences in the EA maximum of up to 4 h between control and cry^{01} flies under long days, phase delays in the maximal staining intensity should be easily observed; but even smaller differences of only 1-2 h, as found in the onset of EA under 12:12 cycles, might be reflected in the EO staining profile.

4.2.2.4 Activity rhythms under constant conditions

Screens for mutations that alter the period length of the free-running rhythm were and are still widely used to identify clock components. Locomotor activity monitoring under DD conditions showed that the loss of Rh7 does not alter free-running rhythms and is thus in agreement with our results under entrained conditions, which strongly suggest a role of Rh7 in light entrainment. Our data confirmed robust free-running rhythms in cry^{01} mutants as previously published by Dolezelova et al. (2007). The same was true for $rh7^{0}$ cry^{01} flies, although we found clearly reduced free-running rhythmicity. Since this alteration was only detected in one of the two $rh7^{0}$ cry^{01} recombinant strains (#39), it is rather unlikely that this effect indeed depends on the mutations, and might also be due to the generally lower activity levels initially observed in $rh7^{0}$ cry^{01}*#39* flies.
In LL, $rh7^{0}$ mutants behaved like wild-type controls and immediately became arrythmic indicating that CRY-dependent resetting mechanisms are not affected in $rh7^{0}$ mutants. In cry^{01}, we observed the splitting phenotype described for *cry* mutant flies under LL of high intensity but only in ~20% of the flies and thus less frequently (Yoshii et al., 2004; Dolezelova et al., 2007). The majority of flies (~65%) exhibited free-running rhythms of long period, but the ratio of these phenotypes seems to be temperature and especially irradiance-dependent (see references above). Interestingly, $rh7^{0}$ cry^{01} double mutants showed only a single long periodic component. Previous results indicated that rhythm dissociation is caused by the external photoreceptors, since LL splitting was absent in $norpA^{P41}$*;;* cry^{b} and so^{1}*;* cry^{b} double mutants (Yoshii et al., 2004). Our $rh7^{0}$ cry^{01} strains gave equivalent results, and thus Rh7 might contribute to or even mediate this rhythm dissociation. However, the number of analyzed flies was low under LL conditions, but if our observation holds true, it would additionally support a photoreceptive function for Rh7 and imply signaling via the classical visual pathway.

4.3 Rh7 – one protein, many abilities

This thesis mainly aimed to characterize Rh7, a yet unknown photoreceptor candidate in *Drosophila*. We could show that *rh7* is expressed in the retina of the compound eye as well as in the adult brain at equally low levels. The predicted Rh7 protein structure is similar to the six previously described rhodopsins including all structural properties required for a photoreceptive function. Furthermore, we confirmed that Rh7 is indeed able to replace Rh1 in several aspects: In *ninaE* mutants, expression of Rh7 in place of Rh1 in R1-R6 photoreceptors 1) prevented retinal degeneration 2) rescued motion vision and 3) restored the wild-type ERG response (Grebler, 2010). These properties

require localization of Rh7 to rhabdomeral microvilli, a light-activated conformational change into the biologically active metarhodopsin state and the subsequent initiation of the common rhodopsin phototransduction cascade by G_q protein interaction. Taken together, these findings clearly show that Rh7 has the ability to function as a classical rhodopsin photoreceptor in *Drosophila*. However, these results solely rely on ectopical expression of Rh7, and there are other arguments favoring different *in vivo* functions. First of all, loss of Rh7 caused an increase in sensitivity to white light and a reduction in the adaptation response (prolonged depolarizing afterpotential or PDA) in the ERG. Moreover, the OR to bright stimuli of low pattern contrast was reduced in $rh7^0$ mutants, thereby confirming impaired light adaptation. Both responses the PDA and the OR depend on Rh1 function suggesting that Rh7 is somehow able to affect Rh1 function. Since flies were more light-sensitive in the absence of Rh7, it would be feasible that Rh7 usually shields incoming light from R1-R6 photoreceptor cells. Thus, less photons would be available to activate rhabdomeral Rh1, thereby probably facilitating optimal adaptation. This theory suggests an indirect effect of Rh7 and would also explain the circadian phenotype of *rh7* null mutants. They prolonged their midday trough just like wild-type flies when experiencing high irradiances (see discussion on entrainment).

Rh7 is expressed at low levels in *D. melanogaster* which is known to prefer low light intensities and to be mostly active around dusk and down under laboratory conditions (Rieger et al., 2007; Rieger et al., 2012). Besides, *rh7* is highly conserved across the *Drosophila* genus (Senthilan, personal communication). In order to test our shielding hypothesis, it would be interesting to analyze *rh7* expression levels of species that are exposed to high light intensities due to their habitat, such as *D. Helvetica*, which lives in the Himalaya above 4000 m altitude. This species is active during midday and thus exposes itself to irradiances of ~120,000 lux in summer (Vanlalhriatpuia et al., 2007). A light-dependent function of Rh7 might also be supported by the finding that wild-type flies reared under darkness conditions for 57 years carried a nonsense mutation in the *rh7* gene resulting in a 21-aa C-terminal truncation of the protein (Izutsu et al., 2012).

Although Rh7 shares sequence similarities to the known *Drosophila* Rhs, phylogenetic analysis revealed more closely related genes of *rh7* in mosquitoes *(A. gambiae)*, the human body louse *(P. humanus corporis)*, pea aphids *(A. pisum)* and, interestingly, in *Daphnia pulex* (Senthilan, unpublished data). This crustacean is believed to represent the ancestral arthropods from which insects originated (Glenner et al., 2006). Thus, Rh7 might be considered an ancient pigment. Unfortunately, nothing is known about the function of any of these gene products. The circadian system of

aphids is currently investigated in our workgroup. This will be a good opportunity to study the expression of *rh7*-related genes as well.

Due to its predicted 7TM domain structure, the suggested shielding function of Rh7 would either require co-expression of Rh7 along with Rh1 in R1-R6 photoreceptors or localization in ommatidia-associated accessory cells. Targeting to R7 and/or R8 cells seems rather unlikely because of their central location. Although the expression of two visual pigments in one photoreceptor was under discussion and even frowned upon for a long time ("one rhodopsin - one PR rule"), co-expression of Rh3 and Rh4 in R7 has been shown in a dorsal subtype of y-ommatidia (Mazzoni et al., 2008). Thus, expression of both Rh1 and Rh7 could theoretically occur in the same photoreceptor cell, although we were skeptical (*ninaE* phenotype). On the other hand, we could not yet provide any experimental evidence for Rh7 biosynthesis in non-photoreceptor cells. As far as we can estimate, expression of Rh7 in the eight photoreceptors of the HB-eyelets could not reflect *rh7* expression levels in the fly brain. For this reason, Rh7 is either present in other than photoreceptor cells or *rh7* transcripts are not translated into protein. In any case, Rh7 might have an additional shielding-independent function in the brain, but further investigation would urgently require specific antibodies.

The *Drosophila* Interactions Database (DroID) is a comprehensive genes and proteins interaction database which predicts interaction with microRNAs for *rh7* (20 in total). These are short non-coding RNAs which specifically regulate (primarily repress) target gene expression at the posttranscriptional level and which are generally important for normal development and also cellular functions (for review, see Ambros, 2004). Even though ~240 miRNAs have been identified in *Drosophila* to date (www.mirbase.org), their functions remained largely unknown. Some of them have been associated with circadian clock function including two of the 20 potential *rh7*-interaction candidates, *miR-8* and *miR-219-1* (Brennecke et al., 2003; Cheng et al., 2007; for review: Pegoraro and Tauber, 2008). Low levels of *rh7* expression might be explained by miRNA-mediated silencing, but database predictions should be treated with caution and require further verification.

Apart from our current model, there are other (previously) suggested functions for Rh7 that could not be further supported by our data. Even though we observed *rh7*-GAL4-mediated reporter gene expression in the antennae, $rh7^{0}$ mutants were not impaired in sound sensing (Piepenbrock, personal communication) and expression of *rh7* in the second antennal segment was below the limit of detection in a recent microarray study (Senthilan, 2010). Thus, Rh7 might not be involved in auditory signaling. Furthermore, Rh7 is probably not the unknown photoreceptor believed to be present in certain DN

clock neurons (Helfrich-Förster et al., 2001; Rieger et al, 2003; Veleri et al., 2003). In order to mediate residual entrainment in *norpA*^{P41}*;; cry*^{b} double mutants, this unknown visual pigment was predicted to signal via a *norpA*-independent pathway. In contrast, Bleyl (2008) did not detect co-expression of PER and *rh7* in gene expression studies neither in the dorsal nor in the lateral brain. Furthermore, Rh7 was able to initiate the classical *norpA*-dependent signal transduction cascade in our experiments. Thus, Rh7 is a rather unsuitable candidate for this role, although an additional PLCβ-independent pathway, which contributes to circadian entrainment, has recently been suggested for Rh5 and Rh6 (Veleri et al., 2007; Szular et al., 2012). A third theory, suggesting an additional catalytic function of Rh7 based on similarities to the vertebrate circadian ocular photoreceptor melanopsin (low expression levels and a lack of the conserved HEK motif) was not further investigated (see Bachleitner, 2008) Thus, the question, if Rh7 could also work as an isomerase remains unanswered for now.

Although this thesis could, without question, contribute to the characterization of Rh7, both main topics localization and function of Rh7 require further investigations. It will be crucial to verify the Rh7 expression pattern in order to gain closer insights into the *in vivo* function of Rh7.

5 Summary

Many organisms evolved an endogenous clock to adapt to the daily environmental changes caused by the earth's rotation. Light is the primary time cue *("Zeitgeber")* for entrainment of circadian clocks to the external 24-h day. In *Drosophila*, several visual pigments are known to mediate synchronization to light: The blue-light photopigment Cryptochrome (CRY) and six well-described rhodopsins (Rh1-Rh6). CRY is present in the majority of clock neurons as well as in the compound eyes, whereas the location of rhodopsins is restricted to the photoreceptive organs – the compound eyes, the ocelli and the HB-eyelets.

CRY is thought to represent the key photoreceptor of *Drosophila's* circadian clock. Nevertheless, mutant flies lacking CRY *(cry^{01})* are able to synchronize their locomotor activity rhythms to light-dark (LD) cycles, but need significantly longer than wild-type flies. In this behavior, cry^{01} mutants strongly resemble mammalian species that do not possess any internal photoreceptors and perceive light information exclusively through their photoreceptive organs (eyes). Thus, a mammalian-like phase-shifting behavior would be expected in cry^{01} flies. We investigated this issue by monitoring a phase response curve (PRC) of cry^{01} and wild-type flies to 1-h light pulses of 1000 lux irradiance. Indeed, cry^{01} mutants produced a mammalian-similar so called type 1 PRC of comparatively low amplitude (< 25% of wild-type) with phase delays to light pulses during the early subjective night and phase advances to light pulses during the late subjective night (~1 h each).

Despite the predominant role of CRY, the visual system contributes to the light sensitivity of the fly's circadian clock, mainly around dawn and dusk. Furthermore, this phase shifting allows for the slow re-entrainment which we observed in cry^{01} mutants to 8-h phase delays of the LD 12 h:12 h cycle. However, cry^{01} also showed surprising differences in their shifting ability: First of all, their PRC was characterized by a second dead zone in the middle of the subjective night (ZT17-ZT19) in addition to the usual unresponsiveness during the subjective day. Second, in contrast to wild-type flies, cry^{01} mutants did not increase their shift of activity rhythms neither in response to longer stimuli nor to light pulses of higher irradiance. In contrast, both 6-h light pulses of 1000 lux and 1-h light pulses of 10,000 lux light intensity during the early subjective night even resulted in phase advances instead of the expected delays. Thus, CRY seems to be not only responsible for the high light sensitivity of the wild-type circadian clock, but is apparently also involved in integrating and processing light information.

Rhodopsin 7 (Rh7) is a yet uncharacterized protein, but became a good photoreceptor candidate due to sequence similarities to the six known *Drosophila* Rhs. The second part of this thesis investigated the expression pattern of Rh7 and its possible functions, especially in circadian photoreception. Furthermore, we were interested in a potential interaction with CRY and thus, tested cry^{01} and $rh7^{0}$ cry^{01} mutants as well.

Rh1 is the main visual pigment of the *Drosophila* compound eye and expressed in six out of eight photoreceptors cells (R1-R6) in each of the ~800 ommatidia. Motion vision depends exclusively on Rh1 function but, moreover, Rh1 plays an important structural role and assures proper photoreceptor cell development and maintenance. In order to investigate its possible photoreceptive function, we expressed Rh7 in place of Rh1. Rh7 was indeed able to overtake the role of Rh1 in both aspects: It prevented retinal degeneration and mediated the optomotor response (OR), a motion vision-dependent behavior.

At the transcriptional level, *rh7* is expressed at approximately equal amounts in adult fly brains and retinas. Due to a reduced specificity of anti-Rh7 antibodies, we could not verify this result at the protein level. However, analysis of *rh7* null mutants ($rh7^{0}$) suggested different Rh7 functions *in vivo*. Previous experiments strongly indicated an increased sensitivity of the compound eyes in the absence of Rh7 and suggested impaired light adaptation. We aimed to test this hypothesis at the levels of circadian photoreception. Locomotor activity rhythms are a reliable output of the circadian clock. $Rh7^{0}$ mutant flies generally displayed a wild-type similar bimodal activity pattern comprising morning (M) and evening (E) activity bouts. Activity monitoring supported the proposed “shielding” function, since $rh7^{0}$ mutants behaved like wild-type flies experiencing high irradiances. Under all investigated conditions, their activity peaks lay further apart resulting in a prolonged midday break. The behavior of cry^{01} mutants was mainly characterized by an unexpectedly high flexibility in the timing of M and E activity bouts which allowed tracking of lights-on and lights-off even under extreme photoperiods. Activity profiles of the corresponding $rh7^{0}$ cry^{01} double mutants reflected neither synergistic nor antagonistic effects of Rh7 and CRY and were dominated by a broad E activity peak. In the future, the different circadian phenotypes will be further investigated on the molecular level by analysis of clock protein cycling in the underlying pacemaker neurons.

The work of this thesis confirmed that Rh7 is indeed able to work as a photoreceptor and to initiate the classical phototransduction cascade. On the other hand, it provided further evidence at the levels of circadian photoreception that Rh7 might serve as a shielding pigment for Rh1 *in vivo*, thereby mediating proper light adaptation.

6 Zusammenfassung

Viele Lebewesen haben eine endogene (circadiane) Uhr entwickelt, um sich an die im 24-Stunden-Rhythmus variierenden Umweltbedingungen anzupassen, die auf der Erdrotation beruhen. Zur Synchronisation auf den externen 24-Stunden-Tag nutzen circadiane Uhren in erster Linie Licht als Zeitgeber. An dieser Lichtsynchronisation sind bei *Drosophila* nachweislich eine Reihe von Sehpigmenten, der Blaulicht Photorezeptor Cryptochrom (CRY) sowie sechs bekannte Rhodopsine (Rh1-Rh6), beteiligt. CRY ist sowohl in der Mehrheit der Uhrneuronen als auch in den Komplexaugen zu finden. Die Lokalisation der Rhodopsine ist im Gegensatz dazu auf die Photorezeptoren – die Komplexaugen, die Ocellen und die HB-Äuglein – beschränkt.

CRY gilt als der entscheidende Photorezeptor in der circadianen Uhr von *Drosophila*. Zwar können Mutanten, die kein CRY besitzen *(cry^{01})*, ihre Laufaktivitätsrhythmen durch Licht-Dunkel-Zyklen synchronisieren, jedoch brauchen sie dafür mehrere Tage und damit erheblich länger als wildtypische Fliegen. In diesem Verhalten ähneln *cry^{01}*-Mutanten den Säugetieren, die nicht über interne Photorezeptoren verfügen und Licht somit ausschließlich über ihre Lichtsinnesorgane (Augen) wahrnehmen. Demnach wären bei *cry^{01}*-Fliegen säugetierähnliche Phasenverschiebungen des Laufaktivitäts-rhythmus auf Lichtpulse zu erwarten. Um diesen Sachverhalt zu untersuchen, wurde sowohl für *cry^{01}*-Mutanten als auch für Wildtyp-Fliegen eine Phasenresponsekurve (PRC) aufgezeichnet, wobei einstündige Lichtpulse mit einer Intensität von 1000 lux als Stimulus dienten. Wir erhielten für die *cry^{01}*-Mutanten tatsächlich eine säugetierähnliche PRC, welche auch als so genannte Typ 1 PRC bezeichnet wird und sich durch eine im Vergleich zum Wildtyp verringerte Amplitude (< 25%) auszeichnete. Die dabei beobachteten maximalen Phasenverschiebungen betrugen ungefähr eine Stunde. Dies galt sowohl für Lichtpulse, die in der ersten Hälfte der subjektiven Nacht gegeben wurden und die Laufaktivität verzögerten (nach hinten verschoben), als auch für Lichtpulse, die in der zweiten Hälfte der subjektiven Nacht gegeben wurden und die Laufaktivität beschleunigten (nach vorne verschoben).

Die für *cry^{01}*-Mutanten ermittelten Reaktionen auf einstündige Lichtpulse erklären die langsame Resynchronisation der Mutanten auf Phasenverschiebungen des Licht-Dunkel-Zyklus (LD-Zyklus). Allerdings zeigte die PRC von *cry^{01}*-Mutanten auch überraschende Besonderheiten, die bisher für kein Tier berichtet wurden. Üblicherweise hat eine PRC eine so genannte „Tot-Zone“ am subjektiven Tag, d. h.

die Tiere reagieren nicht auf Lichtreize, die während des subjektiven Tages verabreicht werden. Die PRC der *cry*^{01}-Mutanten zeichnete sich durch eine zweite solche Tot-Zone in der Mitte der subjektiven Nacht (ZT17-ZT19) aus. Außerdem konnten die Phasenverschiebungen in *cry*^{01}-Mutanten weder durch eine Verlängerung noch durch eine Verstärkung des Reizes gesteigert werden. Dies steht im Gegensatz zu wildtypischen Fliegen und anderen Tieren, deren PRC dosisabhängig ist. Bei *cry*^{01}-Mutanten riefen dagegen sowohl sechsstündige Lichtpulse der zuvor verwendeten Intensität (1000 lux) als auch einstündige Lichtpulse hoher Intensität (10.000 lux) sogar gegenteilige Effekte auf die Phasenverschiebung hervor. Die *cry*^{01}-Mutanten reagierten auf den Stimulus, der jeweils in der ersten Nachthälfte einsetzte, unter beiden Bedingungen mit einer Vorverschiebung ihres Aktivitätsrhythmus anstatt mit der eigentlich erwarteten Verzögerung.
Obwohl CRY sicher die wichtigste Rolle einnimmt, trägt auch das visuelle System zur Lichtsensitivität und Synchronisation der inneren Uhr der Fliege bei. Dies ist vor allem morgens und abends in der Dämmerung der Fall. *Cry*^{01}-Mutanten reagierten auf Lichtpulse, die morgens oder abends gegeben wurden, mit den oben beschriebenen einstündigen Phasenverschiebungen. Dies reicht aus, um die Aktivität der Fliegen auf einen Licht-Dunkel-Zyklus zu synchronisieren.

Rhodopsin 7 (Rh7) ist ein noch nahezu unbeschriebenes Protein, das Ähnlichkeiten in seiner Aminosäuresequenz zu den bereits bekannten *Drosophila*-Rhodopsinen besitzt und daher als potentieller neuer Photorezeptor betrachtet wird. Der zweite Teil dieser Arbeit beschäftigte sich mit dem Expressionsmuster sowie den möglichen Funktionen von Rh7, insbesondere in der circadianen Photorezeption. Darüber hinaus wurden *rh7*^{0} *cry*^{01}-Doppelmutanten getestet, um eine eventuelle Interaktion zwischen Rh7 und CRY zu untersuchen.
Rh1, das in jeweils sechs von acht Photorezeptorzellen (R1-R6) der insgesamt rund 800 Ommatidien exprimiert wird, stellt das häufigste Photopigment im Komplexauge von *Drosophila* dar. Zum einen vermittelt Rh1 die Wahrnehmung von Bewegungen, zum anderen besitzt es wichtige strukturelle Aufgaben, da es sowohl eine normale Entwicklung der Photorezeptorzellen als auch deren Erhaltung gewährleistet. Um eine mögliche Beteiligung in der Lichtwahrnehmung zu untersuchen, wurde Rh7 anstelle von Rh1 exprimiert. Rh7 konnte in der Tat Rh1 unter beiden Aspekten ersetzen. Seine Expression verhinderte nicht nur die Degeneration der Retina, sondern ermöglichte zudem optomotorische Reaktionen, die auf einem intakten Bewegungssehen beruhen. In adulten Fliegen wird Rh7 auf Ebene der Transkription in vergleichbaren Mengen im

Gehirn und in der Retina exprimiert. Aufgrund der geringen Spezifität der anti-Rh7 Antikörper konnte dieses Ergebnis leider nicht auf Proteinebene bestätigt werden. Die Untersuchung von *rh7*-Knockout-Mutanten *($rh7^0$)* befürwortete jedoch eine alternative Funktion von Rh7 *in vivo*. In vorangegangenen Versuchen führte der Verlust von Rh7 zu einer gesteigerten Sensitivität der Komplexaugen, was wahrscheinlich auf einer verminderten Lichtadaptation beruhte. Wir versuchten diese Hypothese auf Ebene der circadianen Photorezeption zu überprüfen und zeichneten dazu die Laufaktivität der Fliegen auf, da ihr Aktivitätsrhythmus einen verlässlichen Output der circadianen Uhr darstellt.

Grundsätzlich wiesen die *$rh7^0$*-Mutanten das für Wildtyp-Fliegen typische bimodale Aktivitätsmuster auf, das sich durch zwei Aktivitätsmaxima auszeichnet, die entsprechend ihrer Lage als Morgen- beziehungsweise Abendaktivitätsgipfel bezeichnet werden. Dabei wurde beobachtet, dass sich *$rh7^0$*-Mutanten wie Wildtyp-Fliegen verhalten, die hohen Lichtintensitäten ausgesetzt sind. So zeigte deren Aktivitätsrhythmus unter allen Versuchsbedingungen eine verlängerte Mittagspause, die durch einen großen Abstand zwischen den beiden Aktivitätsmaxima hervorgerufen wurde. Durch diese Versuche wurde die Hypothese, dass Rh7 als eine Art Schirmpigment wirken könnte, auf Verhaltensebene bestätigt. Das Verhalten der *cry^{01}*-Fliegen zeichnete sich im Wesentlichen durch eine unerwartet hohe Flexibilität der beiden Aktivitätsmaxima aus. Diese konnten auch unter extremen Photoperioden an die Übergänge von Licht und Dunkelheit gekoppelt werden. Der Aktivitätsrhythmus der entsprechenden *$rh7^0$ cry^{01}*-Doppelmutanten wurde durch eine ausgeprägte Abendaktivität bestimmt und erlaubte es nicht, Rückschlüsse auf eine synergistische oder antagonistische Wirkung von Rh7 und CRY zu ziehen. Zukünftige Versuche könnten die verschiedenen circadianen Phänotypen auf molekularer Ebene charakterisieren, z. B. durch Untersuchung der Oszillationen der Uhrproteine in den verantwortlichen Schrittmacher-Neuronen.

Zum einen konnten die Versuche dieser Arbeit bestätigen, dass Rh7 in der Tat über die klassische Phototransduktionskaskade als Photorezeptor wirken kann. Darüber hinaus wurden auf Ebene der circadianen Photorezeption weitere Anzeichen für eine alternative *in vivo* Funktion von Rh7 gesammelt. Diese sprechen für eine Rolle von Rh7 als Schirmpigment für Rh1, wodurch Rh7 an der einwandfreien Lichtadaptation beteiligt wäre.

7 Supplementary

7.1 Appendices

7.1.1 Materials

7.1.1.1 Bacterial strains

Table 28: Bacterial strains used in this thesis.

Strain	Genotype	Source / Reference
Escherichia coli XL1-Blue competent cells	*recA1 endA1 gyrA96 thi-1 hsdR17 supE44 relA1 lac* [F'*proAB*$^{+}$, *lacI*^{q} *lacZΔM15* Tn*10* (Tet^{r})]	Stratagene #200249; Sambrook et al., 1989
NEB 10-beta competent *Escherichia coli*	*araD139 Δ*(*ara-leu*)7697 *fhuA lacX74 galK (*φ80 *Δ*(*lacZ*)*M15*) *mcrA galU recA1 endA1 nupG rpsL* (Str^{R}) *Δ*(*mrr-hsdRMS-mcrBC*)	NEB #103019

Bacterial strains were cultured in LB medium on a rotary shaker or on LB agar plates at 37°C for 14-16 hours.

7.1.1.2 Vectors

Table 29: Vectors used in this thesis; BDGC: Berkeley *Drosophila* Genome Project.

Vector	Size	Resistance	Source / Reference	Details / Purpose
pOT2	1665 bp	Chloramphenicol	Clone from BDGC cDNA library	*Rh7* cDNA clone GH14208
pGEM-T Easy	3015 bp	Ampicillin	Promega #A1360	Intermediate cloning step
pUAST	9050 bp	Ampicillin	Brand and Perrimon, 1993	Germline transformation; *white* marker

7.1.1.3 Oligonucleotides

Table 30: Primers used in this thesis.

Primer (notation)	Sequence (5'-3') in triplets	Annealing temperature	Application
RP49 Fw	CCA AGC ACT TCA TCC GCC ACC	52°C-62°C	Control primer Regensburg
RP49 Rv	GCG GGT GCG CTT GTT CGA TCC	52°C-62°C	Control primer Regensburg

α-tub CG1913-control-5’	TCT GCG ATT CGA TGG TGC CCT TA A	60°C	Control primer Würzburg
α-tub CG1913-control-3	GGA TCG CAC TTG ACC ATC TGG TGG GC	60°C	Control primer Würzburg
5’ Rh7 cDNA EcoRI	GCG AAT TCC ACC TCC AGC AGC AGC	56°C	Amplification of *rh7* cDNA from pOT2
3’ Rh7 cDNA KpnI	GCG GTA CCA GGC GAG TTT CAG ATA TTC C	56°C	Amplification of *rh7* cDNA from pOT2
SP6	TAT TTA GGT GAC ACT ATA G	55°C	Sequencing pGEM-T Easy
T7	TAA TAC GAC TCA CTA TAG GG	55°C	Sequencing pGEM-T Easy
rh7-II-sense	TCA TCA AAT GCC CGA TTG CC	54°C	Real-time PCR *rh7*
rh7-II-antisense	GCA CCA CCA CAT TGT ACC G	54°C	Real-time PCR *rh7*
5’ in E4 C2	CAG TAC CTA TTG TTT TTG TTA TGG	51°C-54°C	*Rh7* deletion mapping
3’ in E1 C1	ATG CTG GCA CTC GTT ATC	51°C-54°C	*Rh7* deletion mapping
5’ up P (P1)	GCC TTG GCA AAC ATG AGT CC	50°C-60°C	*Rh7* deletion mapping; cloning / sequencing
3’ do P (P3)	GCT GCA TAT CTC CAA GAC ATC C	50°C-60°C	*Rh7* deletion mapping; cloning / sequencing
3’ in E4 C1	AAG GGG CGG CCA TCA CAA TAC TG	50°C-60°C	*Rh7* deletion mapping; cloning / sequencing
Rh7 TM S	GTG TGG GCA ATG GCT TCG TCA	60°C-62°C	Identification of $rh7^{0}$ cry^{01} recombinant lines
Rh7 TM AS	AGG CCA CCA CAA ATC CAT AGA GG	60°C-62°C	Identification of $rh7^{0}$ cry^{01} recombinant lines
P-El Fw	TTA TCA ATG AAC ACC CGC CAC ACC	60°C-62°C	Identification of $rh7^{0}$ cry^{01} recombinants lines
P-El Rv	CAT CCG TTG CAT CCC AGA GC	60°C-62°C	Identification of $rh7^{0}$ cry^{01} recombinant lines
5’ up P (P2)	CCG GAA AGC CAA CTT ATG ATG G	50°C-56°C	Confirmation of $rh7^{0}$ cry^{01} recombinant lines
3’ do P (P3)	GCT GCA TAT CTC CAA GAC ATC C	50°C-56°C	Confirmation of $rh7^{0}$ cry^{01} recombinant lines
3’ do P (P4)	CGC CTT TAA GCT GCG AAT TCC	50°C-56°C	Confirmation of $rh7^{0}$ cry^{01} recombinant lines
3’ do P (P5)	GGA AAC AAA AAG GGG GAA GCG	50°C-56°C	Confirmation of $rh7^{0}$ cry^{01} recombinant lines

Rh7-qPCR-2-5'	GAC AAG CAC GTG AAT GAC AGC GTT TC	60°C	qPCR *rh7* brains and retinas
Rh7-qPCR-2-3'	TCC CAC CAC CGA AAT CAG GCA ATA CAG	60°C	qPCR *rh7* brains and retinas
ninaE-qPCR-5'	TCT GTA TTT CGA GAC CTG GGT GCT C	60°C	qPCR *rh1* brains and retinas
ninaE-qPCR-3'	GAC ATG AAC CAG ATG TAG GCA ATC TTG C	60°C	qPCR *rh1* brains and retinas

Desalted oligonucleotides were obtained from Invitrogen (orders from Regensburg), Sigma and AGCTLab (orders from Würzburg).

7.1.1.4 Antibodies and sera

Table 31: Antibodies used in this thesis; DSHB: Developmental Studies Hybridoma Bank; KIT: Karlsruher Institut für Technologie (Zoologisches Institut).

Primary antibody (host animal)	Application (working dilution)	Details	Source / Reference
4C5 Anti-rhodopsin (mouse)	Whole mount brains, retina (1:100)	Anti-rh1; monoclonal antibody	DSHB; de Couet and Tanimura, 1987
Anti-rh7 (rabbit) "Rh7:E"	Whole mount brains (1:1000)	20-mer peptide antibody against Rh7 (intracellular domain; T412-431)	J. Bentrop, KIT Karlsruhe; Bachleitner, 2008
Anti-rh7 (guinea pig; two animals)	Whole mount brains, retina (1:100-1:1000); Western blots (1:1000-1:5000); cryosections (1:1000-1:5000); paraffin sections (1:100-1:300)	18-mer peptide antibody against Rh7 (extracellular domain)	Pineda Antikörper-Service
Anti-rh7 (rabbit; two animals)		18-mer peptide antibody against Rh7 (extracellular domain)	Pineda Antikörper-Service
Anti-24B10 (mouse)	Whole mount brains, retina (1:100)	Anti-chaoptin; monoclonal antibody	Würzburg hybridoma library; Fujita et al., 1982
Anti-nb33 (mouse)	Whole mount brains (1:200)	Anti-PDF-precursor; monoclonal antibody	Würzburg hybridoma library; Hofbauer et al., 2009
Secondary antibody	Application (working dilution)	Details	Source / Reference
Alexa Fluor 488 goat anti-guinea pig	Whole mount brains, retina (1:200)	Highly cross-adsorbed	Molecular Probes (Invitrogen), #A-11073

Alexa Fluor 488 goat anti-rabbit	Whole mount brains, retina (1:200)		Molecular Probes (Invitrogen), #A-11008
Alexa Fluor 532 goat anti-mouse	Whole mount brains, retina (1:200)		Molecular Probes (Invitrogen), #A-11002
Alexa Fluor 635 goat anti-mouse	Whole mount brains, retina (1:200)		Molecular Probes (Invitrogen), #A-31574
Alexa Fluor 680 goat anti-rabbit	Western blot (1:5000)		Invitrogen, #A-21076
IRDye 680 donkey anti-guinea pig	Western blot (1:5000)	Polyclonal antibody, highly cross-adsorbed	LI-COR Biosciences #926-32411
Biotinylated goat anti-guinea pig	Paraffin sections (1:200)	Polyclonal antibody	Vector Laboratories #BA-7000
Vectastain ABC Kit (Rabbit IgG)	Paraffin sections	Includes biotinylated goat anti-rabbit antibody; polyclonal antibody	Vector Laboratories #PK-4001
Serum	Application (working dilution)	Details	Source / Reference
Normal goat serum (NGS)	Immunocytochemistry (2-5%)	Blocking of non-specific binding	Invitrogen #50-197Z

7.1.1.5 Commercial kits

Table 32: Commercial kits used in this thesis.

Kit	Application / Details	Source
Taq DNA Polymerase Master Mix (2x and 2.0 mM $MgCl_2$)	PCR (Würzburg)	VWR #733-2543
QIAquick Gel Extraction Kit	Isolation of DNA fragments from agarose gels	QIAGEN #28704
pGEM-T Easy Vector System I	T/A cloning	Promega #A1360
Big Dye Terminator v1.1 Cycle Sequencing Kit	Sequencing	Applied Biosystems #4337450
QIAprep Spin Miniprep Kit	Plasmid DNA extraction, mini scale (minipreparation)	QIAGEN #27104
QIAfilter Plasmid Midi Kit	Plasmid DNA extraction, medium scale (Regensburg)	QIAGEN #12243
GenElute Plasmid Midi Prep Kit	Plasmid DNA extraction, medium scale (Würzburg)	Sigma-Aldrich #PLD35-1KT

peqGOLD TriFast	RNA extraction (Regensburg)	Peqlab #30-2010
Quick-RNA MicroPrep	RNA extraction (Würzburg)	Zymo Research #R1050
QuantiTect Reverse Transcription Kit	cDNA synthesis	QIAGEN #205311
QuantiTect SYBR Green PCR Kit	Real-time PCR	QIAGEN #204143
Maxima SYBR Green/ROX qPCR Master Mix (2x)	Real-time PCR	Fermentas #KO221

7.1.1.6 Media

Table 33: Media used in this thesis; LB: Lysogeny broth.

Product	Contents / Details
LB_0 liquid medium	1% bacto-tryptone; 0.5% bacto-yeast extract; 1% NaCl; 0.3% NaOH; pH 7.0; culture medium
LB_{Amp} liquid medium	LB_0 with 50-100 µg/ml ampicillin; selective medium
LB_{Amp} agar plates	LB_{Amp} liquid media (100 µg/ml ampicillin) with 1.5% bacto-agar; selective plates
AXI agar plates	LB_{Amp} agar plates with 50 µl 1M IPTG and 50 µl X-Gal (8% in DMSO); blue/white screening
LB_{Cam} liquid medium	LB_0 with 25 µg/ml chloramphenicol; selective medium
LB_{Cam} agar plates	LB_{Cam} liquid media with 1.5% bacto-agar; selective plates
Apple juice agar egg laying plates	25% apple juice; 0.2% bacto-agar; 2.5% sucrose; 0.4% nipagin (in ethanol); embryo collection for germline transformation;
TriKinetics medium	4% sucrose; 2% agar-agar, Danish; medium for tubes

7.1.1.7 Enzymes, markers and ladders

Table 34: Enzymes, markers and ladders used; NEB: New England Biolabs.

Product	Application / Details	Source
Restriction enzymes	Digestion of Plasmid DNA	NEB
CIAP (Calf Intestine Alkaline Phosphatase)	Dephosphorylation of vectors	Fermentas #EF0341
Taq DNA polymerase	Polymerase for test PCR	Generated in the institute
RNase A (90 U/mg)	Plasmid mini preparation; 10 µg/ml	Roth #7156.1
T4 DNA ligase	Ligation reaction	NEB #M0202
FastStart Taq DNA Polymerase	Hot start PCR with increased specificity; sequencing of product	Roche #2 158 264

100 bp DNA ladder	Molecular weight marker; size and mass estimation of DNA fragments ranging from 100-1,517 bp in agarose gel electrophoresis	NEB #N3231
1 kb DNA ladder	Molecular weight marker; size and mass estimation of DNA fragments ranging from 0.5-10.0 kb in agarose gel electrophoresis	NEB #N3232
1 kb DNA ladder	Molecular weight marker; size and mass estimation of DNA fragments ranging from 0.25-10.0 kb in agarose gel electrophoresis	Fermentas #SM0311
Prestained Protein Marker, Broad Range (6-175 kDa)	Molecular weight marker; identification and size estimation of proteins on SDS-PAGE and Western blot	NEB #P7708S
Restriction enzymes	Digestion of Plasmid DNA	NEB and Fermentas
Taq DNA polymerase	Polymerase for test PCR	Generated within the department (Regensburg)
RNase (> 70 U/mg)	Plasmid mini preparation; 10 µg/ml	Roth #7164.1
FastStart Taq DNA Polymerase	Hot start PCR with increased specificity; sequencing of product	Roche #2 158 264

7.1.1.8 Buffers and solutions

Table 35: Buffers and solutions used in this thesis.

Application / Name	Contents / Details
Genomic DNA extraction	
Homogenization buffer	100 mM NaCl; 100 mM Tris, pH 8.0; 50 mM EDTA, pH 8.0; 0.5% SDS
Squishing buffer	50 mM NaOH; 1 M Tris-HCl, pH 8.0
Cloning	
X-Gal solution	8% X-Gal (w/v) in dimethylformamide; blue white selection of positive recombinant colonies
Chloramphenicol (stock)	3.4% chloramphenicol; solved in ethanol
RNA extraction	
DEPC water (RNase free)	0.1% DEPC; leave over night at 37°C, then autoclave
PCR and agarose gel electrophoresis	
10x LSB (low salt buffer)	200 mM Tris-HCl, pH 8.75; 100 mM KCl; 100 mM $(NH_4)_2SO_4$; 20 mM $MgSO_4$; 1 mg/ml BSA
50x TAE (Tris-acetate-EDTA)	242 g Tris base; 57.1 ml acetic acid; 100 ml 0.5 M EDTA, pH 8.0; make up to 1 l with deionized water

6x loading dye	0.001 M EDTA; 50% glycerol (v/v); 0.25% bromphenol blue (w/v); 0.25% xylencyanol (w/v)
Germline transformation	
10x injection buffer	50 mM KCl; 1 mM $NaPO_4$, pH 6.8
Mini-preparation of plasmid DNA	
GTE (Glucose-Tris-EDTA) buffer	50 mM glucose; 25 mM Tris-HCl, pH 8.0; 10 mM EDTA, pH 8.0
Alkaline-SDS solution	0.2 N NaOH; 1% SDS
Acetate solution	5 M potassium acetate; add 5 M glacial acetic acid to pH 4.8
Paraffin sections	
Carnoy's fixative	ethanol, 99%; chloroform; glacial acetic acid in the relative proportions 6:3:1
Semithin sections	
5x toluidine blue staining solution	1% toluidine blue (w/v); 1% sodium tetraborat (w/v)
Western blot	
Protein cracking buffer	10 mM $NaPO_4$, pH 7.2; 1% β-mercaptoethanol; 1% SDS (v/w); 6 M urea; 0.01% bromphenol blue (w/v)
5x electrophoresis buffer	1.5% Tris base; 7.2% glycin; 0.5% SDS
Transfer buffer (semi-dry)	48 mM Tris base; 39 mM glycin; 20% methanol; 0.27% SDS
10x TBS	100 mM Tris-HCl, pH 7.5; 1500 mM NaCl
1x TBST	10 mM Tris-HCl, pH 7.5; 150 mM NaCl; 0.1% Tween-20, add after autoclaving
Blocking buffer	Odyssey Blocking Buffer (LI-COR # 927-40003) and TBS at the ratio of 1:1, 0.02% sodium azide (NaN_3)
Resolving gel 12%	20 ml: 5.16 ml H_2O bidist.; 5.0 ml Tris pH 8.8; 100 µl SDS 20%; 8.0 ml 30% polyacrylamide; 1.63 ml 2% bisacrylamide; 100 µl APS 10%; 10 µl TEMED
Stacking gel 5%	10 ml: 6.63 ml H_2O bidist.; 1.25 ml Tris pH 6.8; 50 µl SDS 20%; 1.67 ml 30% polyacrylamide; 0.34 ml 2 % bisacrylamide; 50 µl APS 10%; 10 µl TEMED
Immunocytochemistry	
PB	0.1 M Na_2HPO_4 / NaH_2PO_4; at the ratio of 4:1 for pH 7.2-7.4
PBS	7 mM Na_2HPO_4; 3 mM Na_2HPO_4; 130 mM NaCl; pH 7.2-7.4
PBT (0.03, 0.1 and 0.5%)	PB with Triton X-100 (v/v) 0.1% and 0.5%; pH 7.2-7.4
Paraformaldehyde	4% PFA in PB or PBT 0.1% (w/v)
Blocking solution	5% NGS in PBT 0.5% or 0.1% (v/v)

7.1.1.9 Other reagents

Table 36: Other reagents used in this thesis.

Product	Application / Details	Source
Fixogum	Removable gum; cover slip sealing	Marabu #290117000
DPX	Embedding medium for semithin sections	Sigma #44581
GelRed Nucleic Acid Gel Stain	Replacement for ethidium bromide; DNA staining in agarose gels	Biotium #41003
Normal goat serum (NGS)	Immunocytochemistry (3-5%); blocking of non-specific binding	Invitrogen #50-197Z
Tissue-Tek O.C.T. Compound	Embedding medium for frozen tissue specimens; cryosections	Sakura #4583
Vectashield	Immunocytochemistry; mounting medium for fluorescence microscopy	Vector Laboratories #H-1000

7.1.1.10 Machines and equipment

Table 37: Machines and equipment used in this thesis; DAM: *Drosophila* Activity Monitoring.

Device	Details / Source
Activity monitoring system	DAMSystem, TriKinetics Inc.; homemade system, workshop of the University of Regensburg
Autoclave	2540 EK, Tuttnauer / Systec
Confocal microscope	Zeiss LSM 510 Meta, Leica TCS SPE
Bench-top centrifuge	Biofuge pico, Heraeus
Cryostat	Leica CM3000
Fluorescence microscope	Leica DMR
Fluorescence microscope camera	Olympus DP20 Leica Reichert 2040 Autocut Mikrotom
Hand-held homogenizer	Roth #9748.1
Imaging system (nucleic acids)	MultiImage light cabinet, INTAS; E-Box VX2, Vilber; visualization of nucleic acids with UV light
Imaging system (proteins)	Odyssey Infrared Imaging System, LI-COR; Western blot
Incubators	MIR-553, Sanyo Biomedica; I-36VL, Percival Scientific (temperature cycle); locomotor activity recording
Microtomes	Reichert-Jung, Heidelberg; paraffin sections; Leica Reichert 2040 Autocut; semithin sections
PCR machines	Robocycler Gradient 40, Stratagene; Mastercycler gradient, Eppendorf
qRT-PCR machines	LightCycler II, Roche; Rotor-Gene Q, QIAGEN

Refrigerated bench-top centrifuge	Eppendorf 5804 R
Refrigerated microcentrifuge	Heraeus Fresco 21, fixed-angle and swing-bucket rotor; plasmid DNA extraction (midi-preparation)
SDS-PAGE Gel electrophoresis unit (big)	SE600, Hoefer
SDS-PAGE Gel electrophoresis unit (small)	SE260, Hoefer
Electro blotting system	PerfectBlue Semi-Dry Electro Blotter; Peqlab; Western blot
Spectrophotometer	Ultrospec 3000, Pharmacia Biotech; NanoDrop 2000c, Thermo Scientific
Stereo microscope	Stemi SV6, Zeiss; SZ61, Olympus
Water system	TKA GenPure xCAD water purification system

7.1.1.11 Software

Table 38: Software used in this thesis; V: Version.

Program	Application / Details	Source
Chromas Lite 2.01	Sequencing data analysis	Technelysium; free software
DAMSystem3 data collection software	Locomotor activity monitoring	TriKinetics
DNASTAR V 5.03	Sequence alignment, primer design	DNASTAR
E-Capt	Agarose gel documentation, image analysis and editing	Vilber
El Temps V 1,236	Actogram plotting	Antoni Diez-Noguera; http://www.el-temps.com
Excel, Picture Manager, PowerPoint, Word 2003	Microsoft Office 2003; various applications	Microsoft
Excel macro Average activity LIGHT V 4.1	Average day calculation	T. Yoshii
Excel macro Periodogram analysis V 4.3	Period length determination	T. Yoshii
Excel template for activity peak determination	Activity peak determination	M. Schlichting
Fiji	Confocal image processing	Free software, http://fiji.sc/
GENtle V 1.9.4	Sequence alignment, cloning strategies	M. Manske, free software
LAS AF Light V 2.4.1	Confocal images	Leica

Lichtorgel	Light program control	G. Stöckl
NanoDrop 2000c	Spectrophotometer data analysis	Thermo Scientific
Odyssey V 1.1	Western blot imaging	LI-COR
Paint V 5.1	Figure and image processing	Microsoft
QtiPlot V 0,9,8,8(1)	Plotting of daily average activity profiles	ProIndep Serv S.r.l.
Rotor-Gene Q Series Software V 2.0.2	qPCR data analysis	QIAGEN
SYSTAT V 11.00.01	Statistics	SYSTAT
Zeiss LSM image browser V 4,2,0,121	Confocal images	Zeiss

7.1.1.12 Online resources

Table 39: Online resources used in this thesis.

Website	Application
http://www.basic.northwestern.edu/biotools/oligocalc.html	Oligonucleotide properties calculator
http://blast.ncbi.nlm.nih.gov/Blast.cgi	Alignment search tool
http://www.ceolas.org/fly/	The WWW Virtual Library: *Drosophila*
http://flyatlas.org/	*Drosophila* gene expression atlas
http://flybase.org/	*Drosophila* database
http://flystocks.bio.indiana.edu/	Bloomington Stock Center
http://www.ncbi.nlm.nih.gov/pubmed/	Literature search
http://sana.tkk.fi/awe/index.html	Academic writing in English
http://topcons.net/	Consensus prediction of membrane protein topology
http://www.sdbonline.org/fly/aimain/1aahome.htm	Guide to *Drosophila* development
http://www.droidb.org	*Drosophila* Interactions Database
http://www.google.de/	Search engine

7.1.1.13 Chemicals, consumables and small devices

Unless stated otherwise, all other chemicals, consumables, and small devices were purchased from the following companies: Amersham Biosciences, AppliChem, Atofina, Behrens, Biometra, BioRad, Biozym, Brand, Consort, Eppendorf, Fermentas, Gilson, Greiner Bio-One, Hartenstein, Heidolph, Hoefer, Integra, Invitrogen, Kimberly-Clark, LI-COR, Liebherr, Lumitronix, Memmert, Menzel, Merck, neoLab, New England

Biolabs (NEB), Pechiney Plastic Packaging, Peqlab, Promega, Qbiogene, QIAGEN, Roche, Roth, Sakura, Sarstedt, Scherf Präzision, Schleicher & Schuell, Scientific Industries, Siemens, Sigma-Aldrich, Tork, VWR and Whatman.

7.1.2 FlyAtlas anatomical expression data

Expression data obtained from http://flyatlas.org/ is presented in the following tables. Please note that two different data sets were provided for *rh7* mRNA levels.

Table 40: Anatomical expression profile for *ninaE*.

Tissue	mRNA Signal	Present Call	Enrichment	Affy Call
Brain	57 ± 10	4 of 4	0.00	Down
Head	5940 ± 192	4 of 4	2.20	Up
Eye	9586 ± 92	4 of 4	3.47	Up
Thoracicoabdominal ganglion	9 ± 2	2 of 4	0.00	Down
Salivary gland	24 ± 2	3 of 4	0.01	Down
Crop	13 ± 2	2 of 4	0.00	Down
Midgut	6 ± 2	0 of 4	0.00	Down
Tubule	9 ± 0	0 of 4	0.00	Down
Hindgut	10 ± 1	3 of 4	0.00	Down
Heart	141 ± 93	4 of 4	0.05	Down
Fat body	12 ± 7	0 of 4	0.00	Down
Ovary	3 ± 0	0 of 4	0.00	Down
Testis	8 ± 1	1 of 4	0.00	Down
Male accessory glands	15 ± 4	2 of 4	0.00	Down
Virgin spermatheca	8 ± 1	3 of 4	0.00	Down
Mated spermatheca	9 ± 1	1 of 4	0.00	Down
Adult carcass	6 ± 3	0 of 4	0.00	Down
Larval CNS	7 ± 2	3 of 4	0.00	Down
Larval Salivary gland	15 ± 2	2 of 4	0.01	Down
Larval midgut	19 ± 4	4 of 4	0.01	Down
Larval tubule	6 ± 1	1 of 4	0.00	Down
Larval hindgut	8 ± 2	1 of 4	0.00	Down
Larval fat body	14 ± 1	2 of 4	0.00	Down
Larval trachea	1516 ± 2880	3 of 4	0.55	None
Larval carcass	7 ± 1	0 of 4	0.00	Down
S2 cells (growing)	6 ± 0	0 of 4	0.00	Down
Whole fly	2761 ± 149	4 of 4		

Table 41: Anatomical expression profile for *rh7*; data set one.

Tissue	mRNA Signal	Present Call	Enrichment	Affy Call
Brain	8 ± 1	2 of 4	1.40	None
Head	11 ± 3	0 of 4	1.90	None
Eye	4 ± 1	0 of 4	0.77	None
Thoracicoabdominal ganglion	9 ± 3	0 of 4	1.50	None
Salivary gland	15 ± 5	0 of 4	2.55	None
Crop	10 ± 4	0 of 4	1.80	None
Midgut	8 ± 2	0 of 4	1.40	None
Tubule	8 ± 0	0 of 4	1.40	Up
Hindgut	6 ± 3	0 of 4	1.10	None
Heart	6 ± 1	0 of 4	1.12	None
Fat body	13 ± 6	0 of 4	2.23	None
Ovary	2 ± 0	0 of 4	0.40	None
Testis	1 ± 0	0 of 4	0.30	None
Male accessory glands	7 ± 3	0 of 4	1.30	None
Virgin spermatheca	8 ± 2	0 of 4	1.47	None
Mated spermatheca	5 ± 2	0 of 4	0.93	None
Adult carcass	8 ± 4	0 of 4	1.50	None
Larval CNS	5 ± 3	0 of 4	1.01	None
Larval Salivary gland	8 ± 1	0 of 4	1.43	None
Larval midgut	4 ± 1	0 of 4	0.75	None
Larval tubule	5 ± 1	0 of 4	0.90	None
Larval hindgut	1 ± 0	0 of 4	0.28	None
Larval fat body	16 ± 5	0 of 4	2.80	None
Larval trachea	7 ± 4	0 of 4	1.30	None
Larval carcass	2 ± 0	0 of 4	0.44	None
S2 cells (growing)	10 ± 2	0 of 4	1.76	None
Whole fly	5 ± 1	0 of 4		

Table 42: Anatomical expression profile for *rh7*; data set two.

Tissue	mRNA Signal	Present Call	Enrichment	Affy Call
Brain	8 ± 1	2 of 4	1.40	None
Head	11 ± 3	0 of 4	1.90	None
Eye	4 ± 1	0 of 4	0.77	None
Thoracicoabdominal ganglion	9 ± 3	0 of 4	1.50	None
Salivary gland	15 ± 5	0 of 4	2.55	None
Crop	10 ± 4	0 of 4	1.80	None
Midgut	8 ± 2	0 of 4	1.40	None
Tubule	8 ± 0	0 of 4	1.40	Up
Hindgut	6 ± 3	0 of 4	1.10	None
Heart	6 ± 1	0 of 4	1.12	None
Fat body	13 ± 6	0 of 4	2.23	None
Ovary	2 ± 0	0 of 4	0.40	None
Testis	1 ± 0	0 of 4	0.30	None
Male accessory glands	7 ± 3	0 of 4	1.30	None
Virgin spermatheca	8 ± 2	0 of 4	1.47	None
Mated spermatheca	5 ± 2	0 of 4	0.93	None
Adult carcass	8 ± 4	0 of 4	1.50	None
Larval CNS	5 ± 3	0 of 4	1.01	None
Larval Salivary gland	8 ± 1	0 of 4	1.43	None
Larval midgut	4 ± 1	0 of 4	0.75	None
Larval tubule	5 ± 1	0 of 4	0.90	None
Larval hindgut	1 ± 0	0 of 4	0.28	None
Larval fat body	16 ± 5	0 of 4	2.80	None
Larval trachea	7 ± 4	0 of 4	1.30	None
Larval carcass	2 ± 0	0 of 4	0.44	None
S2 cells (growing)	10 ± 2	0 of 4	1.76	None
Whole fly	5 ± 1	0 of 4		

7.2 Acknowledgements

An old African proverb says: “It takes a village to raise a child.” This thesis would not have been possible without the advice, the support and the encouragement of the kind people around me, to only some of whom it is possible to give particular mention here.

First and foremost, I would like to thank my supervisor Prof. Dr. Charlotte Förster for giving me the opportunity to stay in her laboratory for the PhD and for being both a great mentor and scientist.

I extend my gratitude to my co-advisors Dr. Susanne Fischer, Dr. Taishi Yoshii, Dr. Pingkalai Senthilan and Dr. Dirk Rieger for their suggestions, patience and guidance and to PD Dr. Alois Hofbauer for being the second referee of this thesis.

I am grateful to the staff and all members both of the Department of Neurobiology and Genetics (Würzburg) and the Department of Developmental Biology (Regensburg) for any kind of academic, technical and administrative support and for promoting a welcoming environment. I am also thankful to the DFG for funding most of this project.

Moreover, I would like to thank my present and former colleagues for their friendship and support, for having a good time – not only in the laboratory.

Last, but by no means least, I thank my friends (old, new, local and international) and my relatives. You always encouraged and supported me, personally and financially.
Finally, I would like to take this opportunity to express my gratefulness to my parents, especially to my mother, for their unconditional support and for keeping me grounded.
I owe a lot to you!

****

An dieser Stelle möchte ich mich bei meinen Verwandten und Freunden bedanken. Ihr seid mir immer mit Rat und Tat zur Seite gestanden, habt viel Verständnis gezeigt und mich dabei in meinen Plänen ermutigt und unterstützt.
Schließlich möchte ich die Gelegenheit nutzen, meinen Eltern von ganzem Herzen zu danken – für ihre bedingungslose Unterstützung und ihren Rückhalt.
Ich habe euch sehr viel zu verdanken!

7.3 Curriculum vitae

Personal information:

Name: Christa Rita Kistenpfennig

Date of birth: 1982/08/06

Place of birth: Regensburg

Nationality: German

Education:

Since 2010	Continuation of PhD study at the University of Würzburg, Department of Neurobiology and Genetics
2008 - 2010	DFG Graduate college fellowship: “Sensory Photoreceptors in natural and artificial systems” (GRK 640)
2008	PhD study at the University of Regensburg, Department of Developmental Biology
2007	Diploma thesis at the University of Regensburg, Department of Developmental Biology: “The effect of the neuropeptide PDF on the circadian clock of short- and long-period *timeless*-mutants”
2004/09 - 2005/01	Erasmus exchange studies, University of Leicester, Department of Genetics, UK
2001 - 2007	Study of Biology at the University of Regensburg with focus on Genetics, Cell and Developmental Biology and Zoology

7.4 Publications

Kistenpfennig C, Hirsh J, Yoshii T and Helfrich-Förster C (2012) Phase-Shifting the Fruit Fly Clock without Cryptochrome. *Journal of Biological Rhythms* 27:117-25.

7.5 Bibliography

Adams MD, Celniker SE, Holt RA, Evans CA, Gocayne JD, Amanatides PG, Scherer SE, Li PW, Hoskins RA, Galle RF, George RA, Lewis SE, Richards S, Ashburner M, Henderson SN, Sutton GG, Wortman JR, Yandell MD, Zhang Q, Chen LX, Brandon RC, Rogers YH, Blazej RG, Champe M, Pfeiffer BD, Wan KH, Doyle C, Baxter EG, Helt G, Nelson CR, Gabor GL, Abril JF, Agbayani A, An HJ et al. (2000) The genome sequence of *Drosophila* melanogaster. *Science* 287:2185-2195.

Ahmad M and Cashmore AR (1993) HY4 gene of *A. thaliana* encodes a protein with characteristics of a blue-light photoreceptor. *Nature* 366:162-166.

Allada R and Chung BY (2011) Circadian organization of behavior and physiology in *Drosophila*. *Annual review of physiology* 72:605-624.

Allada R, White NE, So WV, Hall JC and Rosbash M (1998) A mutant *Drosophila* homolog of mammalian Clock disrupts circadian rhythms and transcription of period and timeless. *Cell* 93:791-804.
Ambros V (2004) The functions of animal microRNAs. *Nature* 431:350-355.

Anh NT, Nishitani M, Harada S, Yamaguchi M and Kamei K (2011) A *Drosophila* model for the screening of bioavailable NADPH oxidase inhibitors and antioxidants. *Molecular and cellular biochemistry* 352:91-98.

Arikawa K, Hicks JL and Williams DS (1990) Identification of actin filaments in the rhabdomeral microvilli of *Drosophila* photoreceptors. *The Journal of cell biology* 110:1993-1998.

Aschoff J (1960) Exogenous and endogenous components in circadian rhythms. *Cold Spring Harbor symposia on quantitative biology* 25:11-28.

Bachleitner W (2008) Photorezeption in *Drosophila melanogaster:* Die Synchronisation der Inneren Uhr durch Mondlicht und die Analyse von Rhodopsin 7 als neues Photopigment. PhD thesis. University of Regensburg, Regensburg.

Bachleitner W, Kempinger L, Wulbeck C, Rieger D and Helfrich-Forster C (2007) Moonlight shifts the endogenous clock of *Drosophila melanogaster*. *Proceedings of the National Academy of Sciences of the United States of America* 104:3538-3543.

Bellen HJ, Levis RW, Liao G, He Y, Carlson JW, Tsang G, Evans-Holm M, Hiesinger PR, Schulze KL, Rubin GM, Hoskins RA and Spradling AC (2004) The BDGP gene disruption project: single transposon insertions associated with 40% of *Drosophila genes*. *Genetics* 167:761-781.

Bentrop J, Schwab K, Pak WL and Paulsen R (1997) Site-directed mutagenesis of highly conserved amino acids in the first cytoplasmic loop of *Drosophila* Rh1 opsin blocks rhodopsin synthesis in the nascent state. *The EMBO journal* 16:1600-1609.

Bergmann A, Agapite J, McCall K and Steller H (1998) The *Drosophila* gene hid is a direct molecular target of Ras-dependent survival signaling. *Cell* 95:331-341.

Bhutani S (2009) Natural entrainment of the *Drosophila melanogaster* circadian clock. PhD thesis. University of Leicester, Leicester.

Blau J and Young MW (1999) Cycling vrille expression is required for a functional *Drosophila* clock. *Cell* 99:661-671.

Bleyl C (2008) Untersuchungen zum Expressionsmuster von Rhodopsin7. Diploma thesis. University of Regensburg, Regensburg.

Bolwig N (1946) Senses and sense organs of the anterior end of the house fly larvae. *Vid Medd dansk nat-hist Foren 109* 109:81-217.

Braitenberg V (1967) Patterns of projection in the visual system of the fly. I. Retina-lamina projections. *Experimental brain research Experimentelle Hirnforschung* 3:271-298.

Brand AH and Perrimon N (1993) Targeted gene expression as a means of altering cell fates and generating dominant phenotypes. *Development* 118:401-415.

Brennecke J, Hipfner DR, Stark A, Russell RB and Cohen SM (2003) bantam encodes a developmentally regulated microRNA that controls cell proliferation and regulates the proapoptotic gene hid in *Drosophila*. *Cell* 113:25-36.

Burg MG, Sarthy PV, Koliantz G and Pak WL (1993) Genetic and molecular identification of a *Drosophila* histidine decarboxylase gene required in photoreceptor transmitter synthesis. *The EMBO journal* 12:911-919.

Busza A, Emery-Le M, Rosbash M and Emery P (2004) Roles of the two *Drosophila* CRYPTOCHROME structural domains in circadian photoreception. *Science* 304:1503-1506.

Cashmore AR, Jarillo JA, Wu YJ and Liu D (1999) Cryptochromes: blue light receptors for plants and animals. *Science* 284:760-765.

Ceriani MF, Darlington TK, Staknis D, Mas P, Petti AA, Weitz CJ and Kay SA (1999) Light-dependent sequestration of TIMELESS by CRYPTOCHROME. *Science* 285:553-556.

Cheng HY, Papp JW, Varlamova O, Dziema H, Russell B, Curfman JP, Nakazawa T, Shimizu K, Okamura H, Impey S and Obrietan K (2007) microRNA modulation of circadian-clock period and entrainment. *Neuron* 54:813-829.

Cheyette BN, Green PJ, Martin K, Garren H, Hartenstein V and Zipursky SL (1994) The *Drosophila* sine oculis locus encodes a homeodomain-containing protein required for the development of the entire visual system. *Neuron* 12:977-996.

Chintapalli VR, Wang J and Dow JA (2007) Using FlyAtlas to identify better *Drosophila melanogaster* models of human disease. *Nature genetics* 39:715-720.

Chou WH, Hall KJ, Wilson DB, Wideman CL, Townson SM, Chadwell LV and Britt SG (1996) Identification of a novel *Drosophila* opsin reveals specific patterning of the R7 and R8 photoreceptor cells. *Neuron* 17:1101-1115.

Colley NJ, Cassill JA, Baker EK and Zuker CS (1995) Defective intracellular transport is the molecular basis of rhodopsin-dependent dominant retinal degeneration. *Proceedings of the National Academy of Sciences of the United States of America* 92:3070-3074.
Curtin KD, Huang ZJ and Rosbash M (1995) Temporally regulated nuclear entry of the *Drosophila* period protein contributes to the circadian clock. *Neuron* 14:365-372.

Daan S (1977) Tonic and phasic effects of light in the entrainment of circadian rhythms. *Annals of the New York Academy of Sciences* 290:51-59.

Darlington TK, Wager-Smith K, Ceriani MF, Staknis D, Gekakis N, Steeves TD, Weitz CJ, Takahashi JS and Kay SA (1998) Closing the circadian loop: CLOCK-induced transcription of its own inhibitors per and tim. *Science* 280:1599-1603.

de Couet HG and Tanimura T (1987) Monoclonal antibodies provide evidence that rhodopsin in the outer rhabdomeres of *Drosophila melanogaster* is not glycosylated. *European journal of cell biology* 44:50-56.

Dolezelova E, Dolezel D and Hall JC (2007) Rhythm defects caused by newly engineered null mutations in *Drosophila's* cryptochrome gene. *Genetics* 177:329-345.

Dolph PJ, Ranganathan R, Colley NJ, Hardy RW, Socolich M and Zuker CS (1993) Arrestin function in inactivation of G protein-coupled receptor rhodopsin in vivo. *Science* 260:1910-1916.

Duffy JB (2002) GAL4 system in *Drosophila*: a fly geneticist's Swiss army knife. *Genesis* 34:1-15.

Emery P, So WV, Kaneko M, Hall JC and Rosbash M (1998) CRY, a *Drosophila* clock and light-regulated cryptochrome, is a major contributor to circadian rhythm resetting and photosensitivity. *Cell* 95:669-679.

Emery P, Stanewsky R, Hall JC and Rosbash M (2000a) A unique circadian-rhythm photoreceptor. *Nature* 404:456-457.

Emery P, Stanewsky R, Helfrich-Forster C, Emery-Le M, Hall JC and Rosbash M (2000b) *Drosophila* CRY is a deep brain circadian photoreceptor. *Neuron* 26:493-504.

Fischbach KF and Dittrich APM (1989) The optic lobe of *Drosophila melanogaster*. I. A Golgi analysis of wild-type structure. *Cell and tissue research* 258:441-475.

Fortini ME and Rubin GM (1990) Analysis of cis-acting requirements of the Rh3 and Rh4 genes reveals a bipartite organization to rhodopsin promoters in *Drosophila melanogaster*. *Genes & development* 4:444-463.

Freeman M (1996) Reiterative use of the EGF receptor triggers differentiation of all cell types in the *Drosophila* eye. *Cell* 87:651-660.

Fujita SC, Zipursky SL, Benzer S, Ferrus A and Shotwell SL (1982) Monoclonal antibodies against the *Drosophila* nervous system. *Proceedings of the National Academy of Sciences of the United States of America* 79:7929-7933.

Gärtner W (2000) Invertebrate visual pigments. . In *Handbook of biological physics*, DG Stavenga, WJ De Grip and EN Pugh, eds, pp 297-388, Elsevier, New York.

Gegear RJ, Casselman A, Waddell S and Reppert SM (2008) Cryptochrome mediates light-dependent magnetosensitivity in *Drosophila*. *Nature* 454:1014-1018.

Giebultowicz JM (2001) Peripheral clocks and their role in circadian timing: insights from insects. *Philosophical transactions of the Royal Society of London* 356:1791-1799.

Glenner H, Thomsen PF, Hebsgaard MB, Sorensen MV and Willerslev E (2006) Evolution. The origin of insects. *Science* 314:1883-1884.

Golombek DA and Rosenstein RE (2010) Physiology of circadian entrainment. *Physiological reviews* 90:1063-1102.

Goodman LJ (1970) The structure and function of the insect dorsal ocellus. *Adv Insect Physiol* 7:97-195.

Graveley BR, Brooks AN, Carlson JW, Duff MO, Landolin JM, Yang L, Artieri CG, van Baren MJ, Boley N, Booth BW, Brown JB, Cherbas L, Davis CA, Dobin A, Li R, Lin W, Malone JH, Mattiuzzo NR, Miller D, Sturgill D, Tuch BB, Zaleski C, Zhang D, Blanchette M, Dudoit S, Eads B, Green RE, Hammonds A, Jiang L, Kapranov P, Langton L, Perrimon N, Sandler JE, Wan KH, Willingham A, Zhang Y, Zou Y, Andrews J, Bickel PJ, Brenner SE, Brent MR, Cherbas P, Gingeras TR, Hoskins RA, Kaufman TC, Oliver B and Celniker SE (2011) The developmental transcriptome of *Drosophila melanogaster*. *Nature* 471:473-479.

Grebler R (2010) Elektrophysiologische Charakterisierung von Rhodopsin 7. Diploma thesis. University of Regensburg, Regensburg.

Griffin EA, Jr., Staknis D and Weitz CJ (1999) Light-independent role of CRY1 and CRY2 in the mammalian circadian clock. *Science* 286:768-771.

Grima B, Chelot E, Xia R and Rouyer F (2004) Morning and evening peaks of activity rely on different clock neurons of the *Drosophila* brain. *Nature* 431:869-873.

Halberg F, Halberg E, Barnum CP and Bittner JJ (1959) Physiologic 24-hour periodicity in human beings and mice, the lighting regimen, and daily routine. In *Photoperiodism and related phenomena in plants and animals*, pp 803-878, Am Assn Adv Sci, Washington, DC.

Halfon MS, Gisselbrecht S, Lu J, Estrada B, Keshishian H and Michelson AM (2002) New fluorescent protein reporters for use with the *Drosophila* Gal4 expression system and for vital detection of balancer chromosomes. *Genesis* 34:135-138.

Hamblen-Coyle MJ, Wheeler DA, Rutila JE, Rosbash M and Hall JC (1992) Behavior of period-altered circadian rhythm mutants of *Drosophila* in light: Dark cycles (Diptera: Drosophilidae). J*ournal of Insect Behavior* 5:417-446.

Hardie RC (1987) Is histamine a neurotransmitter in insect photoreceptors? *J Comp Physiol A* 161:201-213.

Hardie RC (2001) Phototransduction in *Drosophila melanogaster*. *The Journal of experimental biology* 204:3403-3409.

Hardie RC (2012) Phototransduction mechanisms in *Drosophila* microvillar photoreceptors. *Wiley Interdisciplinary Reviews: Membrane Transport and Signaling* 1:162-187.

Hardin PE, Hall JC and Rosbash M (1990) Feedback of the *Drosophila* period gene product on circadian cycling of its messenger RNA levels. *Nature* 343:536-540.

Hargrave PA (2001) Rhodopsin structure, function, and topography the Friedenwald lecture. *Investigative ophthalmology & visual science* 42:3-9.

Hargrave PA, McDowell JH, Feldmann RJ, Atkinson PH, Rao JK and Argos P (1984) Rhodopsin's protein and carbohydrate structure: selected aspects. *Vision research* 24:1487-1499.

Heisenberg M and Böhl K (1979) Isolation of anatomical brain mutants of *Drosophila* by histological means. *Zeitschrift fur Naturforschung* 34:143-147.

Heisenberg M and Buchner E (1977) The role of retinula cell types in visual behavior of *Drosophila melanogaster*. *Journal of comparative physiology* 117:127-162.

Helfrich-Forster C (1998) Robust circadian rhythmicity of *Drosophila melanogaster* requires the presence of lateral neurons: a brain-behavioral study of disconnected mutants. *J Comp Physiol A* 182:435-453.

Helfrich-Forster C (2005) Neurobiology of the fruit fly's circadian clock. *Genes, brain, and behavior* 4:65-76.

Helfrich-Forster C (2009) Does the morning and evening oscillator model fit better for flies or mice? *Journal of biological rhythms* 24:259-270.

Helfrich-Forster C, Edwards T, Yasuyama K, Wisotzki B, Schneuwly S, Stanewsky R, Meinertzhagen IA and Hofbauer A (2002) The extraretinal eyelet of *Drosophila*: development, ultrastructure, and putative circadian function. *J Neurosci* 22:9255-9266.

Helfrich-Forster C, Shafer OT, Wulbeck C, Grieshaber E, Rieger D and Taghert P (2007) Development and morphology of the clock-gene-expressing lateral neurons of *Drosophila melanogaster*. *The Journal of comparative neurology* 500:47-70.

Helfrich-Forster C, Winter C, Hofbauer A, Hall JC and Stanewsky R (2001) The circadian clock of fruit flies is blind after elimination of all known photoreceptors. *Neuron* 30:249-261.

Helfrich C and Engelmann W (1983) Circadian rhythm of the locomotor activity in *Drosophila melanogaster* and its mutants ‘sine oculis’ and ‘small optic lobes’. *Physiological Entomology* 8:257-272.

Hermann C, Saccon R, Senthilan P, Domnik L, Dircksen H, Yoshii T and Helfrich-Forster C The circadian clock network in the brain of different *Drosophila* species. *The Journal of comparative neurolog.* In Press.

Hermann C, Yoshii T, Dusik V and Helfrich-Forster C (2012) Neuropeptide F immunoreactive clock neurons modify evening locomotor activity and free-running period in *Drosophila melanogaster*. *The Journal of comparative neurology* 520:970-987.

Hitomi K, Okamoto K, Daiyasu H, Miyashita H, Iwai S, Toh H, Ishiura M and Todo T (2000) Bacterial cryptochrome and photolyase: characterization of two photolyase-like genes of *Synechocystis* sp. PCC6803. *Nucleic acids research* 28:2353-2362.

Hofbauer A and Buchner E (1989) Does *Drosophila* have seven eyes? *Die Naturwissenschaften* 76:335-336.

Hofbauer A, Ebel T, Waltenspiel B, Oswald P, Chen YC, Halder P, Biskup S, Lewandrowski U, Winkler C, Sickmann A, Buchner S and Buchner E (2009) The Wuerzburg hybridoma library against *Drosophila* brain. *Journal of neurogenetics* 23:78-91.

Hu KG, Reichert H and Stark WS (1978) Electrophysiological characterization of *Drosophila* ocelli. *Journal of Comparative Physiology A: Neuroethology, Sensory, Neural, and Behavioral Physiology* 126:15-24.

Ito K, Awano W, Suzuki K, Hiromi Y and Yamamoto D (1997) The *Drosophila* mushroom body is a quadruple structure of clonal units each of which contains a virtually identical set of neurones and glial cells. *Development* 124:761-771.

Izutsu M, Zhou J, Sugiyama Y, Nishimura O, Aizu T, Toyoda A, Fujiyama A, Agata K and Fuse N (2012) Genome features of "Dark-fly", a *Drosophila* line reared long-term in a dark environment. *PloS one* 7:e33288.

Johnson CH (1999) Forty years of PRCs - what have we learned? *Chronobiology international* 16:711-743.

Johnson CH, Elliott JA and Foster R (2003) Entrainment of circadian programs. *Chronobiology international* 20:741-774.

Johnson CH and Hastings JW (1986) The elusive mechansims of the circadian clock. *American Scientist* 74:29-36.

Katz B and Minke B (2009) *Drosophila* photoreceptors and signaling mechanisms. *Frontiers in cellular neuroscience* 3:2.

Kaushik R, Nawathean P, Busza A, Murad A, Emery P and Rosbash M (2007) PER-TIM interactions with the photoreceptor cryptochrome mediate circadian temperature responses in *Drosophila*. *PLoS biology* 5:e146.

Kirschfeld K (1973) [Neural superposition eye]. *Fortschritte der Zoologie* 21:229-257.

Kirschfeld K and Franceschini N (1977) Evidence for a sensitising pigment in fly photoreceptors. *Nature* 269:386-390.

Kistenpfennig C, Hirsh J, Yoshii T and Helfrich-Forster C (2012) Phase-shifting the fruit fly clock without cryptochrome. *Journal of biological rhythms* 27:117-125.

Klarsfeld A, Malpel S, Michard-Vanhee C, Picot M, Chelot E and Rouyer F (2004) Novel features of cryptochrome-mediated photoreception in the brain circadian clock of *Drosophila*. *J Neurosci* 24:1468-1477.

Koh K, Zheng X and Sehgal A (2006) JETLAG resets the *Drosophila* circadian clock by promoting light-induced degradation of TIMELESS. *Science* 312:1809-1812.

Konopka RJ and Benzer S (1971) Clock mutants of *Drosophila melanogaster*. *Proceedings of the National Academy of Sciences of the United States of America* 68:2112-2116.

Konopka RJ, Pittendrigh C and Orr D (1989) Reciprocal behaviour associated with altered homeostasis and photosensitivity of *Drosophila* clock mutants. *Journal of neurogenetics* 6:1-10.

Kramer JM and Staveley BE (2003) GAL4 causes developmental defects and apoptosis when expressed in the developing eye of *Drosophila melanogaster*. *Genet Mol Res* 2:43-47.

Krishnan B, Levine JD, Lynch MK, Dowse HB, Funes P, Hall JC, Hardin PE and Dryer SE (2001) A new role for cryptochrome in a *Drosophila* circadian oscillator. *Nature* 411:313-317.

Kumar JP and Ready DF (1995) Rhodopsin plays an essential structural role in *Drosophila* photoreceptor development. *Development* 121:4359-4370.

Kurada P and O'Tousa JE (1995) Retinal degeneration caused by dominant rhodopsin mutations in *Drosophila*. *Neuron* 14:571-579.

Lee C, Bae K and Edery I (1999) PER and TIM inhibit the DNA binding activity of a *Drosophila* CLOCK-CYC/dBMAL1 heterodimer without disrupting formation of the heterodimer: a basis for circadian transcription. *Molecular and cellular biology* 19:5316-5325.

Leonard DS, Bowman VD, Ready DF and Pak WL (1992) Degeneration of photoreceptors in rhodopsin mutants of Drosophila. *Journal of neurobiology* 23:605-626.

Lindsley DL and Grell EH (1968) *Genetic variation of Drosophila melanogaster*, Carnegie Institution of Washington Publication No. 627.

Lindsley DL and Zimm GG (1992) *The Genome of Drosophila melanogaster*, Academic Press, Inc., San Diego.

Livak KJ and Schmittgen TD (2001) Analysis of relative gene expression data using real-time quantitative PCR and the 2(-Delta Delta C(T)) Method. *Methods* 25:402-408.

Maeda M (2011) Physiological Functions and Adaptive Roles of *Drosophila* Rhodopsin 7. In N*eurobiology of Drosophila* (Abstract), Cold Spring Harbor, New York.

Malpel S, Klarsfeld A and Rouyer F (2002) Larval optic nerve and adult extra-retinal photoreceptors sequentially associate with clock neurons during *Drosophila* brain development. *Development* 129:1443-1453.

Marion S, Oakley RH, Kim KM, Caron MG and Barak LS (2006) A beta-arrestin binding determinant common to the second intracellular loops of rhodopsin family G protein-coupled receptors. *The Journal of biological chemistry* 281:2932-2938.

Mazzoni EO, Celik A, Wernet MF, Vasiliauskas D, Johnston RJ, Cook TA, Pichaud F and Desplan C (2008) Iroquois complex genes induce co-expression of rhodopsins in *Drosophila*. *PLoS biology* 6:e97.

Medina PM, Worthen RJ, Forsberg LJ and Brenman JE (2008) The actin-binding protein capulet genetically interacts with the microtubule motor kinesin to maintain neuronal dendrite homeostasis. *PloS one* 3:e3054.

Menne D and Spatz H (1977) Colour vision in *Drosophila melanogaster*. *J Comp Physiol* 114:301-312.

Minors DS and Waterhouse JM (1989) Masking and biological rhythms. *Chronobiology international* 6:1-2.

Montell C (2012) *Drosophila* visual transduction. *Trends in neurosciences* 35:356-363.

Moore-Ede MC, Sulzman FM and Fuller CA (1982) Physiology of the Circadian Timing System. In *The Clocks That Time US*, pp 30-133, Harvard University Press, Cambrige, MA.

Morante J and Desplan C (2005) Photoreceptor axons play hide and seek. *Nature neuroscience* 8:401-402.

Moses K and Rubin GM (1991) Glass encodes a site-specific DNA-binding protein that is regulated in response to positional signals in the developing *Drosophila* eye. *Genes & development* 5:583-593.

Mrosovsky N (1999) Masking: history, definitions, and measurement. *Chronobiology international* 16:415-429.

Naidoo N, Song W, Hunter-Ensor M and Sehgal A (1999) A role for the proteasome in the light response of the timeless clock protein. *Science* 285:1737-1741.

Nelson RJ and Zucker I (1981) Photoperiodic control of reproduction in olfactory-bulbectomized rats. *Neuroendocrinology* 32:266-271.

Nichols R and Pak WL (1985) Characterization of *Drosophila melanogaster* rhodopsin. *The Journal of biological chemistry* 260:12670-12674.

Nitabach MN and Taghert PH (2008) Organization of the *Drosophila* circadian control circuit. *Curr Biol* 18:R84-93.

O'Tousa JE, Baehr W, Martin RL, Hirsh J, Pak WL and Applebury ML (1985) The *Drosophila ninaE* gene encodes an opsin. *Cell* 40:839-850.

Ozturk N, Selby CP, Annayev Y, Zhong D and Sancar A (2011) Reaction mechanism of *Drosophila* cryptochrome. *Proceedings of the National Academy of Sciences of the United States of America* 108:516-521.

Papatsenko D, Nazina A and Desplan C (2001) A conserved regulatory element present in all *Drosophila* rhodopsin genes mediates Pax6 functions and participates in the fine-tuning of cell-specific expression. *Mechanisms of development* 101:143-153.

Papatsenko D, Sheng G and Desplan C (1997) A new rhodopsin in R8 photoreceptors of *Drosophila*: evidence for coordinate expression with Rh3 in R7 cells. *Development* 124:1665-1673.

Pearn MT, Randall LL, Shortridge RD, Burg MG and Pak WL (1996) Molecular, biochemical, and electrophysiological characterization of *Drosophila norpA* mutants. *The Journal of biological chemistry* 271:4937-4945.

Pegoraro M and Tauber E (2008) The role of microRNAs (miRNA) in circadian rhythmicity. *Journal of genetics* 87:505-511.

Peschel N and Helfrich-Forster C (2011) Setting the clock--by nature: circadian rhythm in the fruitfly *Drosophila melanogaster*. *FEBS letters* 585:1435-1442.

Peschel N, Veleri S and Stanewsky R (2006) Veela defines a molecular link between Cryptochrome and Timeless in the light-input pathway to *Drosophila's* circadian clock. *Proceedings of the National Academy of Sciences of the United States of America* 103:17313-17318.

Petrovic M and Hummel T (2008) Temporal identity in axonal target layer recognition. *Nature* 456:800-803.

Pflugfelder GO, Schwarz H, Roth H, Poeck B, Sigl A, Kerscher S, Jonschker B, Pak WL and Heisenberg M (1990) Genetic and molecular characterization of the optomotor-blind gene locus in *Drosophila melanogaster*. *Genetics* 126:91-104.

Pittendrigh CS (1954) On Temperature Independence in the Clock System Controlling Emergence Time in *Drosophila*. *Proceedings of the National Academy of Sciences of the United States of America* 40:1018-1029.

Pittendrigh CS (1960) Circadian rhythms and the circadian organization of living systems. *Cold Spring Harbor symposia on quantitative biology* 25:159-184.

Pittendrigh CS (1966) The circadian oscillation in *Drosophila pseudoobscura* pupae: A model for the photoperiodic clock. *Z Pflanzenphysiol* 54:275-307.

Pittendrigh CS (1981) Circadian systems: entrainment. In *Handbook of Behavioral Neurobiology*, J Aschoff, ed, pp 95-124, Biological Rhythms Plenum Press, New York.

Pittendrigh CS and Daan S (1976) A functional analysis of circadian pacemakers in nocturnal rodents. *Journal of Comparative Physiology A: Neuroethology, Sensory, Neural, and Behavioral Physiology* 106:333-355.

Plautz JD, Kaneko M, Hall JC and Kay SA (1997) Independent photoreceptive circadian clocks throughout *Drosophila*. *Science* 278:1632-1635.

Pollock JA and Benzer S (1988) Transcript localization of four opsin genes in the three visual organs of *Drosophila*; RH2 is ocellus specific. *Nature* 333:779-782.

Ready DF, Hanson TE and Benzer S (1976) Development of the *Drosophila* retina, a neurocrystalline lattice. *Developmental biology* 53:217-240.

Renn SC, Park JH, Rosbash M, Hall JC and Taghert PH (1999) A pdf neuropeptide gene mutation and ablation of PDF neurons each cause severe abnormalities of behavioral circadian rhythms in *Drosophila*. *Cell* 99:791-802.

Rieger D, Fraunholz C, Popp J, Bichler D, Dittmann R and Helfrich-Forster C (2007) The fruit fly *Drosophila melanogaster* favors dim light and times its activity peaks to early dawn and late dusk. *Journal of biological rhythms* 22:387-399.

Rieger D, Peschel N, Dusik V, Glotz S and Helfrich-Forster C (2012) The ability to entrain to long photoperiods differs between 3 *Drosophila melanogaster* wild-type strains and is modified by twilight simulation. *Journal of biological rhythms* 27:37-47.

Rieger D, Shafer OT, Tomioka K and Helfrich-Forster C (2006) Functional analysis of circadian pacemaker neurons in *Drosophila melanogaster*. *J Neurosci* 26:2531-2543.

Rieger D, Stanewsky R and Helfrich-Forster C (2003) Cryptochrome, compound eyes, Hofbauer-Buchner eyelets, and ocelli play different roles in the entrainment and masking pathway of the locomotor activity rhythm in the fruit fly *Drosophila melanogaster*. *Journal of biological rhythms* 18:377-391.

Rister J and Heisenberg M (2006) Distinct functions of neuronal synaptobrevin in developing and mature fly photoreceptors. *Journal of neurobiology* 66:1271-1284.

Robinow S, Campos AR, Yao KM and White K (1988) The elav gene product of *Drosophila*, required in neurons, has three RNP consensus motifs. *Science* 242:1570-1572.
Roenneberg T and Merrow M (2003) The network of time: understanding the molecular circadian system. *Curr Biol* 13:R198-207.

Rosato E, Codd V, Mazzotta G, Piccin A, Zordan M, Costa R and Kyriacou CP (2001) Light-dependent interaction between *Drosophila* CRY and the clock protein PER mediated by the carboxy terminus of CRY. *Curr Biol* 11:909-917.

Rutila JE, Suri V, Le M, So WV, Rosbash M and Hall JC (1998) CYCLE is a second bHLH-PAS clock protein essential for circadian rhythmicity and transcription of *Drosophila* period and timeless. *Cell* 93:805-814.

Salcedo E, Huber A, Henrich S, Chadwell LV, Chou WH, Paulsen R and Britt SG (1999) Blue- and green-absorbing visual pigments of *Drosophila*: ectopic expression and physiological characterization of the R8 photoreceptor cell-specific Rh5 and Rh6 rhodopsins. *J Neurosci* 19:10716-10726.
Sambrook J, Fritsch EF and Maniatis T (1989) *Molecular cloning: a laboratory Manual*, Cold Spring Harbor Laboratory Press, Cold Spring Harbor.

Saunders DS (1978) An experimental and theoretical analysis of photoperiodic induction in the flesh-Fly, *Sarcophaga argyrostoma*. *Journal of Comparative Physiology A: Neuroethology, Sensory, Neural, and Behavioral Physiology* 124:75-95.

Scott K, Becker A, Sun Y, Hardy R and Zuker C (1995) Gq alpha protein function in vivo: genetic dissection of its role in photoreceptor cell physiology. *Neuron* 15:919-927.

Sehgal A, Price JL, Man B and Young MW (1994) Loss of circadian behavioral rhythms and per RNA oscillations in the *Drosophila* mutant timeless. *Science* 263:1603-1606.

Senthilan P (2011) Identification and characterization of deafness genes in *Drosophila melanogaster*. PhD thesis. Georg-August-University Göttingen, Göttingen.

Shen WL, Kwon Y, Adegbola AA, Luo J, Chess A and Montell C (2011) Function of rhodopsin in temperature discrimination in *Drosophila*. *Science* 331:1333-1336.

So WV and Rosbash M (1997) Post-transcriptional regulation contributes to *Drosophila* clock gene mRNA cycling. *The EMBO journal* 16:7146-7155.

Sprecher SG and Desplan C (2008) Switch of rhodopsin expression in terminally differentiated *Drosophila* sensory neurons. *Nature* 454:533-537.

Stanewsky R, Kaneko M, Emery P, Beretta B, Wager-Smith K, Kay SA, Rosbash M and Hall JC (1998) The cryb mutation identifies cryptochrome as a circadian photoreceptor in *Drosophila*. *Cell* 95:681-692.

Stavenga DG (1992) Eye regionalization and spectral tuning of retinal pigments in insects. *Trends in neurosciences* 15:213-218.

Stavenga DG and Arikawa K (2008) One rhodopsin per photoreceptor: Iro-C genes break the rule. *PLoS biology* 6:e115.

Stoleru D, Peng Y, Agosto J and Rosbash M (2004) Coupled oscillators control morning and evening locomotor behaviour of *Drosophila*. *Nature* 431:862-868.

Szular J, Sehadova H, Gentile C, Szabo G, Chou WH, Britt SG and Stanewsky R (2012) Rhodopsin 5- and Rhodopsin 6-mediated clock synchronization in *Drosophila melanogaster* is independent of retinal phospholipase C-beta signaling. *Journal of biological rhythms* 27:25-36.

Todo T, Ryo H, Yamamoto K, Toh H, Inui T, Ayaki H, Nomura T and Ikenaga M (1996) Similarity among the *Drosophila* (6-4)photolyase, a human photolyase homolog, and the DNA photolyase-blue-light photoreceptor family. *Science* 272:109-112.

Trujillo-Cenoz O (1965) Some aspects of the structural organization of the intermediate retina of dipterans. *Journal of ultrastructure research* 13:1-33.

Vanlalhriatpuia K, Chhakchhuak V, Moses SK, Iyyer SB, Kasture MS, Shivagaje AJ, Rajneesh BJ and Joshi DS (2007) Effects of altitude on circadian rhythm of adult locomotor activity in Himalayan strains of *Drosophila helvetica*. *Journal of circadian rhythms* 5:1.

Veleri S (2005) Analysis of the light-entrainment pathways for the circadian clock of *Drosophila melanogaster*. PhD thesis. University of Regensburg, Regensburg.

Veleri S, Brandes C, Helfrich-Forster C, Hall JC and Stanewsky R (2003) A self-sustaining, light-entrainable circadian oscillator in the *Drosophila* brain. *Curr Biol* 13:1758-1767.

Veleri S, Rieger D, Helfrich-Forster C and Stanewsky R (2007) Hofbauer-Buchner eyelet affects circadian photosensitivity and coordinates TIM and PER expression in *Drosophila* clock neurons. *Journal of biological rhythms* 22:29-42.

Vogt K and Kirschfeld K (1984) Chemical identity of the chromophores of fly visual pigment. *Die Naturwissenschaften* 71:211-213.

Wang T and Montell C (2007) Phototransduction and retinal degeneration in *Drosophila*. *Pflugers Arch* 454:821-847.

Wang X, Wang T, Jiao Y, von Lintig J and Montell C (2010) Requirement for an enzymatic visual cycle in *Drosophila*. *Curr Biol* 20:93-102.

Wang X, Wang T, Ni JD, von Lintig J and Montell C (2012) The *Drosophila* visual cycle and de novo chromophore synthesis depends on rdhB. *J Neurosci* 32:3485-3491.

Wernet MF, Labhart T, Baumann F, Mazzoni EO, Pichaud F and Desplan C (2003) Homothorax switches function of *Drosophila* photoreceptors from color to polarized light sensors. *Cell* 115:267-279.

Wheeler DA, Hamblen-Coyle MJ, Dushay MS and Hall JC (1993) Behavior in light-dark cycles of *Drosophila* mutants that are arrhythmic, blind, or both. *Journal of biological rhythms* 8:67-94.

Wimmer EA (2003) Innovations: applications of insect transgenesis. *Nature reviews* 4:225-232.

Winfree AT (1970) Integrated view of resetting a circadian clock. *Journal of theoretical biology* 28:327-374.

Wolff T and Ready DF (1993) Pattern formation in the *Drosophila* retina. In *The development of Drosophila melanogaster*, M Bate and A Martinez-Arias, eds, pp 1277-1325, Cold Spring Harbor Laboratory Press.

Yamaguchi S, Desplan C and Heisenberg M (2010) Contribution of photoreceptor subtypes to spectral wavelength preference in *Drosophila*. *Proceedings of the National Academy of Sciences of the United States of America* 107:5634-5639.

Yamaguchi S, Wolf R, Desplan C and Heisenberg M (2008) Motion vision is independent of color in *Drosophila*. *Proceedings of the National Academy of Sciences of the United States of America* 105:4910-4915.

Yasuyama K and Meinertzhagen IA (1999) Synaptic connections of PDF-immunoreactive lateral neurons projecting to the dorsal protocerebrum of *Drosophila melanogaster*. *The Journal of comparative neurology* 518:292-304.

Yeh E, Gustafson K and Boulianne GL (1995) Green fluorescent protein as a vital marker and reporter of gene expression in *Drosophila*. *Proceedings of the National Academy of Sciences of the United States of America* 92:7036-7040.

Yoshii T, Ahmad M and Helfrich-Forster C (2009) Cryptochrome mediates light-dependent magnetosensitivity of *Drosophila's* circadian clock. *PLoS biology* 7:e1000086.

Yoshii T, Funada Y, Ibuki-Ishibashi T, Matsumoto A, Tanimura T and Tomioka K (2004) *Drosophila* cryb mutation reveals two circadian clocks that drive locomotor rhythm and have different responsiveness to light. *Journal of insect physiology* 50:479-488.

Yoshii T, Todo T, Wulbeck C, Stanewsky R and Helfrich-Forster C (2008) Cryptochrome is present in the compound eyes and a subset of *Drosophila's* clock neurons. *The Journal of comparative neurology* 508:952-966.

Zuker CS, Cowman AF and Rubin GM (1985) Isolation and structure of a rhodopsin gene from *D. melanogaster*. *Cell* 40:851-858.